

AD-A056 093

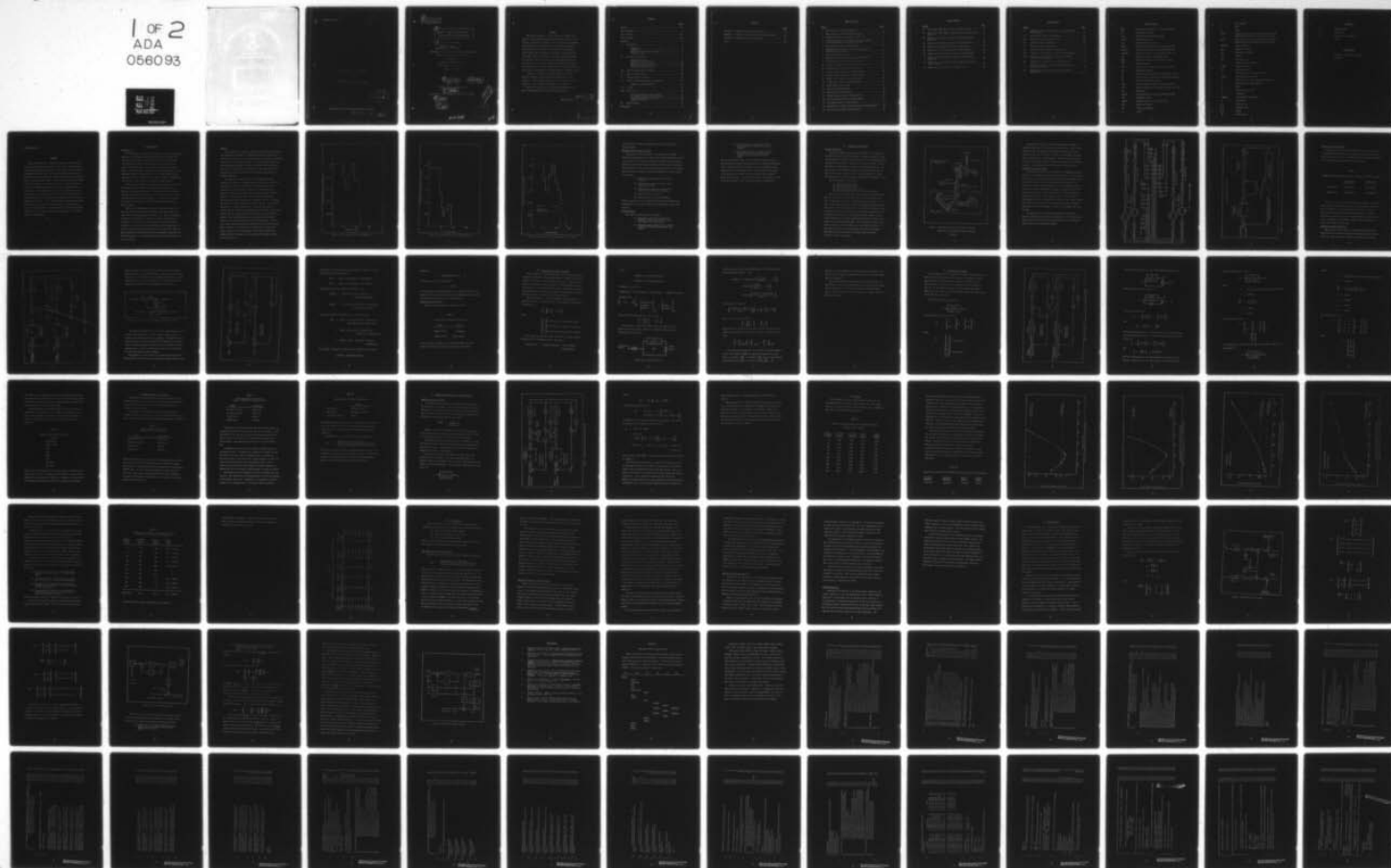
AIR FORCE INST OF TECH WRIGHT-PATTERSON AFB OHIO SCH--ETC F/G 20/6
ANALYSIS AND DESIGN MODIFICATION OF AN AIRBORNE MIRROR ALIGNMEN--ETC(U)
MAR 78 P D NUTZ

UNCLASSIFIED

AFIT/GAE/AA/78M-12

NL

1 OF 2
ADA
056093

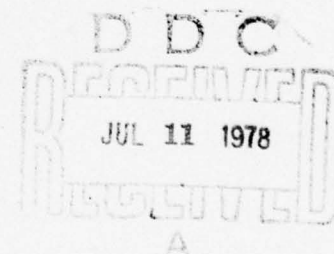


AFIT/GAE/AA/78M-12

ANALYSIS AND DESIGN MODIFICATION OF
AN AIRBORNE MIRROR ALIGNMENT SYSTEM

THESIS

AFIT/GAE/AA/78M-12 Patrick D. Nuts
2d Lt USAF



Approved for public release; distribution unlimited

78 07 10 09 2

14

AFIT/GAE/AA/78M-12

8

ANALYSIS AND DESIGN MODIFICATION OF
AN AIRBORNE MIRROR ALIGNMENT SYSTEM

9

Master's THESIS

Presented to the Faculty of the School of Engineering
of the Air Force Institute of Technology
Air University
in Partial Fulfillment of the
Requirements for the Degree of
Master of Science

by

10

Patrick D. Nutz

2d Lt USAF

12

119p.

Graduate Aeronautical Engineering

11

March 1978

Approved for public release; distribution unlimited.

16

1987

17

01

012225

1473

DDC
REGISTERED
JUL 11 1978
REGISTERED
A

Preface

This thesis attempts to analyze and solve a control system problem of the Airborne Dynamic Alignment System. This system is actually a subsystem of a current Air Force project, the Airborne Laser Laboratory. The Airborne Laser Laboratory is based at Kirtland AFB, NM, and thanks to the people of the LRO branch of the Weapons Lab at Kirtland, I was able to study the problem first hand. They sponsored me in this thesis and also provided the opportunity for a four week stay at Kirtland AFB during the initial phase of this study. Special thanks are due Capt Garth Corey of LRO, who spent many hours walking me through the difficult first steps of understanding the Airborne Dynamic Alignment System.

I also wish to express my sincere appreciation to Capt Gary Reid and Capt Jim Silverthorne who comprised my thesis committee. Without their help and guidance I would never have learned as much as I did while working on this thesis.

Finally, I would like to thank my loving wife, Joyce, who kept me alive during this difficult learning period.

Patrick D. Nutz

ACCESSION NO.	
RTIR	White Section <input checked="" type="checkbox"/>
AND	Buff Section <input type="checkbox"/>
UNANNOUNCED	<input type="checkbox"/>
JUSTIFICATION	
BY	
DISTRIBUTION/AVAILABILITY CODES	
Doc	AVAIL. CODE OR SPECIAL
A	

Contents

	<u>Page</u>
Preface	ii
List of Figures	v
List of Tables	vii
List of Symbols	viii
Abstract	xi
I. Introduction	1
Background	1
Problem	2
General Problem Solution Approach	6
Limits of Study	6
II. Analysis of Present ADAS	8
General Description	8
Electronic Control System	10
Reduction of Control System	13
Need for Electronic Decoupling	13
Discussion of Error Limits	18
III. ADAS Frequency Domain Simulation	19
IV. ADAS State Space Model	23
V. Numerical Extent of Problem	29
VI. Control System Modification and Predictions	32
Addition of Low Pass Filter	32
VII. Results	36
VIII. Conclusions	46
Open Loop Frequency Domain Analysis	46
Closed Loop Frequency Domain Analysis	47
State Space Eigenvalue Analysis	49
Overall Conclusions	50
IX. Recommendations	52
Bibliography	61

Contents

	<u>Page</u>
Appendix A : Frequency Domain Computer Program	62
Appendix B : Diagrams of Two for One Beam Steering Movement . . .	85
Appendix C : Supplementary Figures and Tables	91
Vita	104

List of Figures

<u>Figure</u>		<u>Page</u>
1	ADAS Statement of Work PSD (Angular)	3
2	ADAS Statement of Work PSD (Translational)	4
3	Comparison of ADAS SOW and CYCLE III ROLL PSD	5
4	Functional Diagram of the Optical Train and Components of the Airborne Dynamic Alignment Assembly	9
5	ADAS Frequency Response Block Diagram	11
6	Representative Single Loop in ADAS Block Diagram of Electronic Control System	12
7	Two Loop ADAS Control System	14
8	ALPHA-P, Y-TRANS Electronic Cross-coupling Network	15
9	D.C. Version of ADAS 2 Loop Control System	16
10	Location of States in ADAS Two Loop Control System	24
11	Modified ADAS Control System (Two Loop)	33
12	A1 Motor Torque Required vs Cutoff Frequency	38
13	A2 Motor Torque Required vs Cutoff Frequency	39
14	ALPHA-P Error Signal vs Cutoff Frequency	40
15	Y-TRANS Error Signal vs Cutoff Frequency	41
16	Block Diagram of Basic ADAS	54
17	Basic ADAS Tracking Problem	57
18	Optimal ADAS Tracking Problem	60
19	Initial Position of Beam Steering Mirrors	87
20	Pure Translational Error in Beam Alignment	88
21	Pure Angular Error in Beam Alignment	89
22	Combination of Angular and Translational Beam Misalignment . .	90
23	ADAS State Space Model Computer Program	92

List of Figures

<u>Figure</u>		<u>Page</u>
24	State Matrix $[A]$ for ADAS Two Loop Control System	93
25	State Space Matrix $[A]$ for Modified ADAS Two Loop Control System	94
26	ALPHA-P Open Loop Error Rejection with Various Cutoff Frequencies	95
27	Comparison of Translational ADAS SOW and Filter PSDs	96
28	ADAS SOW PSD and State Space Filter Approximation	97
29	ALPHA-P Open Loop Response (800 Hz Cutoff Frequency)	98
30	ALPHA-P Open Loop Response (1,100 Hz Cutoff Frequency)	99
31	ALPHA-P Open Loop Response (1,600 and 4,000 Hz Cutoff Frequency)	100
32	ALPHA-P Open Loop Response (8,000, 12,000, and 16,000 Hz Cutoff Frequency)	101
33	ALPHA-P Open Loop Response of Original System	102

List of Tables

<u>Table</u>		<u>Page</u>
I.	Comparison of Error Output Between 4 Loop and 2 Loop Control System	13
II.	Error Limits in Angle and Translation	18
III.	Eigenvalues of ADAS Control System	28
IV.	Baseline Closed Loop Response	29
V.	Worst Case Closed Loop Response	30
VI.	Open Loop Data for ALPHA-P Control Loop	31
VII.	Comparison of Complimentary Filter Cutoff Frequencies . .	36
VIII.	Closed Loop Response with No ALPHA-P \rightarrow Y-TRANS Electronic Cross-coupling	37
IX.	Comparison of ALPHA-P Open Loop Characteristics	43
X.	ADAS Two Loop Control System Response with Various Cutoff Frequencies	45
XI.	Eigenvalue Comparison with Various Filter Cutoff Frequencies	103

List of Symbols

[A]	Matrix that is dependent on system components
AAS	<u>A</u> uto <u>A</u> lignment <u>S</u> ystem
ADAS	<u>A</u> irborne <u>D</u> ynamic <u>A</u> lignment <u>S</u> ystem
A(DIS)	Angular disturbance
ALL	<u>A</u> irborne <u>L</u> aser <u>L</u> aboratory
ALPHA	Angular rotation axis of beam steering mirrors
ALPHA(1)	ALPHA axis rotation of beam steering Mirror #1
ALPHA(2)	ALPHA axis rotation of beam steering Mirror #2
APT	<u>A</u> utomatic <u>P</u> ointing and <u>T</u> racking Device
[B]	Matrix which represents the external inputs
BAS	<u>B</u> eam <u>A</u> ngle <u>S</u> ensor
BETA	Angular rotation axis of beam steering mirrors
BSM	<u>B</u> eam <u>S</u> teering <u>M</u> irror
C_1	Signal leaving Y-Translation compensation network
C_2	Signal leaving ALPHA-Prealign compensation network
\hat{d}	Estimated disturbance vector
E(A)	Error in angular alignment of main laser beam
E(T)	Error in translational alignment of main laser beam
FM	<u>F</u> old <u>M</u> irror
FRQRSP	Frequency Response Computer Simulation Program
GDL	<u>G</u> as <u>D</u> ynamic <u>L</u> aser
GLOWPS	Transfer function for low pass filter
HPG	<u>H</u> igh <u>P</u> ower <u>G</u> rating
Hz	Hertz, cycles/second
in	inches

J	Cost function
j	$\sqrt{-1}$
lb	Pound
KA1AP	Electronic cross-coupling sensitivity between the ALPHA-Prealign and Y-Translation control loops
KA2YT	Electronic cross-coupling sensitivity between the ALPHA-Prealign and Y-Translation control loops
NODE2SIG	Signal at Node #2
PAS	<u>P</u> re <u>A</u> lignment <u>S</u> ensor
PSD	<u>P</u> ower <u>S</u> pectral <u>D</u> ensity
rad	Radians
RMS	<u>R</u> oot <u>M</u> ean <u>S</u> quare
s	Laplace transform variable
SIGMA	Standard deviation
SOW	<u>S</u> tatement <u>O</u> f <u>W</u> ork
T	Cutoff frequency of low pass filter
T(DIS)	Translational disturbance
W	White noise, zero mean, Gaussian statistics
w	Frequency, hertz (Hz), rad/sec
X	State
\hat{x}	Estimated state vector
Y	Y direction
YTERSIG	Y-Translation error signal
Z	Z direction
→	To or goes to
	Absolute value
[]	Matrix
Δ	Greater than

Subscripts

A	Angle, angular
d	Disturbance
T	Translation, translational
x	State

Super Scripts

•	Derivative (with respect to time)
^	Estimated

Abstract

This study deals with an electronic control system modification to solve a torque limitation problem in the Airborne Dynamic Alignment System aboard the Airborne Laser Lab. This control system is reduced in complexity and modeled in the frequency and state space domains. Closed loop system response over a desired frequency range is obtained from the frequency domain model. Stability data is calculated through eigenvalue analysis of the state space model. A low pass filter is introduced to decrease the demand on the torque saturated motor. The main result of this modification is that the filter does not appreciably alter the closed loop response. This is due to the fact that the cutoff frequency of the filter must be extremely high to keep the modified system stable. It is concluded that the complimentary filter does not solve the torque saturation problem. A recommendation is made that further analysis be concentrated in the time domain through modern state space techniques and the design approach to an optimal controller is presented.

I. Introduction

Background

The background of the mirror alignment system lies in the design progression of the Airborne Laser Lab (ALL) based at Kirtland AFB, Albuquerque, New Mexico. The mission of the ALL is to demonstrate the technology involved in firing a laser from an aircraft in an actual flight environment. This project was divided into several phases. The initial phases involved the design and fabrication of the individual components aboard the ALL. In the final phases all the components will be installed in the aircraft and tested. Immediately, the need for certain subsystems to the ALL was acknowledged.

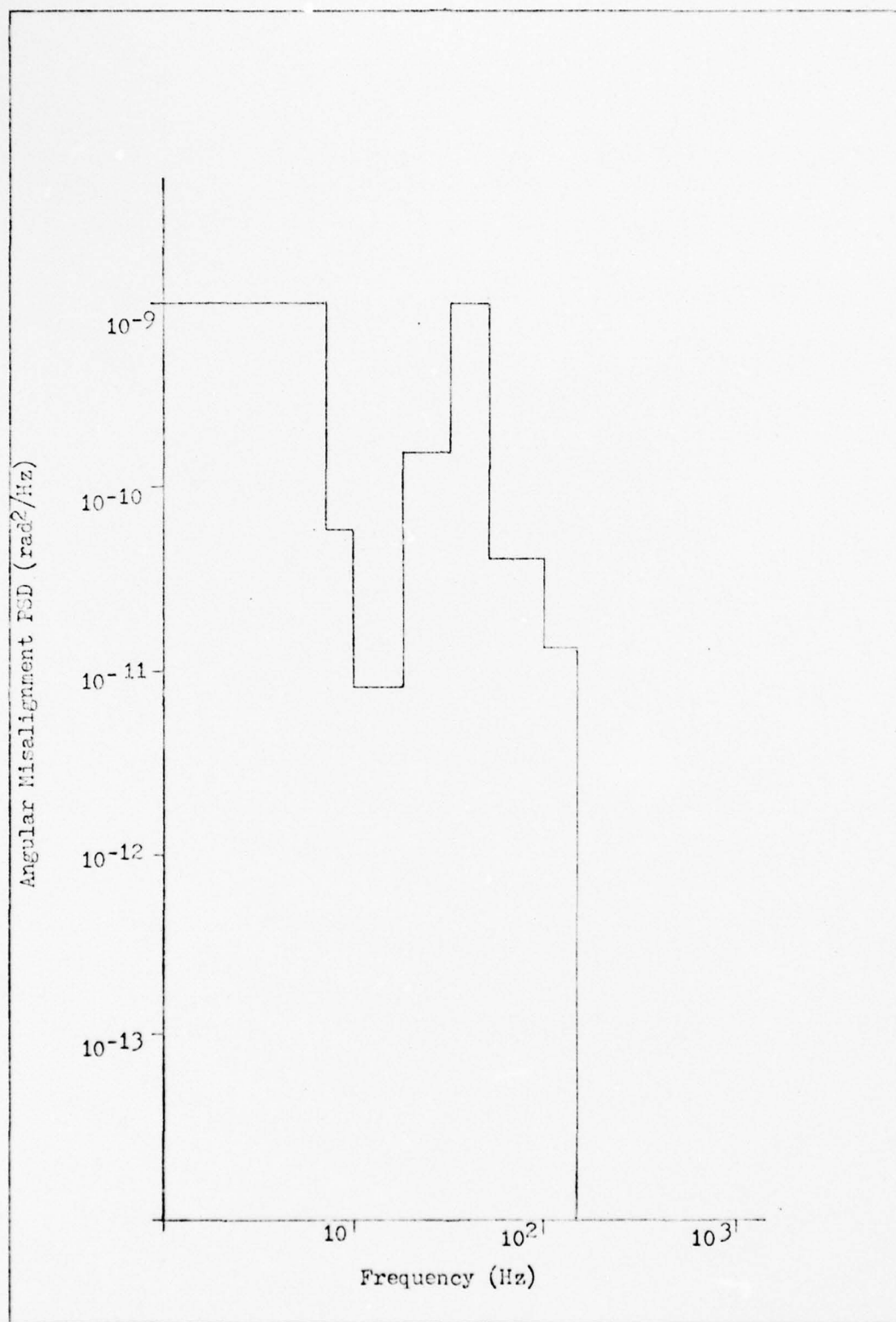
These included the actual beam generation mechanism: specifically the Gas Dynamic Laser (GDL), and a highly specified Automatic beam Pointing and Tracking (APT) device. Upon further analysis, however, the need for an active beam alignment system between the laser and the pointing/tracking device became apparent. The main catalyst behind this need was the unique vibrational environment encountered in a flying aircraft.

The ALL is a highly modified KC-135 (Boeing 707) aircraft. An aircraft of this size would have significant structural vibrations that would cause misalignments in the laser beam. This is especially critical due to the fact that the ALL is carrying the GDL which is primarily a turbojet engine. Therefore the vibration of the GDL coupled with the normal twisting and bending of the aircraft present quite an adverse vibrational environment to the laser beam. Thus, the Airborne Dynamic Alignment System (ADAS) was designed to eliminate any beam misalignment due to structural flexures of the ALL and the vibration of the GDL.

Problem

The main problem in designing the ADAS was quantitatively defining the vibrational environment. A considerable amount of information on the structural vibration of an ordinary KC-135 is available. Nonetheless the ALL was not an ordinary airplane. For example, major structural modification was necessary to install the GDL and a hole was cut in the roof of the aircraft to mount the APT. Also, there was little information on just how the GDL vibrations would couple with the aircraft vibrations.

With all this in mind, a "first cut" approximation of the vibrations was derived. A complex mathematical model of the ALL was obtained and a "Nastran" based (Ref. 2) structural analysis was performed. The result of this effort was the ADAS Statement Of Work (SOW) Power Spectral Density (PSD). (Ref. 3:2.29 and see Fig.'s 1 and 2). It was with this ADAS SOW disturbance spectrum that Perkin-Elmer designed the actual ADAS hardware. (Ref. 6). The system was delivered to the Air Force to be used in the ALL. It was tested and found to be within specifications. Using a small laser for testing, the ADAS and APT were installed in the aircraft. Flight tests revealed that the actual vibrational environment was worse than predicted. There were significant large magnitude, high frequency vibrations that were not present in the SOW PSD for ADAS. Furthermore, these large magnitude high frequency disturbances were causing ADAS to saturate. Essentially, the system could not respond fast enough to null the beam misalignment. Since this knowledge was a result of CYCLE II testing, the new vibration PSD became the CYCLE III PSD (see Fig. 3).



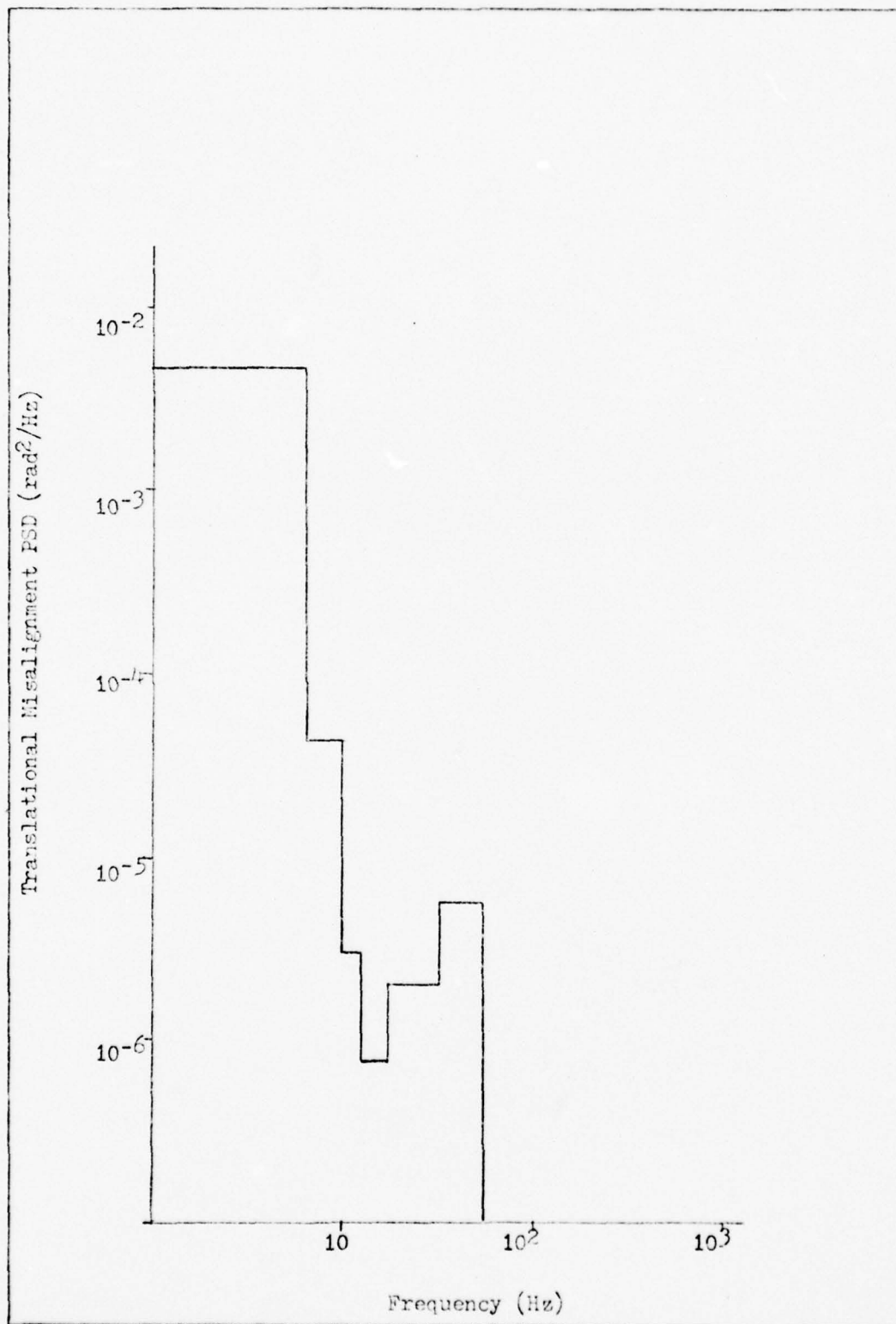


Fig.2 . ADAS Statement of Work PSD (Translational)

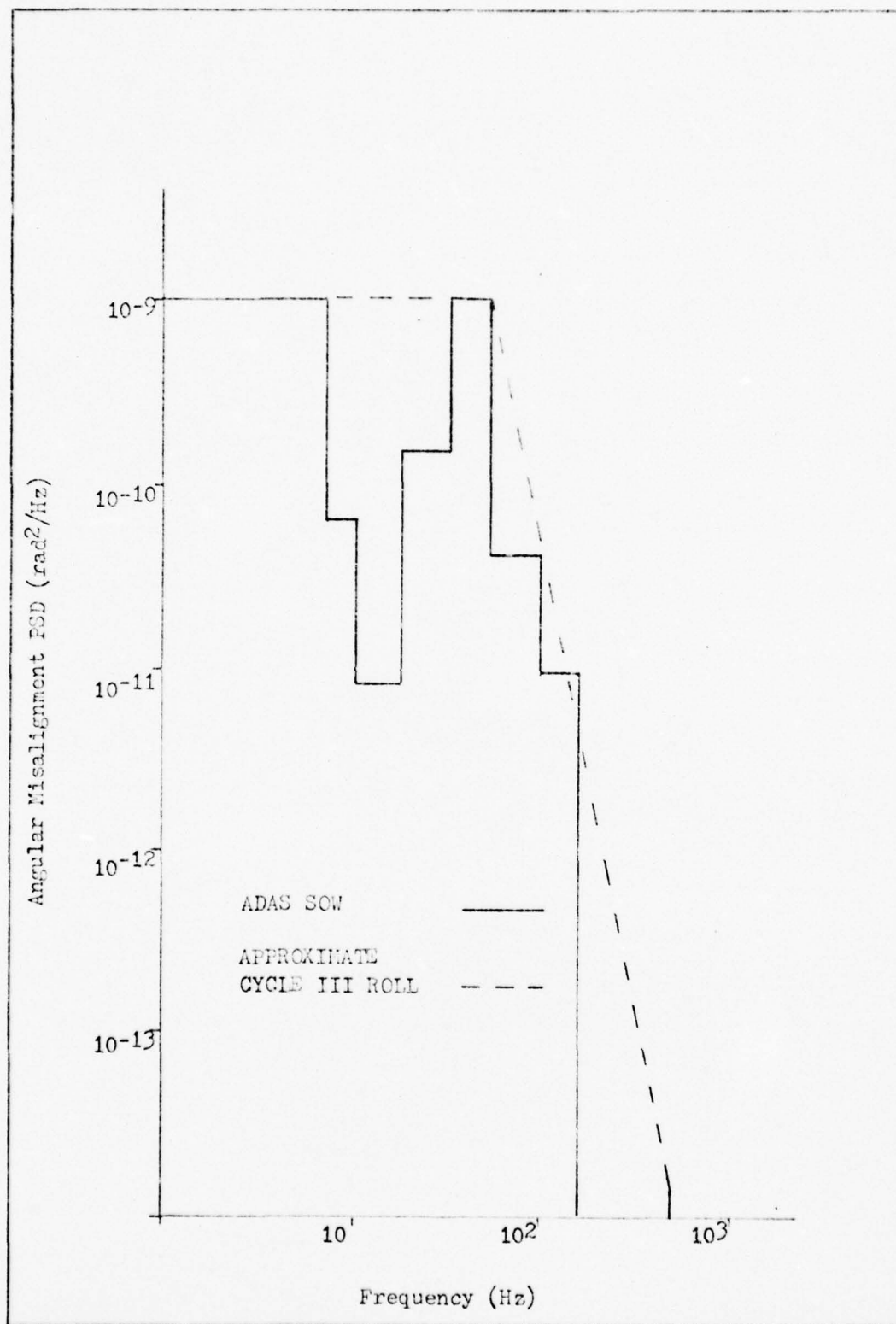


Fig. 3 . Comparison of ADAS SOW and CYCLE III ROLL PSD

and a decision was made to improve ADAS to meet this new input disturbance PSD.

General Problem Solution Approach

The reason the ADAS saturates in the presence of the high frequency disturbances is the torque limit of the mirror actuator motors. In this report it is proposed to accept the torque limit that exists and correct the problem through electronic control system modification. This is possible because the present translation error is very low and more error may be tolerated. The general approach to find a solution is as follows:

- 1.) Conduct an indepth analysis of the present ADAS.
- 2.) Quantitatively define the extent of the saturation problem.
- 3.) Mathematically simplify the present system for ease of analysis and design.
- 4.) Modify the control system.
- 5.) Examine results of above modification.

Finally, conclusions will be drawn from the above investigation and recommendations for further action will be made based on those conclusions.

Limits of Study

The limits of this study are as follows:

- 1.) Modification will deal only with the electronic control system, and no hardware changes were investigated.
- 2.) Frequency domain analysis will be limited to using the ADAS frequency domain simulation.

- 3.) All electronic non-linearities in the frequency domain simulation of ADAS are ignored.
- 4.) No attempt was made to examine the interactive effects of ADAS modification on the APT or the Auto Alignment System (AAS).

The non-linearities in ADAS are in the form of a current limit in the compensation networks and a torque limit to each mirror-actuator motor. Ignoring the limits will allow use of a completely linear representation of the control system. The RMS value of the signal in the compensation networks and to each motor will be computed during the simulation. In this way, violations of the limits and the resulting saturation of the control system will be identified.

II. Analysis of Present ADAS

General Description

The Airborne Dynamic Alignment System (ADAS) is a subsystem of the Airborne Laser Lab (ALL) and serves to maintain alignment between the Gas Dynamic Laser (GDL) and the entrance of the Automatic Pointing and Tracking device (APT). The ADAS is mounted to the APT. In this way there is no misalignment problems between the APT and ADAS. The two sources of beam vibration or "jitter" come from the GDL and the flexure of the ALL. Since the ADAS is not hard mounted to the GDL, the aircraft flexure is considered the larger beam misalignment source.

The ADAS included the following;

- A. translation sensor (TS)
- B. prealignment sensor (PAS)
- C. beam angle sensor (BAS)
- D. two beam steering mirrors (BSM)
- E. associated power sources and control electronics

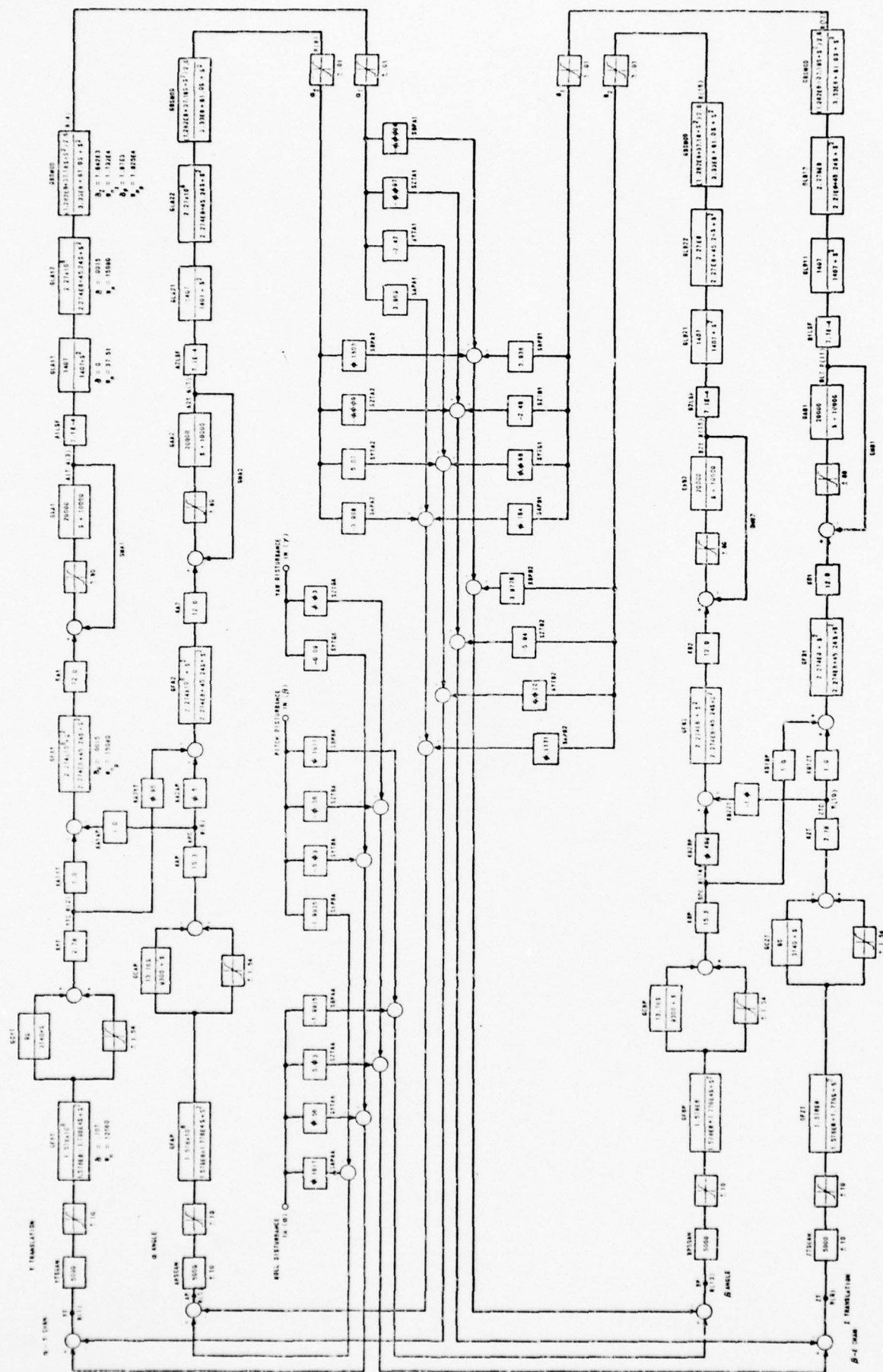
The PAS and TS each have their own active light source. (Ref. 4). This is to allow the use of the PAS and TS before the actual laser beam is generated. The BAS is used only during the operation of the GDL. It maintains a constant "sample" of the precise angular position of the beam. All three sensors, PAS, TS, and BAS are utilized to sense misalignments from a nominal position and feed this information to the electronic control system. The translation sensor measures translational misalignment in the ADAS optical train between the GDL and the translation sensor Fold Mirror (FM). The prealignment sensor measures angular alignment between the GDL and its fold mirror (PAS FM). The beam angle sensor gets its sample of the main beam from the High Power Grating (HPG) and senses the precise angle of the beam between the grating and the GDL.

The electronic control system uses this sensor information to command the movement of the two beam steering mirrors. The two beam steering mirrors are mounted to an optical bench which is in turn mounted to the floor of the ALL. The stop to stop angular displacement of each mirror is 10 microradians. Vibration isolation mounts are used on the bench and GDL to effectively reduce their vibrational coupling. The functional layout of the ADAS is shown in Fig. 4.

The Electronic Control System

The control system works in essentially two independent channels. These are the Y-ALPHA channel and the Z-BETA channel. Y and Z are the two translational errors and ALPHA and BETA are the two angular errors. Each of the two mirrors has two separate axes of rotation. Two separate mirrors are necessary because it is not physically possible to null out angular error without inducing translational error with only one mirror. (Ref. 3:2.4, and Appendix B). The block diagram of the control system is shown in Fig. 5. Each of the four loops is functionally the same. A representative single loop is shown in Fig. 6. Each loop basically consists of a compensation network, electronic decoupling, mirror-motor dynamics, optical cross coupling, and unity feedback.

The electronic cross coupling is necessary to decouple the physical (optical) cross coupling. Essentially, it is with this electronic decoupling networks that translational error is not induced while nulling a pure angular disturbance.



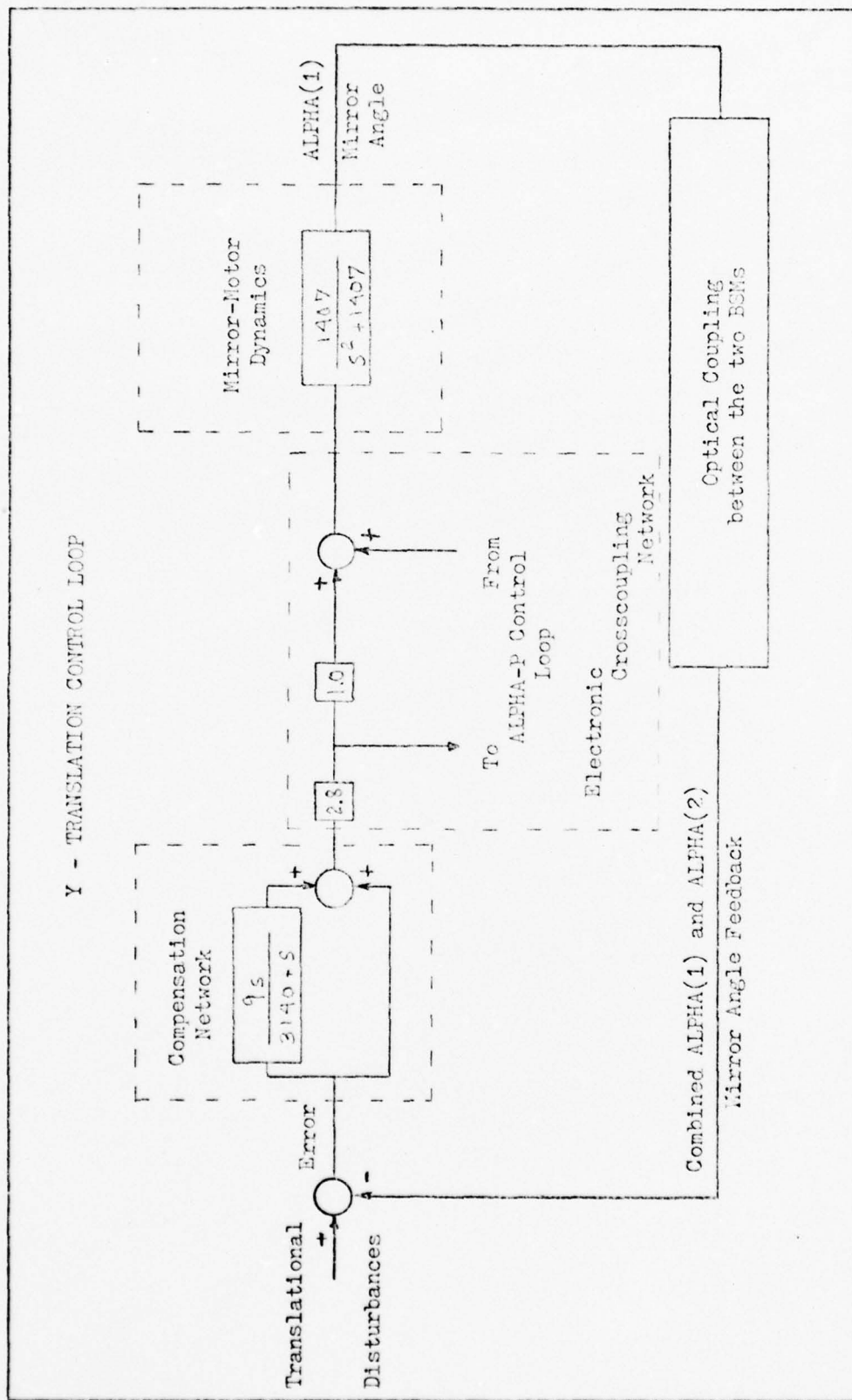


Fig. 6. Representative Single Loop in ADAS Block Diagram of Electronic Control System

Reduction of Control System

Reduction of the four loop control system to a two loop system is straightforward considering the sensitivity coefficients between the control loops (Fig. 5). Furthermore, this will reduce the difficulty in understanding and handling the control system.

Table I

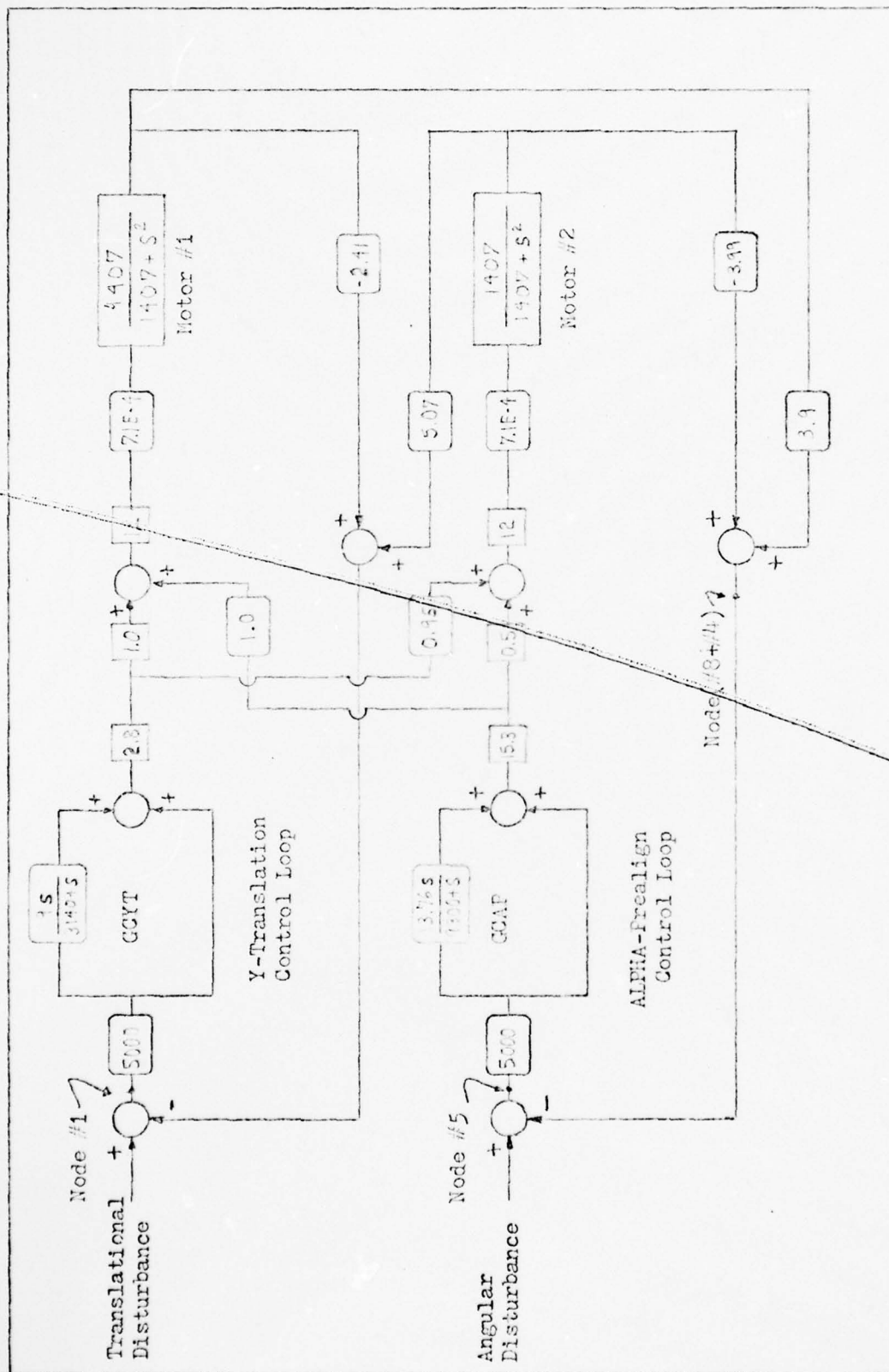
Comparison of Error Output Between 4 Loop and 2 Loop Control System

	<u>4 Loop System</u>	<u>2 Loop System</u>
Y-TRANS Error	4.164 inches	4.165 inches
ALPHA-P Error	1.707 radians	1.705 radians

In Table I, the results of the reduction are shown. This is the error output with the ADAS SOW input at the ALPHA-P disturbance point with no modification to the control system. The two loop system gives almost exactly what the four loop system gives. Therefore, the two loop system (Fig. 7) will be used in place of the four loop system. Essentially, the Y-TRANS — ALPHA-P loops are exactly the same as the Z-TRANS — BETA-P loops.

Need for Electronic Decoupling

The fact that there is optical coupling between the two beam steering mirrors necessitated electronic decoupling between the control loops. Each mirror has an ALPHA and a BETA axis of rotation.



They are defined so that ALPHA of mirror #1 couples with ALPHA of mirror #2 and the same for the BETA axis. The electronic decoupling network for the Y-TRANSLATION and the ALPHA-PREALIGN control loops is shown in Fig. 8. This cross-coupling is of the same form as that between the Z-TRANSLATION and BETA-PREALIGN control loops.

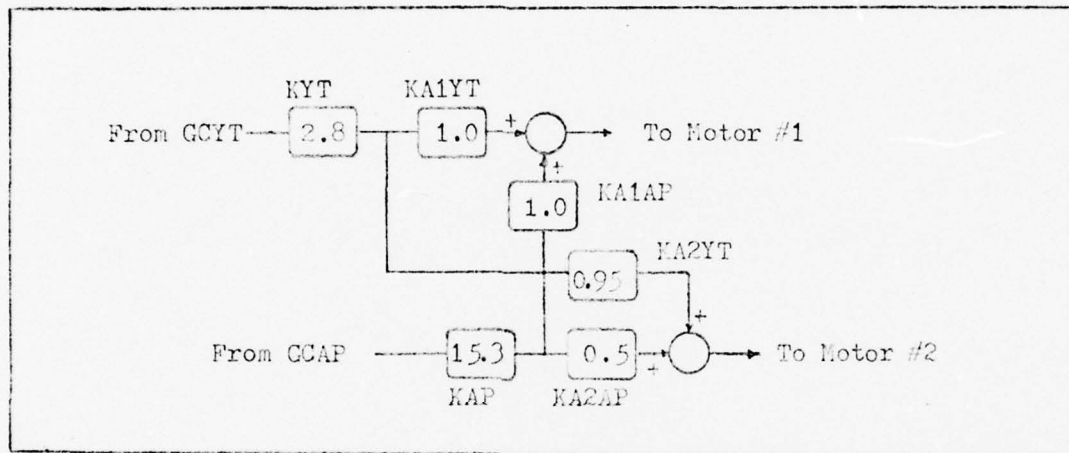


Fig. 8. ALPHA-P, Y- TRANS Electronic Crosscoupling Network

The Y-TRANS and ALPHA-P control loops are shown separated from the main block diagram in Fig. 9. In this figure, however, only the constant gains and sensitivities are included. The electronic cross-coupling sensitivities (KA1AP and KA2YT) are labeled A and B respectively. The high frequency blocks are also not included for further simplification. In this way the control loops are as they would be at a very low frequency ($s \rightarrow 0$) condition.

The equations for each error will be written and the values of A and B will be found such that a pure angular disturbance (A(DIS)) will

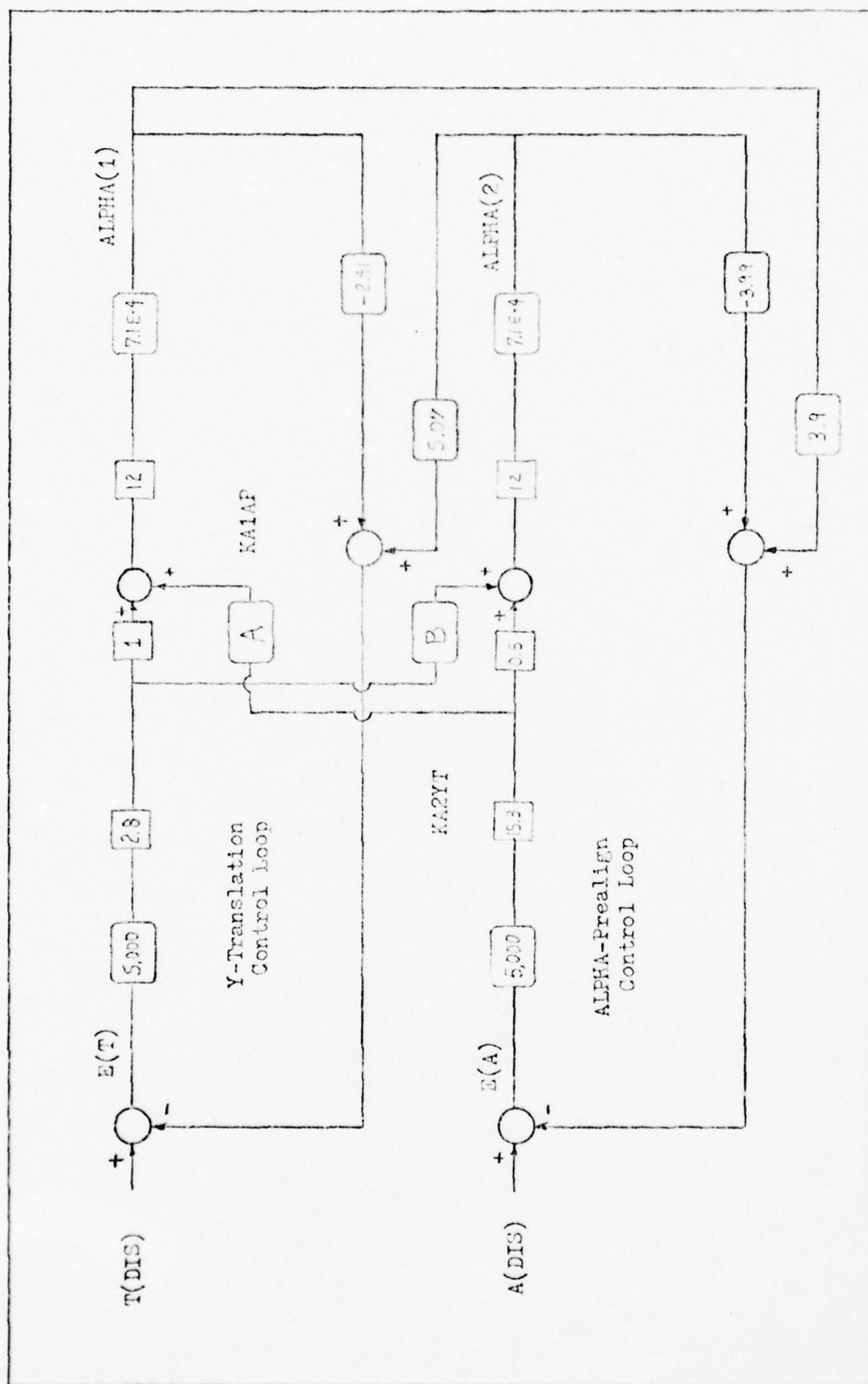


Fig. 9. D.C. Version of ADAS 2 Loop Control System

not induce a translational disturbance (T(DIS)). Equations describing the errors E(T) and E(A) are:

$$E(T) = T(DIS) + 2.41 \text{ ALPHA}(1) - 5.05 \text{ ALPHA}(2)$$

$$E(A) = A(DIS) + 3.998 \text{ ALPHA}(2) - 3.86 \text{ ALPHA}(1)$$

The equations describing ALPHA(1) and ALPHA(2) are:

$$\begin{aligned} \text{ALPHA}(1) = & (12) (7.1E-4) (2.78) (5000) (E(T)) \\ & + (B) (2.78) (5000) E(A) \end{aligned}$$

$$\begin{aligned} \text{ALPHA}(2) = & (12) (7.1E-4) (0.477) (15.3) (5000) (E(A)) \\ & + (B) (2.78) (5000) E(T) \end{aligned}$$

Substituting ALPHA(1) and ALPHA(2) into the E(T) equation:

$$\begin{aligned} E(T) = & T(DIS) + (2.41) (118.4) E(T) + A(651.8) E(A) \\ & - 5.05 (310.9) E(A) + B(118.4) E(T) \\ = & T(DIS) + (285.3) E(T) + A(1570.8) E(A) \\ & - B(598) E(T) - (1570.05) E(A) \\ = & T(DIS) + (285.3 - 598B) E(T) + (1570.8A \\ & - 1570.05) E(A) \end{aligned}$$

Now in order to make E(T) a function only of T(DIS) and not of E(A):

$$(1570.8A - 1570.05) \text{ MUST EQUAL } 0$$

Therefore:

$$A = (1570.05)/(1570.8) = 1.0$$

By the same process B is found to be:

$$B = 0.965$$

In the original block diagram (Fig. 5), $A = 1.0$ and $B = 0.95$, so the electronic cross-coupling (decoupling) does indeed decouple the angle and translation control loops at low frequencies.

Discussion of Error Limits

The error limits specified in the ADAS SOW are:

Table II

Error Limits In Angle And Translation

Signal	Limit
ALPHA-P, BETA-P	3.0 radians
Y-TRANS, Z-TRANS	2,500.0 inches

In the interest of keeping this report unclassified, the exact scale of the limits and closed loop response is not exact.

III. ADAS Frequency Domain Simulation

ADAS is modeled in the frequency domain through a general purpose program called FRQRSP. FRQRSP was developed at Oklahoma State University (Ref. 4) for the Air Force Weapons Laboratory. FRQRSP solves a system of simultaneous linear equations by the Gauss-Jordan elimination method over a specified frequency range. The program is capable of accepting input information in several modes including disturbance spectrum data such as the ADAS SOW and CYCLE III PSD.

ADAS was modeled by a set of 16 equations, each representing a particular node in the control system. The 16 equations are written in the matrix form:

$$\begin{bmatrix} A \end{bmatrix} \begin{bmatrix} R \end{bmatrix} = \begin{bmatrix} B \end{bmatrix}$$

where

$$\begin{bmatrix} R \end{bmatrix} \text{ is the vector of the unknown states}$$
$$\begin{bmatrix} B \end{bmatrix} \text{ is the vector of inputs to the system}$$
$$\begin{bmatrix} A \end{bmatrix} \text{ is the matrix that describes the system}$$

As an example of the way in which the system is modeled, examine the equation for Y-Translation error. From Fig. 7:

$$\begin{aligned} \text{Y-TRANS Error} &= \text{Y-TRANS Disturbance} - (-2.41) \text{ ALPHA}(1) \\ &\quad - (5.07) \text{ ALPHA}(2) \end{aligned}$$

where:

ALPHA(1) is the Angle of Mirror #1

ALPHA(2) is the Angle of Mirror #2

Rearranging the equation:

$$\text{Y-TRANS Error} + (-2.41) \text{ ALPHA}(1) + (5.07) \text{ ALPHA}(2) = \text{Y-TRANS Disturbance}$$

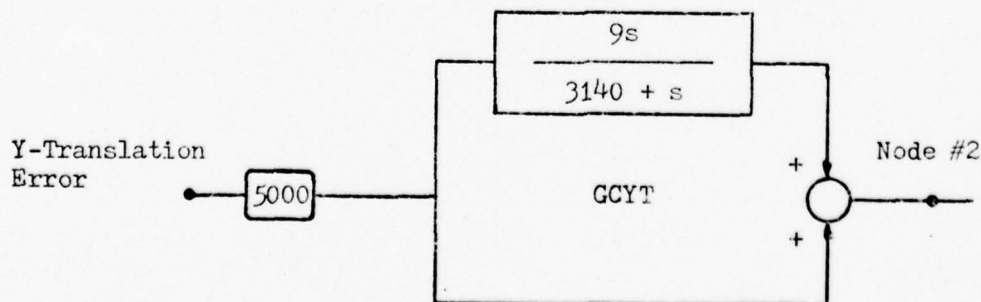
In matrix form:

$$\begin{bmatrix} 1 & -2.41 & 5.07 \end{bmatrix}_{1 \times 3} \begin{bmatrix} \text{Y-TRANS Error} \\ \text{ALPHA}(1) \\ \text{ALPHA}(2) \end{bmatrix}_{3 \times 1} = \begin{bmatrix} \text{Y-TRANS Disturbance} \end{bmatrix}_{1 \times 1}$$

Thus the Y-TRANS Error equation is in the form:

$$\begin{bmatrix} A \end{bmatrix} \begin{bmatrix} R \end{bmatrix} = \begin{bmatrix} B \end{bmatrix}$$

As an example in which the frequency sensitive portions of the control system are modeled, examine the compensation network in the Y-Translation control loop:



(This segment taken from Fig. 7)

Let the signal at Node #2 equal NODE2SIG and let the Y-Translation error signal equal YTERSIG. Then:

$$\begin{aligned}
 \text{NODE2SIG} &= (\text{YTERSIG}) (5000) \left[\frac{9s}{3140 + s} + 1.0 \right] \\
 &= \text{YTERSIG} \left[\frac{45,000s}{3140 + s} + 5000 \right] \\
 &= \text{YTERSIG} \left[\frac{1.57E + 7 + (5.0E + 4)s}{3140 + s} \right]
 \end{aligned}$$

Rearranging this equation:

$$\left[\frac{1.57E + 7 + (5.0E + 4)s}{3140 + s} \right] [\text{YTERSIG}] = [\text{NODE2SIG}]$$

which is in the correct form of:

$$\begin{bmatrix} A \end{bmatrix} \begin{bmatrix} R \end{bmatrix} = \begin{bmatrix} B \end{bmatrix}$$

This procedure is followed for the other 14 nodes and then all the equations are combined. The result is a system of equations in the form:

$$\begin{bmatrix} A \end{bmatrix}_{16 \times 16} \begin{bmatrix} R \end{bmatrix}_{16 \times 1} = \begin{bmatrix} B \end{bmatrix}_{16 \times 1}$$

Since the frequency response of the system is desired, replace s by jw . Then evaluate $[A]$ at a particular frequency w and the result is a complex $[A]$. The complex $[A]$ matrix is then inverted and multiplied with $[B]$ to result in a complex $[R]$. The

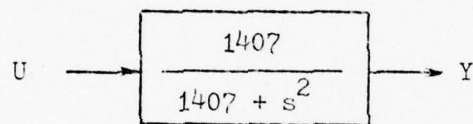
procedure is then repeated for a certain range of frequencies. The overall result is then the complete system response over that certain range of frequencies.

The computer simulation model of ADAS is limited in that it is not possible to model the nonlinearities such as motor torque limits and current limits. It is also not possible to program multiple inputs. However, once the system of equations is solved, output may come from any node.

IV. ADAS State Space Model

ADAS is modeled in state space form to satisfy the need for more precise stability information. This section will develop the state equations, and the shaping filters designed to simulate the input disturbance PSDs. The states of the control system are labeled in Fig. 10. In this particular figure, only the Y-TRANS and ALPHA-P control loops are shown. The figure would be exactly the same for the Z-TRANS BETA-P control loops.

The block diagram for each motor is:



The state equations for each motor is:

$$\dot{\underline{X}} = \begin{bmatrix} 0 & 1 \\ -1407 & 0 \end{bmatrix} \underline{X} + \begin{bmatrix} 0 \\ 1407 \end{bmatrix} U$$

where:

$$\underline{X} = \begin{bmatrix} x_1 \\ x_2 \end{bmatrix}, \text{ for motor \#1}$$

$$= \begin{bmatrix} x_3 \\ x_4 \end{bmatrix}, \text{ for motor \#2}$$

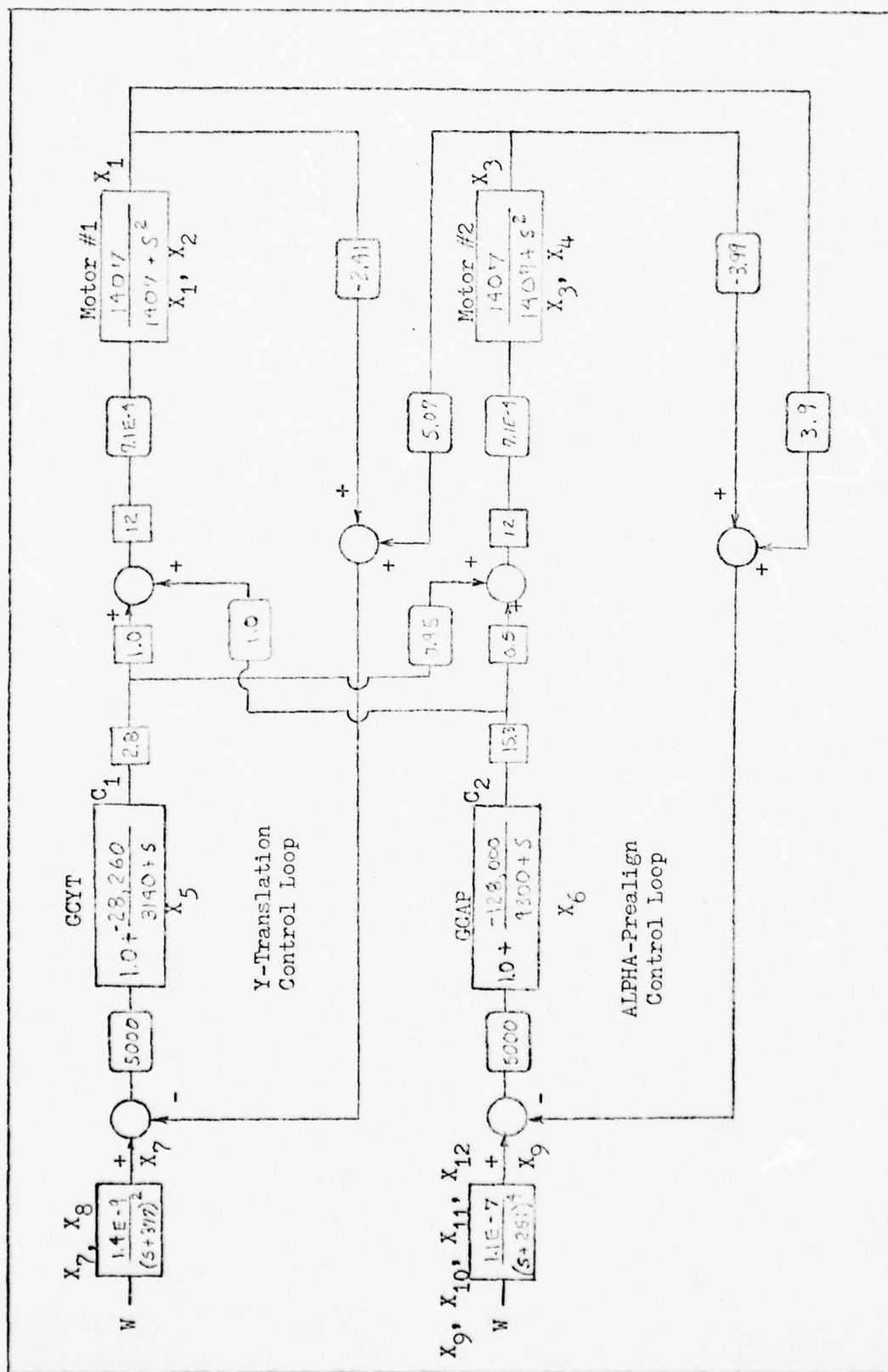
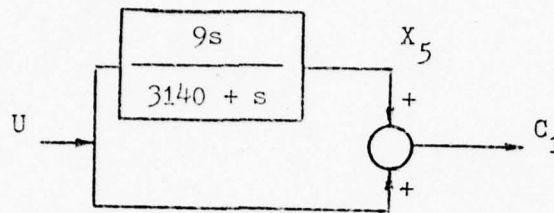
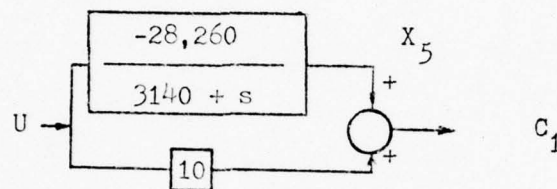


Fig. 10. Location of States in ADAS Two Loop Control System

The actual block diagram for the Y-TRANS (GCYT) compensation is:



This block diagram may be written as:



The X_5 state equation is:

$$\dot{X}_5 = \begin{bmatrix} -3140 \end{bmatrix} X_5 + \begin{bmatrix} -28,260 \end{bmatrix} U$$

and

$$C_1 = \begin{bmatrix} 1 \end{bmatrix} X_5 + \begin{bmatrix} 10 \end{bmatrix} U$$

The state representation of the ALPHA-P compensation is the same form as the Y-TRANS representation. It contains state X_6 and the equation for X_6 is:

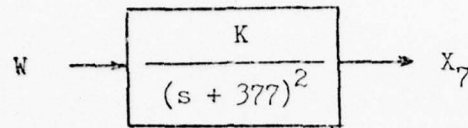
$$\dot{X}_6 = \begin{bmatrix} -9,300 \end{bmatrix} X_6 + \begin{bmatrix} -127,953 \end{bmatrix} U$$

and

$$C_2 = \begin{bmatrix} 1 \end{bmatrix} X_6 + \begin{bmatrix} 14.76 \end{bmatrix} U$$

The input disturbances must be approximated by white noise passed through a shaping filter. The shaping filter for the ADAS SOW PSD

for the Y-TRANS control loop is:



where

W = white noise, zero mean, Gaussian statistics

K = $0.141E-10$

$$\frac{X_7}{W} = \frac{K}{s^2 + Bs + C}$$

B = $7.54E+2$

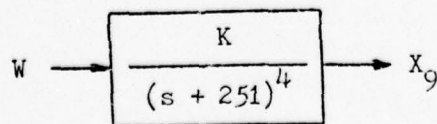
C = $1.42E+2$

The state equations are:

$$\dot{X} = \begin{bmatrix} 0 & 1 \\ -C & -B \end{bmatrix} X + \begin{bmatrix} 0 \\ K \end{bmatrix} W$$

$$X = \begin{bmatrix} X_7 \\ X_6 \end{bmatrix}$$

The shaping filter for the ADAS SOW PSD for the ALPHA-P control loop disturbance is:



where

W = white noise, zero mean, Gaussian statistics

K = $0.110E-8$

$$\frac{X_9}{W} = \frac{K}{s^4 + Bs^3 + Cs^2 + Ds + E}$$

B = $1.0E+4$

C = $3.78E+5$

D = $6.34E+7$

E = $3.97E+9$

The state equations are:

$$\dot{X} = \begin{bmatrix} 0 & 1 & 0 & 0 \\ 0 & 0 & 1 & 0 \\ 0 & 0 & 0 & 1 \\ -E & -D & -C & -B \end{bmatrix} X + \begin{bmatrix} 0 \\ 0 \\ 0 \\ K \end{bmatrix} W$$

where

$$X = \begin{bmatrix} x_9 \\ x_{10} \\ x_{11} \\ x_{12} \end{bmatrix}$$

The origin of these shaping filters is better understood by plotting the magnitude versus frequency curves for the ADAS SOW and approximate disturbances. These plots for the Y-TRANS and ALPHA-P control loops are shown in Fig.'s 27 and 28 respectively.

The combined state space $[A]$ matrix is shown in Fig. 24 in Appendix C. The eigenvalues of this $[A]$ matrix correspond to the roots of the characteristic equation of the closed loop transfer function. The eigenvalues for this control system are shown in Table III.

Table III

Eigenvalues of ADAS Control System

(2 Loop)

$$-4184 \pm 844i$$

$$-1497 \pm 1086i$$

$$-897$$

$$-179$$

$$-388$$

$$-365$$

$$-202 \pm 24i$$

$$-297 \pm 83i$$

The fact that all eigenvalues are negative means the original ADAS is stable. (Ref. 5:576). A listing of program EIGEN that solves for the eigenvalues and eigenvectors of $[A]$ is in Appendix C. Consult Ref. 7 for explanation of subroutine RGEIG used in computer program EIGEN.

V. Numerical Extent of the Problem

The baseline performance for ADAS using the Statement Of Work (SOW) disturbance is given in Table IV. These baseline figures will be used in comparison to the worst case disturbance and also the results of any compensation.

As noted in the introduction, the worst case disturbance is called the CYCLE III disturbance. Since the angular errors are of a much greater concern than the translational disturbances, the CYCLE III

Table IV

Baseline Closed Loop Response
(input is ADAS SOW at Node #5)

Signal	Output (RMS)
A1 Torque Required	1.29 in-lb
A2 Torque Required	0.62 in-lb
Y-TRANS Error	4.16 in
ALPHA-P Error	1.71 rad

ROLL BASE MOTION PSD will be used. Due to the physical layout of the ADAS in the ALL, the roll base motion directly affects the angular control loops. Similarly, pitch base motion affects the translational control loops. It is for this reason that for a single input the worst case system output occurs when CYCLE III ROLL BASE MOTION PSD is input at the ALPHA-P disturbance point. The results of this worst case are listed in Table V.

Table V

Worst Case Closed Loop Response
(input is CYCLE III ROLL PSD at Node #5)

Signal	Output(RMS)
A1 Torque Required	4.73 in-lb
A2 Torque Required	2.74 in-lb
Y-TRANS Error	5.30 in
ALPHA-P Error	3.42 rad

Observe that for both the baseline and the worst case input, the torque-required-ratio of motors A1 and A2 is two to one (2:1). Under the CYCLE III Roll input this two for one torque demand exceeds the torque available for motor A1. This condition occurs due to the high frequency, large amplitude disturbances in the CYCLE III ROLL PSD.

Of equally great concern is the increase in ALPHA-P error over the baseline figure. The ALPHA-P error caused by the CYCLE III ROLL PSD (worst case is well over the specified limit, see Table II). Since these figures are derived from a linear simulation of ADAS, the actual system would have an even higher ALPHA-P error. This is because as the torque limits are exceeded the control system would saturate and the motors would no longer respond to correct for errors.

Documentation is also necessary in the form of ALPHA-P open loop response. The modification will directly affect the open loop response of the angular control loop. Therefore, it is important to know the response of the original system. This data is shown in Table VI.

Table VI

Open Loop Data for ALPHA-P Control Loop

	ALPHA-P
Gain Margin	+3.4 dB @ 920 Hz
Phase Margin	+22 degrees @ 725 Hz
0 dB Gain Crossover	725 Hz

The magnitude and phase angle plot is shown in Fig. 33. Since the open loop stability response is independent of the magnitude of disturbance input, there is no need for a baseline/worst case comparison.

The ALPHA-P open loop transfer function is defined as:

$$G(s) = \frac{\text{angular position of laser beam}}{\text{error in angular alignment of the laser beam}}$$

The error in angular alignment is measured at Node #5 in Fig. 7 and the angular position of the beam is Node (#8 + #4). The open loop response is measured this way to ensure unity feedback between Node (#8 + #4) and the disturbance/error summing point.

VI. Control System Modification and Predictions

Addition of Low Pass Filter

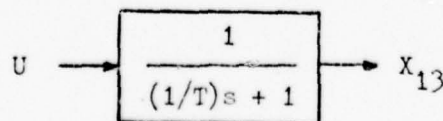
The control system is modified by placing a low pass filter in the electronic cross-coupling. In the frequency domain, this filter replaced the block labeled KA1AP (see Fig. 8) in the branch coming from the ALPHA-P control loop to the Y-TRANS control loop (Fig. 11). The filter is named GLOWPS, and is of the form:

$$\text{GLOWPS} = \frac{1.0}{(1/T)s + 1.0}$$

GLOWPS is essentially a filter with T as the cutoff frequency. A first order filter was chosen because of simplicity and the desire not to introduce more poles into the system than necessary.

The cutoff frequency T was varied between 0 and 700 Hz. Closed loop response data was calculated at each frequency to compare errors and required torques. Open loop data for the ALPHA-P loop will be gathered for stability considerations.

In the state space model the complimentary filter will add another state to the system. The state matrix $[A]$ will be of dimension 13X13 for the modified control system. Again the filter will replace the block labeled KA1AP. The state space representation of the filter is:



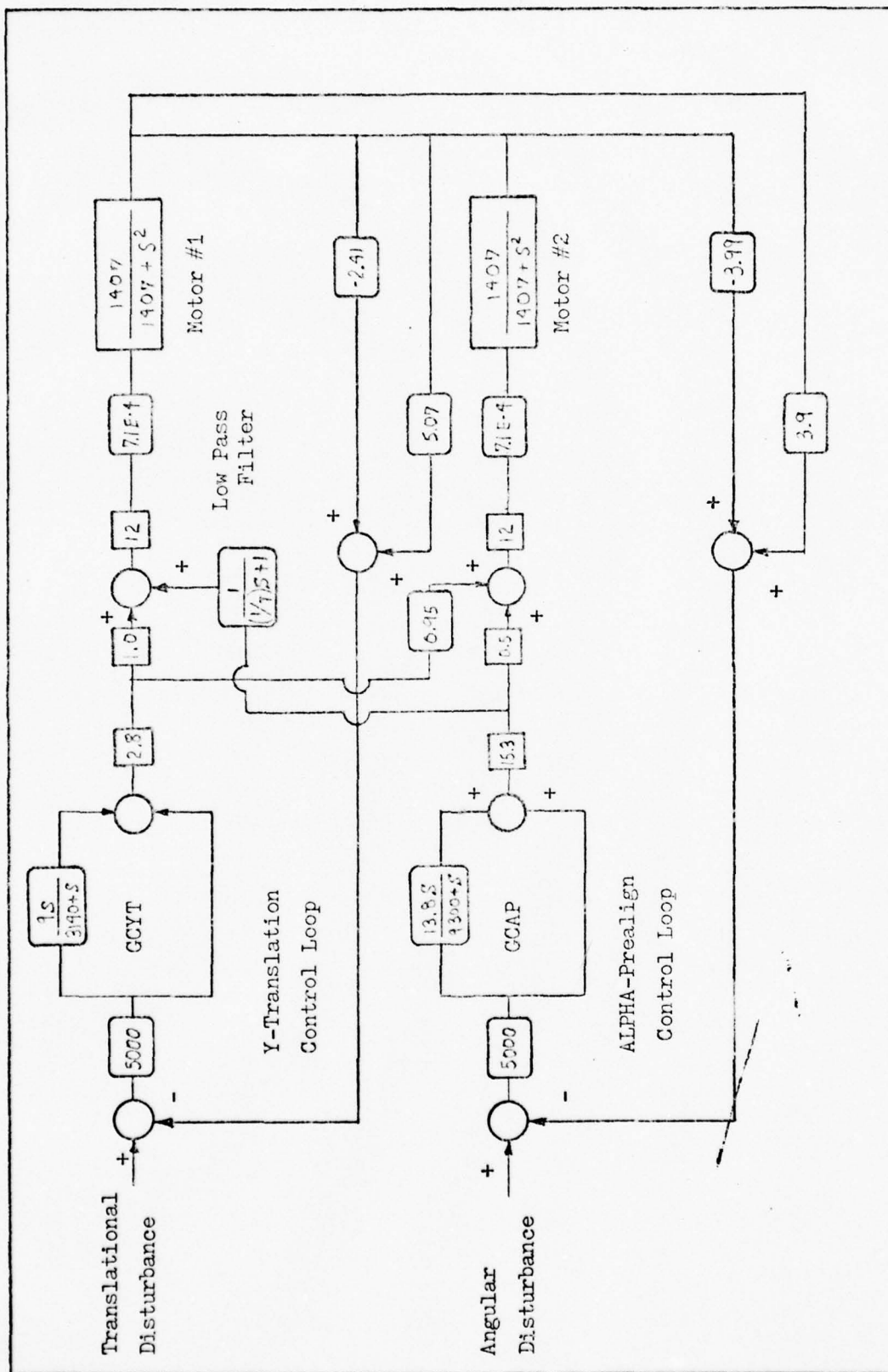


Fig.11. Modified ADAS Control System (Two Loop)

where

$$\dot{X}_{13} = [-T] \dot{X}_{13} + [T] U$$

substituting expression for U,

$$\begin{aligned} \dot{X}_{13} = & -(T) \dot{X}_{13} - (T) \left[-4.4E+6 \dot{X}_1 \right. \\ & \left. + 4.51E+6 \dot{X}_3 + (15.3) \dot{X}_6 + 1.13E+6 \dot{X}_9 \right] \end{aligned}$$

The addition of state X_{13} also changes the X_2 equation. The form of X_2 equation for the modified control system is:

$$\begin{aligned} \dot{X}_2 = & -1407 \dot{X}_1 + 1407 U \\ = & -1407 \dot{X}_1 \\ & + (1407) \left[(12) (7.1E-4) \right] \left[(2.8C_1) + 12 \dot{X}_{13} \right] \\ = & 4.03E+6 \dot{X}_1 - 8.5E+6 \dot{X}_3 + (33.6) \dot{X}_5 + 1.68E+6 \dot{X}_7 \\ & + 12.0 \dot{X}_{13} \end{aligned}$$

The full state matrix $[A]$ for the modified control system is Fig. 22 in Appendix C.

The function of this filter is to pass the low frequency content of the signal crossing from the ALPHA-P control loop to the Y-TRANS control loop and attenuate the higher frequency portion. Thus, the intent of the filter is to cut down on the torque requirement command of Motor #1. The big difference between the ADAS SOW and the CYCLE III roll disturbance is the large magnitude, high frequency error in CYCLE III roll. The filter will effectively reduce the CYCLE III

torque required signal to something similar to the ADAS SOW for Motor #1.

Reducing the Motor #1 torque will destroy the 2:1 mirror rotation for a pure angular error. Therefore, it is expected that translation error will increase with the addition of the filter. Since it is possible to correct for angular error with one to one movement of the mirrors, the angular error is not expected to increase. However, with the physical and electrical cross-coupling present, the direct effect on the angular error is not obvious.

VII. Results

The frequency domain closed loop response results with the complimentary filter in ADAS is shown in Table VII. The cutoff frequency is varied from 32 Hz to 700 Hz and the input is CYCLE III ROLL PSD at the ALPHA-P disturbance point.

Table VII

Comparison of Complimentary Filter Cutoff Frequencies
(Output in RMS; 1-SIGMA)

<u>Cutoff Frequency</u> (Hz)	<u>A1 Torque Required</u> (in-lb)	<u>A2 Torque Required</u> (in-lb)	<u>ALPHA-P Error</u> (rad)	<u>Y-TRANS Error</u> (rad)
32	1.90	2.27	1.75	6.20
56	1.71	2.26	1.90	6.42
64	1.65	2.25	1.95	6.49
111	1.25	2.22	2.33	6.87
143	1.00	2.20	2.64	7.09
150	0.96	2.19	2.71	7.13
190	0.88	2.18	3.14	7.34
200	0.92	2.18	3.25	7.39
350	2.93	2.49	4.90	7.56
700	14.80	8.49	11.30	8.90

This frequency domain closed loop data versus cutoff frequency is graphed in Fig.'s 12, 13, 14, and 15. On each of the four graphs the original system value is plotted as a dotted line for comparison. From the plot of Y-TRANS versus cutoff frequency, it is significant that for every frequency the modified system yields a higher value of error than the original system. This is as predicted. It was not predicted that the Y-TRANS error would increase with increasing cutoff frequency. This result did not seem likely due to the modification involved. As the cutoff frequency gets larger in a low pass filter, one would expect closer agreement with the original system.

This phenomena may also be observed in the ALPHA-P error graph. The low cutoff frequencies give the desired reduction in error (from the original system), but high cutoff frequencies give the reverse effect. From these two plots, one may see that the lowest cutoff frequency yields the least error. In fact, 0 Hz cutoff (no ALPHA-P \rightarrow Y-TRANS electronic coupling) would appear to be the best. Completely eliminating the ALPHA-P \rightarrow Y-TRANS electronic cross-coupling was not in the original plan, but the results are shown in Table VIII.

Table VIII

Closed Loop Response With No ALPHA-P \rightarrow Y-TRANS Electronic Cross-coupling

<u>A1 Torque Required</u>	<u>A2 Torque Required</u>	<u>ALPHA-P Error</u>	<u>Y-TRANS Error</u>
2.12 in-lb	2.28 in-lb	1.65 rad	5.86 in

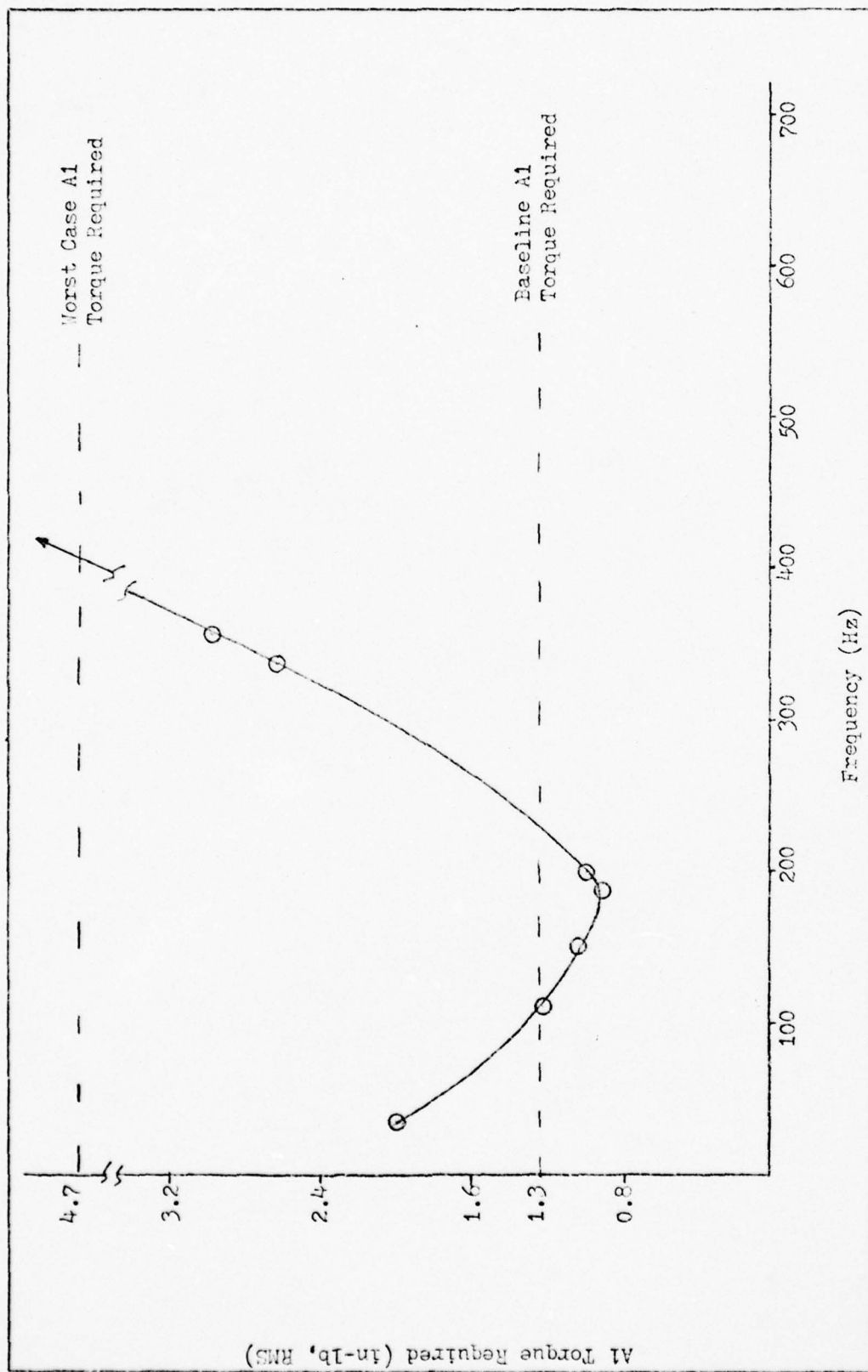


Fig. 12. AI Torque Required vs Cutoff Frequency

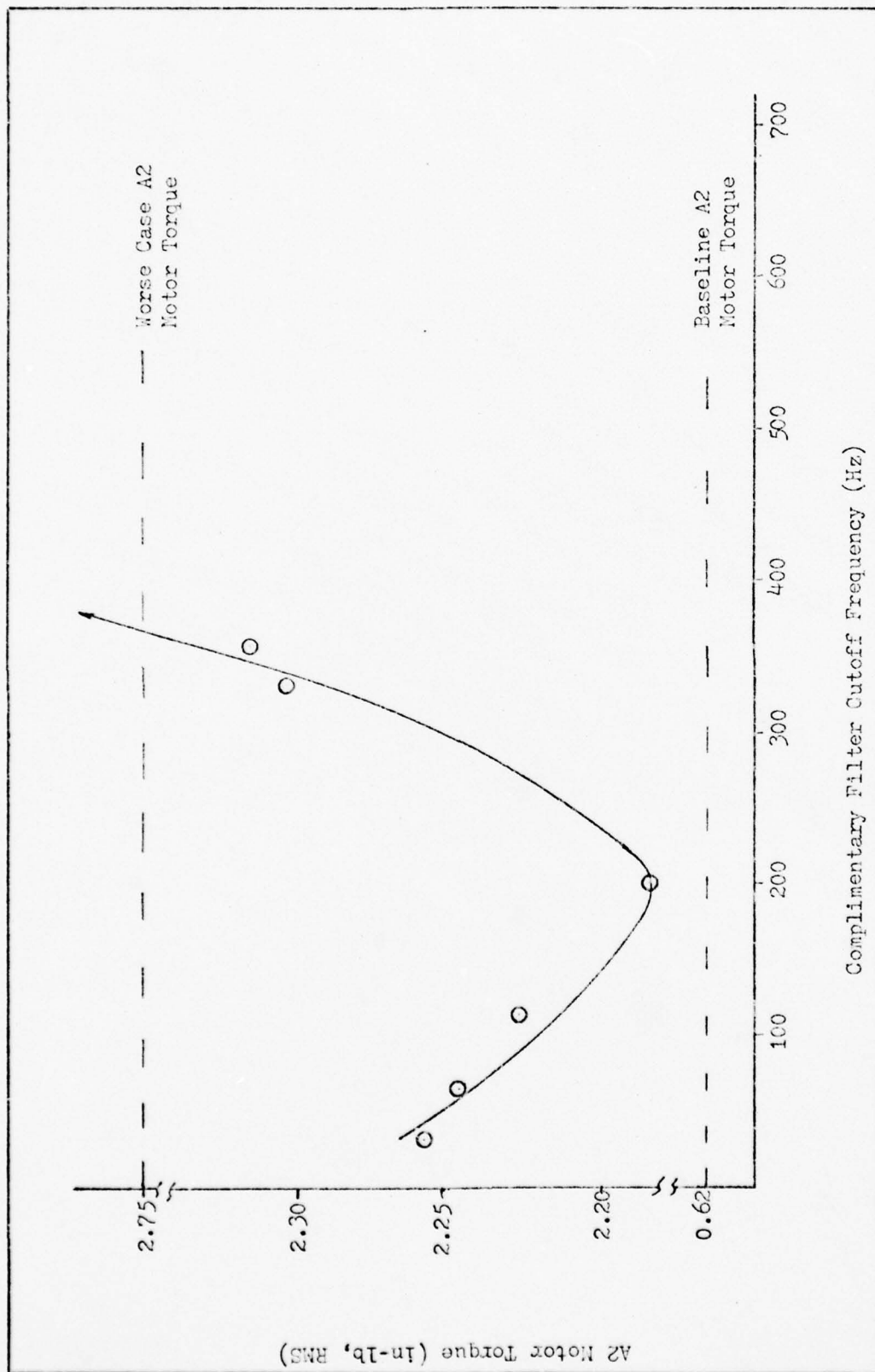


Fig.13. A2 Motor Torque Required vs Cutoff Frequency

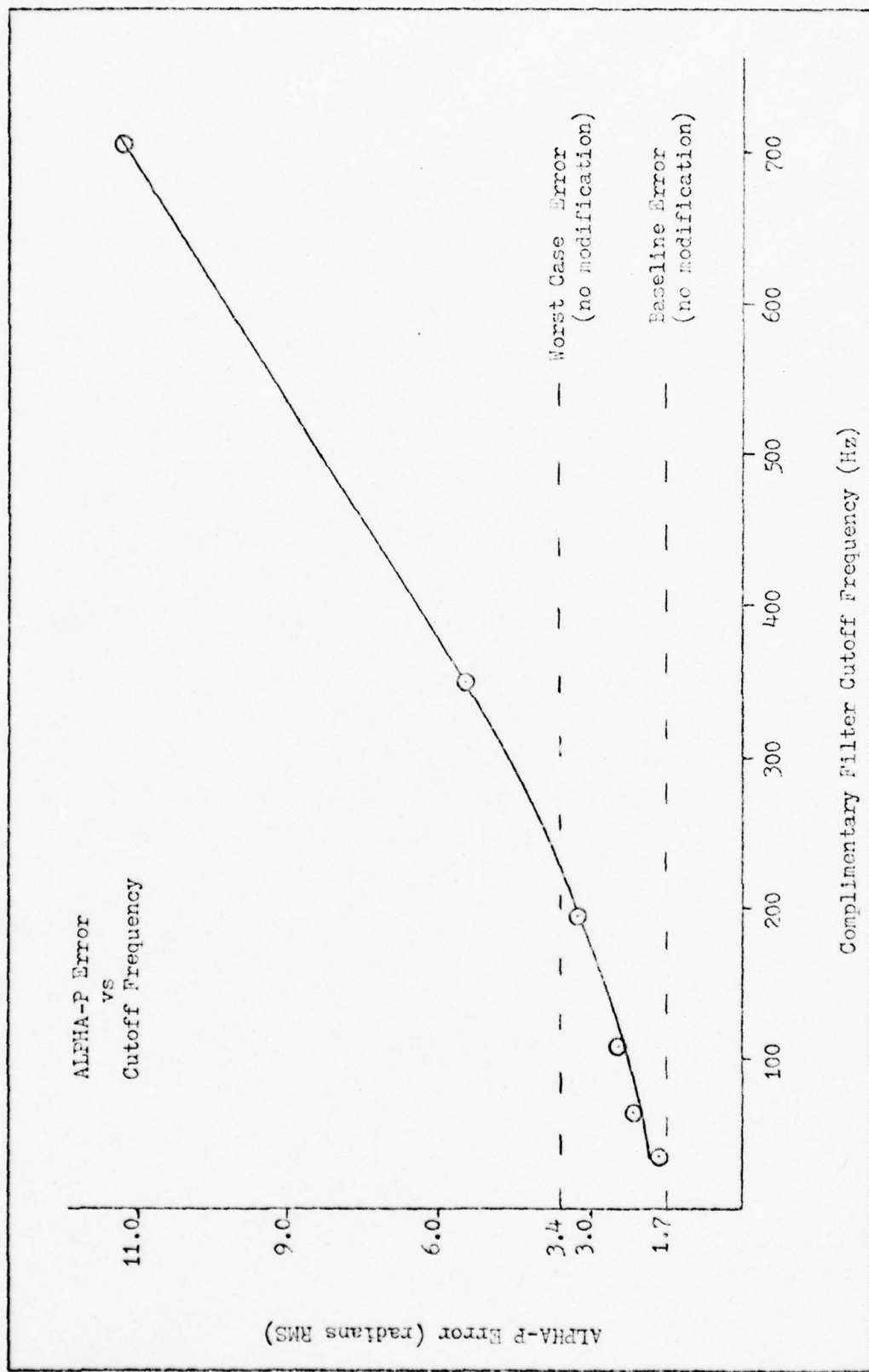


Fig.14 . ALPHA-P Error Signal vs Cutoff Frequency

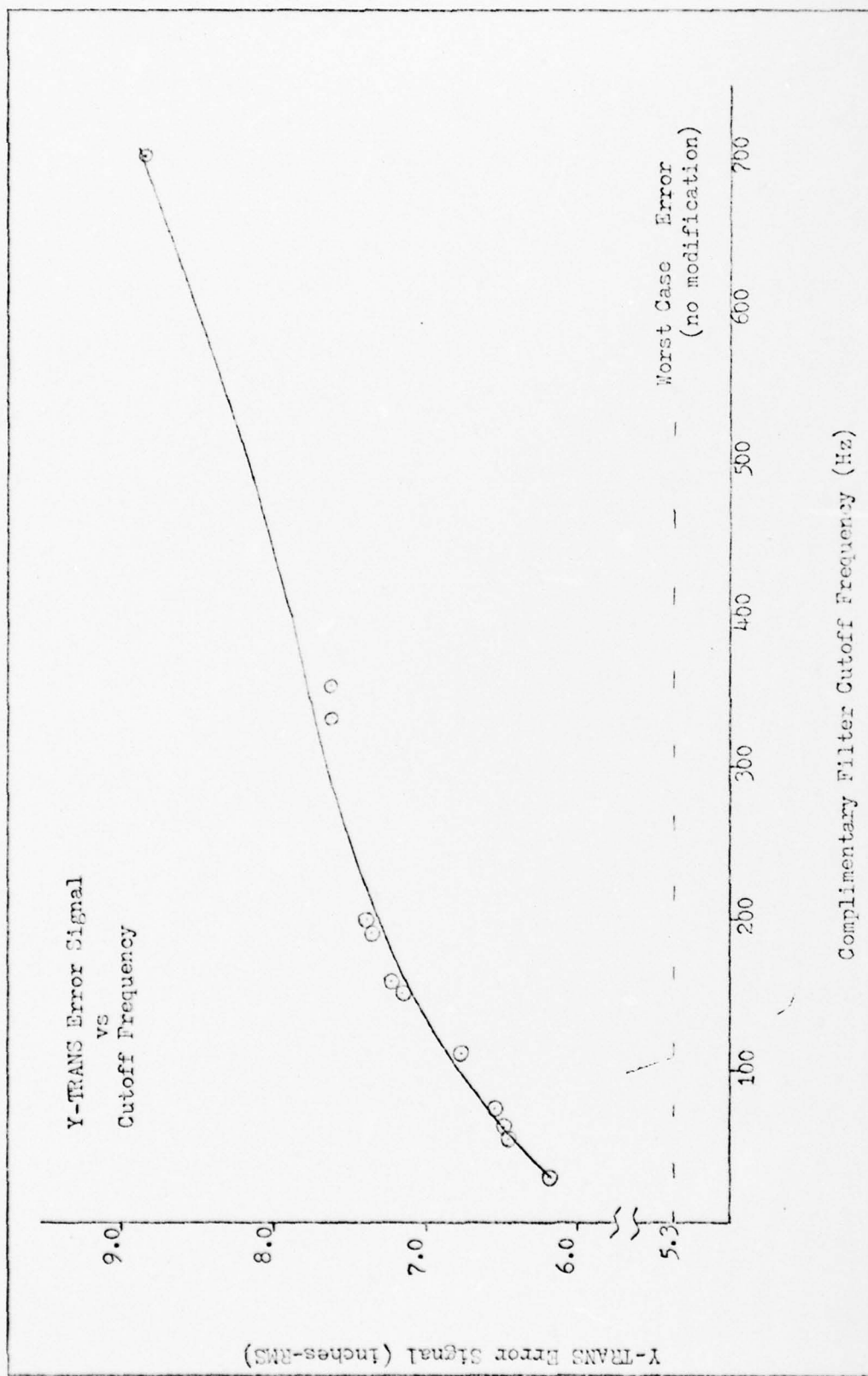


Fig.15. Y-TRANS Error Signal vs Cutoff Frequency

The A1 and A2 motor torque plots each yield a minimum at about 200 Hz. The A1 torque was considerably reduced as predicted. It was not expected that the A1 motor torque requirement would fall below that of the A2 motor.

The ALPHA-P open loop results are shown in Table IX on the next page. This table shows the increase in frequency response stability parameters from the original system to the system with no ALPHA-P \rightarrow Y-TRANS electronic cross-coupling. This result reinforces the data from the ALPHA-P and Y-TRANS error plots. The 190 \rightarrow 200 Hz cutoff, which was the minimum region for the torque required curves yields an unstable open loop phase margin. ALPHA-P open loop error rejection curves for various cutoff frequencies shown in Appendix C.

The state space analysis results in a set of eigenvalues and associated eigenvectors. The system is considered stable if all the eigenvalues are negative. The results of the eigenvalue analysis are as follows:

- 1.) The 0 Hz cutoff frequency (no ALPHA-P \rightarrow Y-TRANS electronic coupling) produces a positive eigenvalue.
- 2.) It is not until the cutoff frequency is greater than 725 Hz that all eigenvalues become negative.
- 3.) The system does not appear to be well damped (Damping Ratio Δ 0.707) until the cutoff frequency is moved past 5,000 Hz.
- 4.) At approximately 16,000 Hz cutoff frequency, the modified system eigenvalues are within 15% of the original system eigenvalues.

The exact numerical results are presented in Appendix C, Table XI.

As a result of the above eigenvalue information more frequency domain information was needed. This time the cutoff frequency was

Table IX

Comparison of ALPHA-P Open Loop Characteristics
with Various Filter Cutoff Frequencies

Cutoff Frequency (Hz)	0 dB Gain Crossover (Hz)	Phase Margin (degrees)	Gain Margin (dB)
0	397	+45	+12 @ 918 Hz
32	397	+43	+9 @ 775 Hz
56	380	+40	+9 @ 775 Hz
64	400	+40	+9 @ 775 Hz
111	140	+150	+7.5 @ 725 Hz
150	460	-380	*
200	140	-351	*
330	550	+5	+2.1 @ 600 Hz
350	550	+5	+1.9 @ 600 Hz
700	652	0	+2.5 @ 623 Hz
Worst Case	725	+22	+3.4 @ 920 Hz

* Phase angle never equals -180 degrees below 10,000 Hz

varied from 800 to 16,000 Hz. The results are shown in Table X. More information concerning the erratic nature of the open loop response is shown in Fig.'s 29 - 32.

Table X
ADAS Two Loop Control System Response with Various Cutoff Frequencies

Cutoff Freq. (Hz)	Y-TRANS Error (inches)	ALPHA-P Error (radians)	A1 Motor Error (in-lb)	A2 Motor Torque (in-lb)	ALPHA-P Phase Margin (degrees)	ALPHA-P Gain Margin (dB)
800	75.0	11.0	16.0	8.8	-1 @ 650 Hz	+0.3 @ 650 Hz
1,100	31.0	5.8	8.1	4.1	+0 @ 675 Hz	0 @ 675 Hz
1,600	18.0	4.6	6.3	3.1	+0 @ 700 Hz	0 @ 700 Hz
4,000	8.1	3.8	5.2	2.5	+8 @ 775 Hz	+4 @ 880 Hz
8,000	6.1	3.6	4.9	2.4	+14 @ 775 Hz	+3 @ 880 Hz
12,000	5.7	3.5	4.9	2.4	+14 @ 775 Hz	+3 @ 880 Hz
16,000	5.6	3.5	4.8	2.4	+14 @ 775 Hz	+3 @ 880 Hz
Worst Case	5.3	3.4	4.7	2.75	+22 @ 725 Hz	+3 @ 918 Hz

VIII. Conclusions

Three types of basic analysis efforts were accomplished to analyze the performance of the proposed low pass filter compensator:

- 1.) Open loop frequency domain analysis
- 2.) Closed loop frequency domain analysis
- 3.) State space eigenvalue analysis

The conclusions of each approach are discussed separately and then the summary of the overall conclusions is presented.

Open Loop Frequency Domain Analysis

The ALPHA-P open loop transfer function is defined as follows:

$$G(s) = \frac{\text{angular position of laser beam}}{\text{error in angular alignment of laser beam}}$$

This is shown more clearly in Fig. 7. The error in angular alignment is Node #5 and the angular position of the beam Nodes (#8 + #4). The ALPHA-P open loop transfer function contains the ALPHA-P compensation and the dynamics from mirror-motors #1 and #2. The transfer function is defined this way to include the optical coupling between the two beam steering mirrors (see Appendix B) and the electronic decoupling from ALPHA-P to Y-TRANS loop. Since the open loop response is independent of input the modified system is compared to the original system independent of input angular disturbance. The open loop results of the original system are shown in Table VI and Fig. 33. This is the response when the block labeled KA1AP in Fig. 8 contain a constant gain equal to 1.0.

To implement the low pass filter, KA1AP was reduced with $\frac{1.0}{(1/T)s + 1}$,

where T is the cutoff frequency. The cutoff frequency is varied from 0 to 16,000 Hz and the results are shown in Table IV, Table X and Fig.'s 29 - 32.

The conclusion is that the modified system improved the ALPHA-P open loop stability with cutoff frequencies below 100 Hz. With cutoff frequency above 100 Hz, the modified system actually decreased the stability of the control system. The gain and phase margins became very erratic as cutoff frequency increased. Although it is not clear, the fact that the ALPHA-P and Y-TRANS loops are no longer exactly decoupled may explain the instability. The poor stability data could be a result of the way the ALPHA-P open loop transfer function is defined. With the optical coupling and electronic decoupling between the two loops, straightforward frequency domain stability analysis is questionable if not impossible. For this reason, the accuracy of the improved stability figures at low cutoff frequencies must not be trusted. Clearly the stability analysis of the modified control system should not be done in the frequency domain.

Closed Loop Frequency Domain Analysis

Using the two loop ADAS control system shown in Fig. 7, the CYCLE III Roll angular disturbance PSD was input to the ALPHA-P control loop. The translational disturbance was kept equal to zero. The four main points for measuring the closed loop response were: the signal (torque command) to mirror-motors #1 and #2, and, the Y-TRANS and ALPHA-P error signals. The results of this simulation are shown in Table V and are called worst case figures. A first order low pass filter is substituted for block labeled KA1AP (see Fig. 8) and the

cutoff frequency was varied from 0 \rightarrow 16,000 Hz. The closed loop results are presented in Tables VII, VIII, and X, and Fig.'s 12-15.

At low cutoff frequencies (below 200 Hz) the modified system closed loop response was greatly improved over the worst case. The torque requirements went down and the ALPHA-P error was reduced. The Y-TRANS error increased slightly but is still well within the limits of the system (see Table II). The torque requirements to the Beam Steering Mirror (BSM) #1 and #2 were minimized at about 200 Hz cutoff frequency. However, overall system response seemed best at very low or zero cutoff frequencies. The errors were at their lowest value with a zero Hz cutoff and the torque requirements to each BSM were well below their worst case values. Using a 0 Hz cutoff frequency resulted in an almost one-for-one mirror torque requirement. This means that both mirror-motors are being driven by exactly the same amount. There is no longer a two-for-one torque requirement between BSM #1 and BSM #2. This two-for-one torque requirement is undesirable because BSM #1 reaches its torque limit and the control system saturates. Table VII shows that the two-for-one torque requirement is reduced to one-to-one at the expense of increasing the Y-TRANS error. For 0 Hz cutoff, the Y-TRANS error is still well within the limit (see Table VIII and Table II).

However, as cutoff frequency is increased between 250 and 700 Hz, the ALPHA-P error exceeds the worst case error (see Fig. 14). Since the effect of the low pass filter decreases as the cutoff frequency increases, the result that the ALPHA-P error exceeded the worst case was unanticipated.

For cutoff frequencies between 800 and 16,000 Hz, the closed loop

response does approach the worst case figures. The problem is that the closed loop errors and torque approach the worst case figures from the high side. This means that, above 250 Hz cutoff frequency, the low pass filter does not provide any improvement in performance. Also, above about 700 Hz the modified system results are academic because the system response is not this high.

The conclusion from this closed loop frequency domain analysis is that the cutoff frequency must be below 250 Hz for the low pass filter to improve the performance of the system. In fact, from an error control standpoint, 0 Hz cutoff frequency seems to be the best. A low pass filter with 0 Hz cutoff frequency is the same as completely eliminating the electronic cross-coupling from the ALPHA-P to the Y-TRANS control loops. This conclusion supports the belief that the exact decoupling must be reduced or eliminated to reduce the torque saturation problem on BSM #1 and also control errors.

State Space Eigenvalue Analysis

The closed loop eigenvalues for the original and modified systems were calculated. The original system was characterized by 12 states (see ADAS State Space Model) and the addition of the first order low pass filter added an additional state. The eigenvalues were calculated from the closed loop system matrix $[A]$ using program EIGEN (listed in Appendix C) and subroutine RCEIG (Ref. 7).

Analysis of the original closed loop system yielded 12 eigenvalues with negative real parts (see Table III). This means that the original closed loop system is stable. (Ref. 5:576). The eigenvalues were then calculated for the modified control system with the low pass filter

cutoff frequency varied from $0 \rightarrow 160,000$ Hz. The first 7 eigenvalues for each case are shown in Table XI. The last 6 eigenvalues correspond to the 6 states of the disturbance shaping filters (see ADAS State Space Model). These 6 eigenvalues have no influence on the stability of the system so they are not shown.

The eigenvalues of the modified system show that it is unstable for cutoff frequencies below about 725 Hz. As the cutoff frequency is increased above 725 Hz the modified system eigenvalues approach the original system eigenvalues. The only difference is the presence of an eigenvalue corresponding to the low pass filter. As cutoff frequency is increased, the effect of this eigenvalue of the filter decreases. This result is as expected and corresponds to the declining effect of the low pass filter as cutoff frequency goes to infinity.

Since the open loop response of the control system is not greater than 725 Hz, any filter with cutoff frequency above 725 Hz would have no effect on the system. And since the modified system is always unstable at cutoff frequencies below 725 Hz, the low pass filter is not successful in improving the system.

Overall Conclusions

Combining the conclusions of the three analysis techniques, the overall conclusion is that the modified ADAS control system offers no improvement in performance over the original system. However, it is interesting to compare and contrast the results and conclusions of the frequency domain techniques with those of the state space analysis. Both the open and closed loop frequency domain results pointed to an improved stable modified system at low cutoff frequencies. The

eigenvalue analysis showed a large unstable closed loop pole at low cutoff frequencies. Thus, at low frequencies the two separate analysis techniques are in direct conflict. The real problem is then to decide which technique is giving correct results.

At high cutoff frequencies (200 → 800 Hz), there is less difference between frequency domain and state space analysis results. The eigenvalue analysis continues to show an unstable closed loop pole until cutoff frequency is higher than 725 Hz. This unstable pole could explain the erratic nature of the open loop stability figures. It could also explain the closed loop response figures exceeding the worst case figures. As a result, the state space approach seems to be the correct way to analyze the modified system. This modern control approach has become quite refined and is particularly suitable to multi-input, multi-output control system analysis.

IX. Recommendations

The ADAS control system is basically a multiple-input/multiple-output system. In the original ADAS control system design, a great deal of effort went into ensuring the angle and translation loops were completely decoupled electronically. Among other things, this allowed frequency domain techniques to be used in designing the compensation networks. If the vibrational environment was well defined and mirror-motors with infinite torque and acceleration capability were available, this technique would have worked. Since these things are not available some compromises must be made. The thrust of this study was to ignore the exact decoupling and decrease the torque/acceleration demand to motor #1. Since the translational errors are not as critical as the angular errors, more translational error would be accepted in order to decrease this torque/acceleration requirement.

However, as soon as the exact decoupling is altered, the limits of the frequency domain model are violated. It is no longer possible to assume single-input/single-output relationships. Since accepting more translational error and eliminating exact decoupling remains a viable solution, it is clear that another modeling and analysis technique is necessary.

It is recommended that modern state space control techniques be applied to this problem. A state space model of ADAS would be capable of handling multiple-inputs and multiple-outputs. Since a new model is recommended, it is further recommended that completely new feedback and compensation be designed. In this way the resulting

design would not be a modification to the original control system but a completely new design.

To illustrate this new design philosophy, a block diagram of the basic Airborne Dynamic Alignment System is shown in Fig. 16. Again the design will be performed on a two loop control system. In the final design the two basic two loop systems could be joined together for the full ADAS system. Note that there is no mirror angle feedback, electronic decoupling, or compensation network that appears in the present control system.

The open loop state matrix equations that describe the system are as follows;

$$\dot{\underline{X}}(t) = [\underline{A}] \underline{X}(t) + [\underline{B}] \underline{u}(t)$$

$$\underline{y} = [\underline{C}] \underline{X}(t)$$

$$\underline{z} = [\underline{D}] \underline{X}(t)$$

$$\underline{e} = \underline{d} - \underline{z}$$

where

$$[\underline{A}] = \begin{bmatrix} 0 & 1 & 0 & 0 \\ -1407 & 0 & 0 & 0 \\ 0 & 0 & 0 & 1 \\ 0 & 0 & -1407 & 0 \end{bmatrix}$$

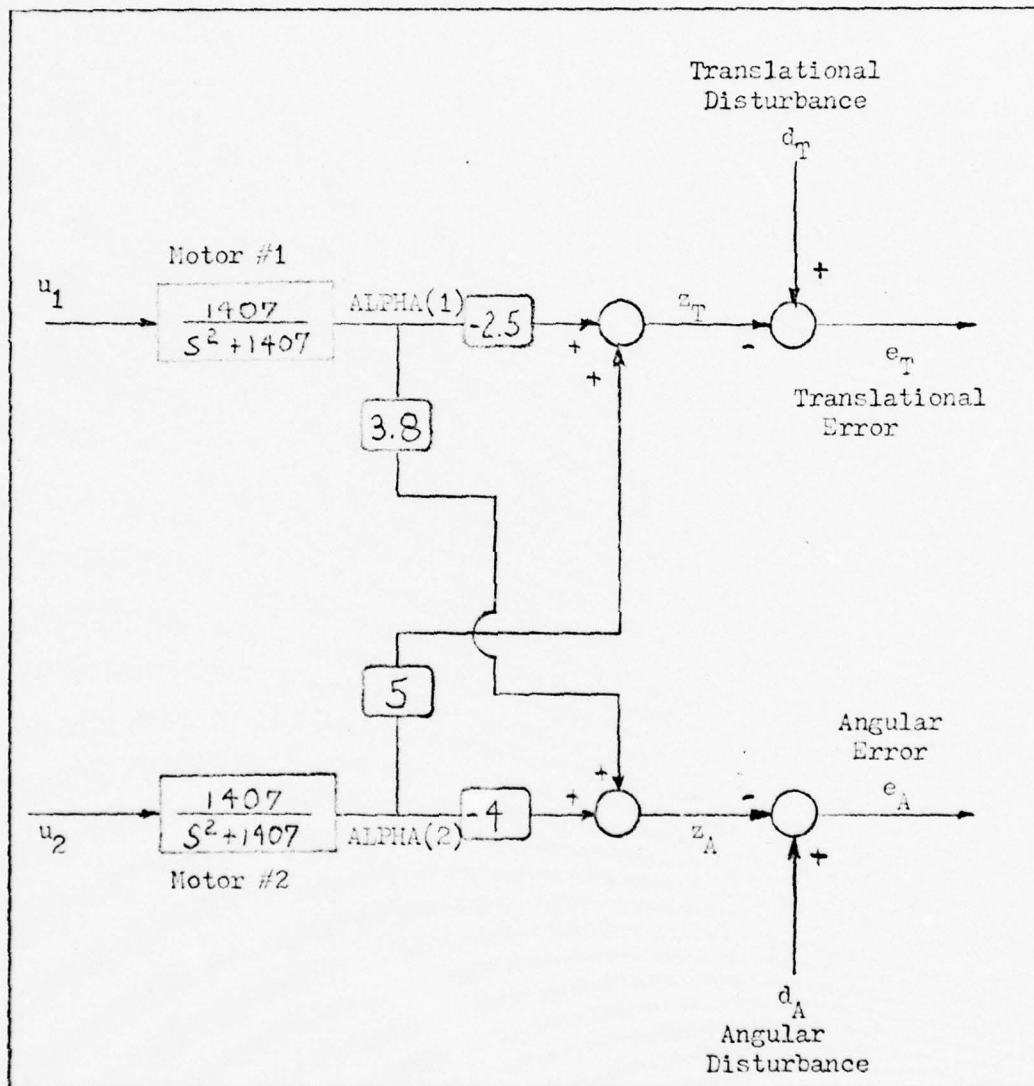


Fig.16. Block Diagram of Basic ADAS

$$\underline{x}(t) = \begin{bmatrix} x_1(t) \\ x_2(t) \\ x_3(t) \\ x_4(t) \end{bmatrix}$$

$$\underline{x}(t) = \begin{bmatrix} x_1(t), \text{ Angular Displacement of BSM \#1} \\ x_2(t), \text{ Rotational Velocity of BSM \#1} \\ x_3(t), \text{ Angular Displacement of BSM \#2} \\ x_4(t), \text{ Rotational Velocity of BSM \#2} \end{bmatrix}$$

$$[B] = \begin{bmatrix} 0 & 0 \\ 1407 & 0 \\ 0 & 0 \\ 0 & 1407 \end{bmatrix}$$

$$\underline{u}(t) = \begin{bmatrix} u_1(t) \\ u_2(t) \end{bmatrix} = \begin{bmatrix} \text{Command to Motor \#1} \\ \text{Command to Motor \#2} \end{bmatrix}$$

$$[C] = \begin{bmatrix} 1 & 0 & 0 & 0 \\ 0 & 0 & 1 & 0 \end{bmatrix}$$

$$\underline{z}(t) = \begin{bmatrix} z_T(t) \\ z_A(t) \end{bmatrix} = \begin{bmatrix} \text{Translation of Beam} \\ \text{Angle of Beam} \end{bmatrix}$$

$$[D] = \begin{bmatrix} -2.5 & 0 & 5 & 0 \\ 3.8 & 0 & -4 & 0 \end{bmatrix}$$

$$\underline{e}(t) = \begin{bmatrix} e_T(t) \\ e_A(t) \end{bmatrix} = \begin{bmatrix} \text{Trans Error of Beam} \\ \text{Angle Error of Beam} \end{bmatrix}$$

$$\underline{d}(t) = \begin{bmatrix} d_T(t) \\ d_A(t) \end{bmatrix} = \begin{bmatrix} \text{Translational Disturbance of Beam} \\ \text{Angular Disturbance of Beam} \end{bmatrix}$$

When this basic system is shown in a state matrix diagram, it is easily identified as a basic tracking problem. This state matrix diagram is in Fig. 17. The significance of identifying this basic tracking problem is that there are several systematic ways available of solving this problem. (Ref. 1:253).

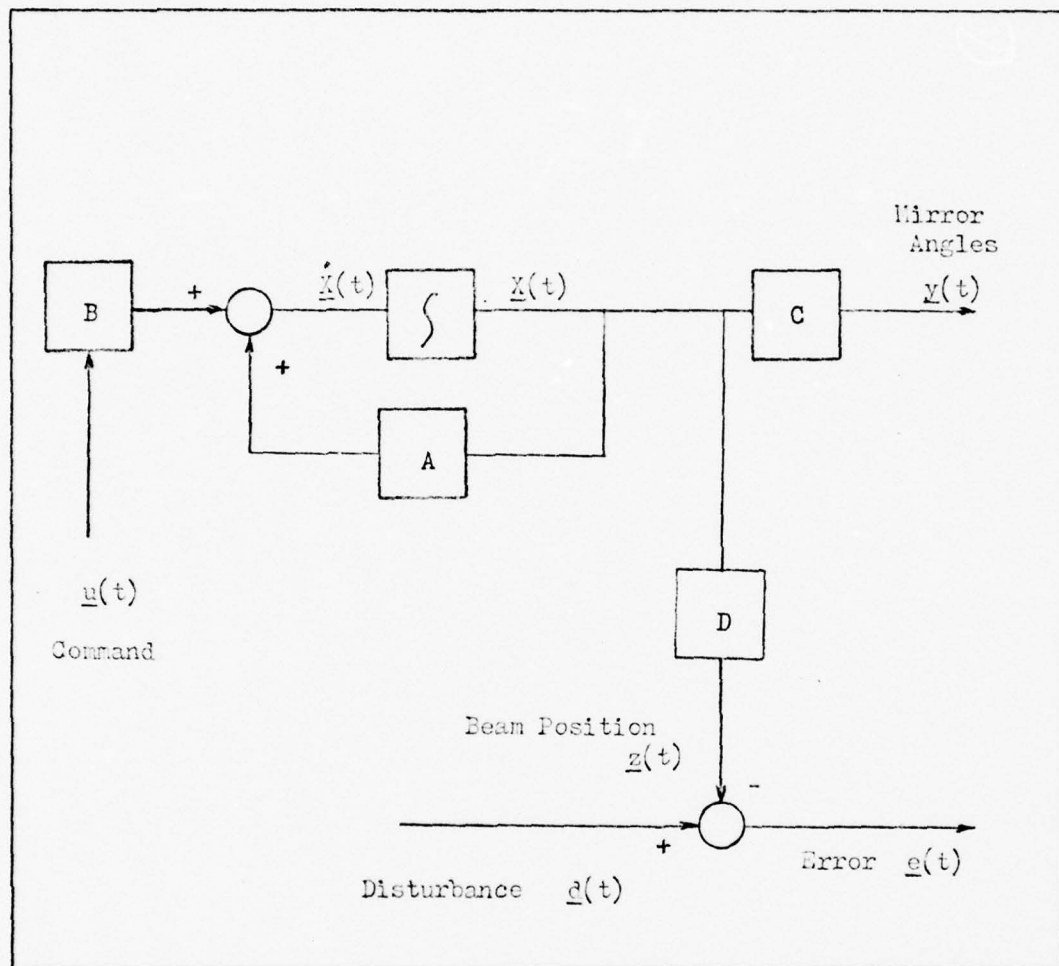


Fig.17. Basic ADAS Tracking Problem

With the insight gained from conducting the previous study of ADAS in the frequency domain, the following is an outline of the solution approach for the state space ADAS tracking problem;

- 1.) Improve "open loop" mirror-motor damping by feeding the states $(X(t))$ through a matrix $\begin{bmatrix} F_x \end{bmatrix}$ to the input $u(t)$.

- 2.) Improve overall system closed loop response by feedback of the disturbance through a matrix $\begin{bmatrix} F_d \end{bmatrix}$ to the input $u(t)$.

When the states are fed back through matrix $\begin{bmatrix} F_x \end{bmatrix}$, the control $u(t)$ becomes;

$$\underline{u}(t) = \begin{bmatrix} F_x \end{bmatrix} \underline{X}(t)$$

substituting $u(t)$ into the $\underline{X}(t)$ equation:

$$\begin{aligned} \underline{X}(t) &= \begin{bmatrix} A \end{bmatrix} \underline{X}(t) + \begin{bmatrix} B \end{bmatrix} \begin{bmatrix} F_x \end{bmatrix} \underline{X}(t) \\ &= \begin{bmatrix} A + BF_x \end{bmatrix} \underline{X}(t) \end{aligned}$$

Thus, $\begin{bmatrix} A + BF_x \end{bmatrix}$ becomes the new matrix that defines the closed loop response between $\underline{u}(t)$ and $\underline{X}(t)$. Now, with the proper choice of the state feedback matrix $\begin{bmatrix} F_x \end{bmatrix}$ the closed loop eigenvalues may be changed to improve the damping of the system. (Ref. 8).

When the disturbance ($\underline{d}(t)$) is fed back to the input ($\underline{u}(t)$) with the revised open loop system the control system will respond to correct any input disturbance. The new closed loop system equation is now:

$$\underline{X}(t) = \begin{bmatrix} A + BF_x \end{bmatrix} \underline{X}(t) + \begin{bmatrix} B \end{bmatrix} \begin{bmatrix} F_d \end{bmatrix} \underline{d}(t)$$

It is through this $\begin{bmatrix} F_d \end{bmatrix}$ matrix that the relative importance of the translational and angular errors may be specified. Since the angular error is of greater importance, $\begin{bmatrix} F_d \end{bmatrix}$ may be designed with a heavier weighting on angular errors. The best way to design $\begin{bmatrix} F_d \end{bmatrix}$ is through linear optimal control theory. A cost function (J) would be defined to make angular error control more important than

translational error control. The cost function (J) is also the place to define the weighting of the controls u_1 and u_2 .

The only problem in implementing the above recommendations is that two of the states (X_2 and X_4) and both disturbances $d_T(t)$ and $d_A(t)$ are not directly available. Again, modern control theory provides a solution to this dilemma. Since two of the states X_1 and X_3 are available through output $y(t)$, an observer may be used to estimate the states X_2 and X_4 . All four states may then be fed back through $[F_x]$ to improve the system damping. The disturbances ($d(t)$) are also estimated using a Kalman filter. (Ref. 1:341). The Kalman filter used the errors that are available from the sensors and the states from the observer to estimate $d(t)$. Finally $d(t)$ is multiplied by $[F_d]$ and fed into the control $u(t)$. The state matrix of the total system is shown in Fig. 18.

Several more details need to be examined before the control system shown in Fig. 18 will work properly. These include: picking actual eigenvalues to give the desired closed loop response, and determination of weighting matrices on $e_T(t)$, $e_A(t)$, $u_1(t)$, and $u_2(t)$. Additionally, the observer and Kalman filter would need to be "fine tuned" for optimal estimates of the states and disturbances. A computer program would have to be designed to simulate this new control system. It would then be through simulation of the system that these details could be worked out. Such a design approach is felt to be advantageous because it is inherently capable of dealing with the multi-input and multi-output system. For this particular system, it does not appear beneficial to exactly decouple and treat as two single-input/single-output system designs.

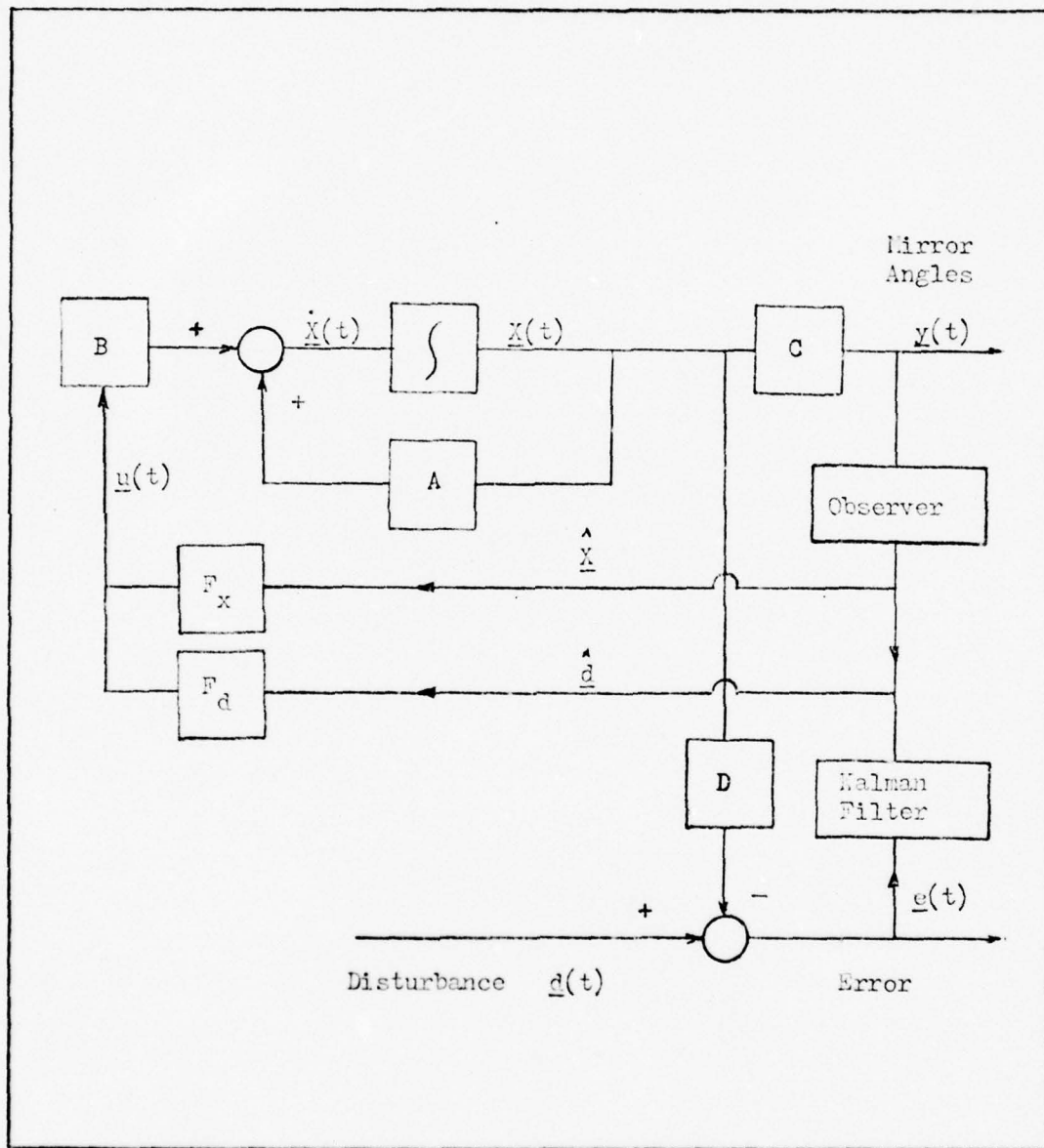


Fig.18. Optimal ADAS Tracking Problem

Bibliography

1. Kwakernaak, Huibert and Raphael Sivan. Linear Optimal Control Systems. New York, New York: Wiley-Interscience, 1972.
2. McCormick, C. W. (Editor). The Nastran Users Manual (Level 15), NASA SP-222(01), With Level Updates. NASA, Washington, D. C.: June 1972.
3. Oklahoma State University. Addendum Five To Advanced Simulation Concepts, User Manual for OSUAPT 3.1 and FRQAPT, Airborne Dynamic Alignment System Simulation. Contract Number F29601-75-C-0121, Air Force Weapons Laboratory, Kirtland AFB, NM: March 1976.
4. Oklahoma State University, School of Mechanical and Aerospace Engineering. User Guide for Frequency Response Analysis Program, FRQRSP. USAF Weapons Lab. Contract Number F29601-75-C-0121, Stillwater, Oklahoma: 28 September 1977.
5. Padulo, Louis and Michael A. Arbib. System Theory. Philadelphia: W. B. Saunders Company, 1974.
6. Perkin-Elmer Corporation, Electro-Optical Division. Mathematical Model of the ADAS System, Memorandum to ADAS File by J. Gottesman. Perkin-Elmer Corporation, Norwalk, Connecticut: December 1975.
7. Purdue University. RGEIG. Eispack Eigensystem Package, on file at Wright-Patterson AFB, Ohio.
8. Reid, J. Gary. Lecture materials distributed in EE 6.60, Feedback Systems Design. School of Engineering, Air Force Institute of Technology, Wright-Patterson AFB: February 1978.

Appendix A

Frequency Domain Computer Program

ADAS is modeled in the frequency domain through a general purpose frequency domain program called "FRQRSP." The total program consists of 22 subroutines and a small main program. The function of the main program (FRQPGM) is to initialize the run and call the main subroutine "FRQRSP." The calling sequence is shown below.

(1)	(2)	(3)	(4)	(5)	(6)
<hr/>					
FRQRSP					
	FIRST				
	FUNCTIONG				
	GET				
	LAST				
	FUNCTIONPSD				
		PRINT			
	SAVE				
	SOLVER				
		COEF			
			COEFADS		
				CONADS	
			COEFAPT		BLOCKADAS
				CONAPT	
			COEFAAS		BLOCKAPT
				CONAAS	
		SIEDEL			
		SPARSE			
	PIVSEL				
	STEP				
	FRPLOT				

Subroutines; FRQRSP, SAVE, GET, SOLVER, SPARSE, PIVSEL, SIEDEL, FRPLOT, STEP, and PRINT belong to the general purpose package.

Subroutines; COEF, COEFADS, CONADS, BLOCKADAS, COEFAPT, CONAPT, BLOCKAPT, COEFAAS, CONAAS, and FUNCTIONG are used to describe the APT, AAS, and ADAS subsystems to the ALL. All of these subroutines were retained in the simulation during this study to facilitate later total system integration. COEFADS, CONADS, BLOCKADAS, and FUNCTIONG are the only subroutines that were altered for the ADAS control system modification. These subroutines are listed at the end of this appendix. The "FRQRSP USER GUIDE", (Ref. 3) contains a detailed description of the rest of the subroutines. It also gives the user the information necessary to adapt FRQRSP to any particular problem.

Output is in tabular and graphical form. Frequency is in both radians per second and Hertz. Amplitude is in magnitude of $G(s)$ and decibels, where one decibel equals $20 \log_{10} |MAC(G)|$. The phase of $G(s)$ is tabulated in degrees as the imaginary part of $G(s)$. Also, phase is corrected to account for phase beyond ± 180 degrees.

2 BLOCKADAS
3 BLOCKADAS
4 BLOCKADAS
5 BLOCKADAS
6 BLOCKADAS
7 BLOCKADAS
8 BLOCKADAS
9 BLOCKADAS
12 COMPFIL2
11 BLOCKADAS
12 BLOCKADAS
13 BLOCKADAS
14 BLOCKADAS
15 BLOCKADAS
16 BLOCKADAS
17 BLOCKADAS
18 BLOCKADAS
19 BLOCKADAS
20 BLOCKADAS
21 BLOCKADAS
22 BLOCKADAS
23 BLOCKADAS
24 BLOCKADAS
25 BLOCKADAS
26 BLOCKADAS
27 BLOCKADAS
28 BLOCKADAS
29 BLOCKADAS
30 BLOCKADAS
31 BLOCKADAS
13 COMPFIL2
33 BLOCKADAS

BLOCK DATA ADAS

REAL KZT,KBP,K91,K92,KYT,KAP,KAI,K42,KR1ZT,KR2ZT,
1 KR1BP,K92BP,KAIYT,K42YT,KAIAP,K42AP
COMPLEX GFZT,GCZT,GFBI,GAB1,GM81,SLB11,GLB12,GF8P,GC8P,
1 GF82,GB82,GM82,GLB21,GLB22,GELZT,GELBP,GM81,GM82,
2 GFYT,GCYT,GFBI,GAA1,GLA11,GLA12,
3 GFAP,GCAP,GFAP,GA2,GA2,GLA21,GLA22,
4 GELYT,GELAP,GM81,GM82,GB8MOO,GLOWPS

COMMON/ALL/P(150),NR,NW,ISTART,METHOD
COMMON /CADAS/ SYTAA,SAPAA,SZTAA,SBPAA,SYTBA,SAPBA,SZTBA,SBPBA,
1 YT,AP,ZT,8P,KYT,KAP,KAI,K42,KZT,KBP,KBI,KR2,
2 YTCW2,YTCW1,APCW2,APCW1,ZTCW2,ZTCW1,3PCW2,3PCW1,
3 YTSKAN,APSGAN,AIMFRO,A2MFRO,
4 ZTSKAN,3PSKAN,81MFRO,82MFRO,
5 A1LSF,A2LSF,B1LSF,B2LSF,
7 WFYT,ZFYT,WFA1,ZFA1,WFA2,ZFA2,
8 WLA11,ZLA11,WLA12,ZLA12,WLA21,ZLA22,ZLA22,
9 WFZT,ZFZT,WFB1,ZFB1,WFB2,ZFB2,
A WLB11,ZLB11,WLB12,ZLB12,WLB21,ZLB22,ZLB22,
B SYTAA,SYTAA,SYTBA,SYTBA,SAPAA,SAPAA,SAPBA,SAPBA,
C SZTAA,SZTAA,SZTBA,SZTBA,SBPAA,SBPAA,SBPBA,SBPBA,
D KR1ZT,KR2ZT,KR1BP,KR2BP,YAIYT,K42YT,K41AP,K42AP,
E SYTGA,SAPGA,SZTGA,SBPGA
COMMON /GADAS/
1 GFZT,GCZT,GFBI,GAB1,GM81,SLB11,GLB12,GF8P,GC8P,
2 GF82,GB82,GM82,GLB21,GLB22,GELZT,GELBP,GM81,GM82,
3 GFYT,GCYT,GFBI,GAA1,GLA11,GLA12,
4 GFAP,GCAP,GFAP,GA2,GA2,GLA21,GLA22,
GELYT,GELAP,GM81,GM82,GB8MOO,GLOWPS

BLOCKADAS 34
 FIRST 116
 FIRST 117
 BLOCKADAS 37
 BLOCKADAS 38
 BLOCKADAS 39
 BLOCKADAS 40
 BLOCKADAS 41
 BLOCKADAS 42
 BLOCKADAS 43
 BLOCKADAS 44
 BLOCKADAS 45
 BLOCKADAS 46
 BLOCKADAS 47
 BLOCKADAS 48
 BLOCKADAS 49
 BLOCKADAS 50
 BLOCKADAS 51
 PROVEIT 5
 PROVEIT 6
 PROVEIT 7
 PROVEIT 8
 PROVEIT 9
 BLOCKADAS 55
 COMFIL2 15
 COMFIL2 16
 BLOCKADAS 58
 BLOCKADAS 59
 BLOCKADAS 60

DATA SYTAA, SAPAA, SZTAA, SBPA/0.35, .1611, 0.0, 0.0, 0.0/
 DATA SYTBA, SAPBA, SZTBA, SBPA/-5.03, -1.9935, 0.0, 0.0, 0.0/
 DATA KYT, KAP, KA1, KA2/2.78, 15.3, 12.0, 12.0/
 DATA KZT, KBP, KB1, KB2/2.78, 15.3, 12.0, 12.0/
 DATA YTCW2, YTCW1, APCW1/3140., 314., 3300., 630./
 DATA ZTCW2, ZTCW1, BPCW1/3140., 314., 9300., 630./
 DATA YTSGAN, APSCAN, A1MFRQ, A2MFRQ/5000., 5000., 10000., 10000./
 DATA ZTSGAN, BPSCAN, B1MFRQ, B2MFRQ/5000., 5000., 10000., 10000./
 DATA A1LSF, A2LSF, B1LSF, B2LSF/4*7.1E-4/
 DATA WFT, ZFT, WFA1, ZFA1/12560., 1.414, 12560., 1.414/
 DATA WFA1, ZFA1, WFA2, ZFA2/15080., 0.003, 15080., 0.003/
 DATA WLA11, ZLA11, WLA12, ZLA12/37.51, 0.0, 15080., 0.003/
 DATA WLA21, ZLA21, WLA22, ZLA22/37.51, 0.0, 15080., 0.003/
 DATA WFT, ZFT, WFB1, ZFB1/12560., 1.414, 12560., 1.414/
 DATA WFB1, ZFB1, WFB2, ZFB2/15080., 0.003, 15080., 0.003/
 DATA WLB11, ZLB11, WLB12, ZLB12/37.51, 0.0, 15080., 0.003/
 DATA WLB21, ZLB21, WLB22, ZLB22/37.51, 0.0, 15080., 0.003/
 DATA SYTA1, SYTA2, SYTB1, SYTB2/-2.42, 5.07, 0.0, 0.0/
 DATA SAPA1, SAPA2, SAPB1, SAPB2/3.859, -3.906, 0.0, 0.0/
 DATA SZTA1, SZTA2, SZTB1, SZTB2/0.0, 0.0, 0.0, 0.0/
 DATA SPPA1, SPPA2, SPPB1, SPPB2/0.0, 0.0, 0.0, 0.0/
 DATA KP1ZT, KR2ZT, KR1BP, KR2BP/1.0, -1.0, 1.0, -.498/
 DATA KA1YT, KA2YT, KA1AP, KA2AP/1.0, .95, 0.00497, .5/
 DATA SYTGA, SAPGA, SZTGA, SBPGA/-0.9, 0.0, .33, 0.0/
 END

2	CONADS		
3	CONADS		
4	CONADS		
5	CONADS		
6	CONADS		
7	CONADS		
8	CONADS		
9	COMPFIL2		
10	CONADS		
11	CONADS		
12	CONADS		
13	CONADS		
14	CONADS		
15	CONADS		
16	CONADS		
17	CONADS		
18	CONADS		
19	CONADS		
20	CONADS		
21	CONADS		
22	CONADS		
23	CONADS		
24	CONADS		
25	CONADS		
26	CONADS		
27	CONADS		
28	CONADS		
29	CONADS		
30	CONADS		

1	COMPLEX	GFZT,GCZT,GFRI,GAR1,GM71,GLB11,GLB12,GFDP,GORP,
2		1 GFR2,GAB2,GM32,GLB21,GLB22,GELZT,GELBP,GM1B1,GM1B2,
3		2GFTY,GCYT,GFAL,GA11,GM11,GLA11,GLA12,
4		3 GFAP,GCAP,GFAL,GA12,GM12,GLA21,GLA22,
		GFELT,GFELP,GM1A1,GM1A2,GRSMOD,GLONPS

1	COMPLEX	S
2		
3		
4		
5		
6		
7		
8		
9		
10		
11		
12		
13		
14		
15		
16		
17		
18		
19		
20		
21		
22		
23		
24		
25		
26		
27		
28		
29		
30		

1	REAL	KZT,KBP,KB1,KB2,KYT,KAP,KA1,KA2,KR1ZT,KR2ZT,
2		1 KB1BP,KR2BP,KA1YT,KA2YT,KA1AP,KA2AP

1	COMMON/ALL/P(150),NR,NW,ISTART,METHOD
2	COMMON /CADAS/ SYTAA,SAPAA,SZTAA,SBPAA,SYTBA,SAPBA,SZTBA,SBPBA,
3	YT,AP,ZT,BP,KYT,KAP,KA1,KA2,KZT,KBP,KB1,KB2,
4	YTCW2,YTCW1,APCW2,APCW1,ZTCW2,ZTCW1,BPCW2,BPCW1,
5	YTCGAN,APSGAN,A1MFRQ,A2MFRQ,
6	ZTCGAN,BPSCGAN,B1MFRQ,B2MFRQ,
7	A1LSF,A2LSF,B1LSF,B2LSF,
8	WFTY,ZFYT,WFBP,ZFBP,WFA1,ZFA1,WFA2,ZFA2,
9	WLA11,ZLA11,WLA12,ZLA12,WLA21,ZLA21,WLA22,ZLA22,
10	WFTZ,ZFTZ,WFBP,ZFBP,WFB1,ZFB1,WFB2,ZFB2,
11	WLB11,ZLB11,WLB12,ZLB12,WLB21,ZLB21,WLB22,ZLB22,
12	SYTA1,SYTA2,SYTD1,SYTD2,SAPA1,SAPA2,SAPB1,SAPB2,
13	SZTA1,SZTA2,SZTB1,SZTB2,SBPA1,SBPA2,SBPB1,SBPB2,
14	KR1ZT,KR2ZT,KR1BP,KR2BP,KA1YT,KA2YT,KA1AP,KA2AP,
15	SYTGA,SAPGA,SZTGA,SBPGA

THIS PAGE IS BEST QUALITY PRACTICABLE
FROM COPY FURNISHED TO DDG

COMMON /GADAS/	GFZT,GCZT,GFBI,GAB1,GMB1,GLB11,GLB12,GFBP,GCBP,	CONADS	31
1	GFBI2,GAB2,GMB2,GLB21,GLB22,GELZT,GELBP,GMLB1,GMLB2,	CONADS	32
2	GFYT,GCYT,GFBI,GAB1,GMB1,GLB11,GLB12,	CONADS	33
3	GFAP,GCAP,GFBI2,GAB2,GMB2,GLB21,GLB22,	CONADS	34
4	GELYT,GELAP,GMLA1,GMLA2,GBSMOD,GLOWPS	COMPFIL2	10
		CONADS	35
		CONADS	36
		COMPFIL2	37
		CONADS	11
		CONADS	38
		CONADS	39
		CONADS	40
		CONADS	41
		CONADS	42
		CONADS	43
		CONADS	44
		CONADS	45
		CONADS	46
		CONADS	47
		CONADS	48
		CONADS	49
		CONADS	50
		CONADS	51
		CONADS	52
		CONADS	53
		CONADS	54
		CONADS	55
		CONADS	56
		CONADS	57

GLOWPS=1.0/(KA1AP*S+1.0)	
GBSMOD=(1.0+2.9E-7*S+7.6E-9*S*S)/(1.0+1.83E-7*S+3.0E-9*S*S)	
GFZT=1.0/((S/WFZT)**2+ZFZT*(S/WFZT)+1.0)	
GCZT=1.0/(ZTCW2/77CW1-1.0)*S/(S+77CW2)	
GFBI=(1.0+(S/WFBI)**2)/((S/WFBI)**2+ZFBI*(S/WFBI)+1.0)	
GAB1=2.0*B1MFRQ/(S+B1MFRQ)	
GMB1=GAB1/(1.0+GAB1)	
GLB11=1.0/((S/WLB11)**2+ZLB11*(S/WLB11)+1.0)	
GLB12=1.0/((S/WLB12)**2+ZLB12*(S/WLB12)+1.0)	
GFBP=1.0/((S/WFBP)**2+ZFBP*(S/WFBP)+1.0)	
GCBP=1.0/(BPCW2/OPCW1-1.0)*S/(S+OPCW2)	
GFBI2=(1.0+(S/WFBI2)**2)/((S/WFBI2)**2+ZFBI2*(S/WFBI2)+1.0)	
GAB2=2.0*B2MFRQ/(S+B2MFRQ)	
GMB2=GAB2/(1.0+GAB2)	
GLB21=1.0/((S/WLB21)**2+ZLB21*(S/WLB21)+1.0)	
GLB22=1.0/((S/WLB22)**2+ZLB22*(S/WLB22)+1.0)	
GELZT=ZTSGAN*GFZT*GCZT*KZT	
GELBP=SPSGAN*GFBP*GCBP*KBP	
GMLB1=KB1*GFBI2*GMB1*P1LSF*GLB11*GLB12*GBSMOD	
GMLB2=KB2*GFBI2*GMB2*P2LSF*GLB21*GLB22*GBSMOD	
GFYT=1.0/((S/WFYT)**2+ZFYT*(S/WFYT)+1.0)	

C C

CONADS 58
CONADS 59
CONADS 60
CONADS 61
CONADS 62
CONADS 63
CONADS 64
CONADS 65
CONADS 66
CONADS 67
CONADS 68
CONADS 69
CONADS 70
CONADS 71
CONADS 72
CONADS 73
CONADS 74
CONADS 75
CONADS 76
CONADS 77

GCT=1.0+(YTCW2/YTCW1-1.0)*S/(S+YTCW2)
GFA1=(1.+(S/WFA1)**2)/((S/WFA1)**2+ZFA1*(S/WFA1)+1.0)
GAA1=2.0*A1MFRQ/(S+A1MFRQ)
GMA1=GAA1/(1.+GAA1)
GLA11=1.0/((S/WLA11)**2+ZLA11*(S/WLA11)+1.0)
GLA12=1.0/((S/WLA12)**2+ZLA12*(S/WLA12)+1.0)
GFAP=1.0/((S/WFAP)**2+ZFA1*(S/WFAP)+1.0)
GCAP=1.0+(APCW2/APCW1-1.0)*S/(S+APCW2)
GFA2=(1.0+(S/WFA2)**2)/((S/WFA2)**2+ZFA2*(S/WFA2)+1.0)
GAA2=2.0*A2MFRQ/(S+A2MFRQ)
GMA2=GAA2/(1.+GAA2)
GLA21=1.0/((S/WLA21)**2+ZLA21*(S/WLA21)+1.0)
GLA22=1.0/((S/WLA22)**2+ZLA22*(S/WLA22)+1.0)
GELYT=YTCGAN*GFYT*GCT*KYT
GELAP=APSCAN*GFAP*GCAP*KAP
GMLA1=KA1*GFA1*GMA1*A1SF*GLA11*GLA12*GPSMOD
GMLA2=KA2*GFA2*GMA2*A2LSF*GLA21*GLA22*GPSMOD
RETURN
END

C

C	2	COEFADS	
C	3	COEFADS	
C	4	COEFADS	
C	5	COEFADS	
C	6	COEFADS	
C	7	COEFADS	
	8	COEFADS	
	9	COEFADS	
	10	COEFADS	
	11	COEFADS	
	12	COMPFIL2	
	13	COEFADS	
	14	COEFADS	
	15	COEFADS	
	16	COEFADS	
	17	COEFADS	
	18	COEFADS	
	19	COEFADS	
	20	COEFADS	
	21	COEFADS	
	22	COEFADS	
	23	COEFADS	
	24	COEFADS	
	25	COEFADS	
	26	COEFADS	
	27	COEFADS	
	28	COEFADS	
	29	COEFADS	
	30	COEFADS	
	31	COEFADS	
	32	COEFADS	
	33	COEFADS	

SUBROUTINE COEFADS(A,P,ICOL,NEON,NROW,NCOL,S,N,R,NAOS)

THIS SUBROUTINE FOR TWO CHANNEL
COUPLED ADAS SYSTEM. WRITTEN BY MERPITT
USINF MATRIX FROM COREY. 5 JAN 77.

COMPLEX GF7T,GC2T,GF8T,GAB1,GB11,GLB12,GF8P,GOBP,
1 GF82,GAB2,GB22,GLB21,GLB22,GEL2T,GELBP,GBLB1,GBLB2,
2 GFYT,GCYT,GFAT,GAAT,GBAT,GBAT2,
3 GFAP,GCAP,GFAT2,GAAT2,GBAT2,GBAT2,
4 GELYT,GELAP,GBLAT,GBLAT2,GBS400,GBOWPS

COMPLEX A,R,S,P
REAL P
REAL K7T,KBP,K01,K02,KYT,KAP,KAI,KAZ,K01ZT,K02ZT,
1 K01BP,K02BP,KAIYT,KAZYT,KAIAP,KAZAP

COMMON/ALL/P(150),NR,NW,ISTART,MET40D
COMMON /CADAS/ SYTAA,SAPAA,SZTAA,SRPAA,SYTBA,SAPBA,SZTBA,SRPBA,
1 YT,AP,ZT,RP,KYT,KAP,KAI,KAZ,KYT,KBP,K01,K02,
2 YTCW2,YTCW1,APCW2,APCW1,ZTCW2,ZTCW1,BPCW1,BPCW2,
3 YTSKAN,APSGAN,A1MFRQ,A2MFRQ,
4 ZTSKAN,APSGAN,B1MFRQ,B2MFRQ,
5 A1LSF,A2LSF,B1LSF,B2LSF,
6 WFTT,7FTT,WFBP,7FBP,WFA1,7FA1,WFA2,7FA2,
7 WLA11,7LA11,WLA12,7LA12,WLA21,7LA21,WLA22,7LA22,
8 WFTT,7FTT,WFBP,7FBP,WFB1,7FB1,WFB2,7FB2,
9 WLB11,7LB11,WLB12,7LB12,WLB21,7LB21,WLB22,7LB22,
A SYTAA,SYTAA2,SYTAA,SYTAA2,SAPAA,SAPAA2,SAPAA,SAPAA2,
B SYTAA,SYTAA2,SYTAA,SYTAA2,SAPAA,SAPAA2,SAPAA,SAPAA2,
C SZTAA,SZTAA2,SZTAA,SZTAA2,SRPAA,SRPAA2,SRPAA,SRPAA2,
D K01ZT,K02ZT,K01BP,K02BP,KAIYT,KAZYT,KAIAP,KAZAP,
E SYTGA,SAPGA,SZTGA,SRPGA

C	A(NADS+6,1)=GELAP \$ ICOL(NADS+5,1)=NADS+5	COEFADS	68
C	A(NADS+6,2)=1. \$ ICOL(NADS+6,2)=NADS+5	COEFADS	69
C	A(NADS+7,1)=-KAZYT \$ ICOL(NADS+7,1)=NADS+2	COEFADS	70
C	A(NADS+7,2)=-KAZAP \$ ICOL(NADS+7,2)=NADS+5	COEFADS	71
C	A(NADS+7,3)=1. \$ ICOL(NADS+7,3)=NADS+7	COEFADS	72
C	A(NADS+8,1)=-GMLA2 \$ ICOL(NADS+8,1)=NADS+7	COEFADS	73
C	A(NADS+8,2)=1. \$ ICOL(NADS+8,2)=NADS+8	COEFADS	74
C	A(NADS+9,1)=-SZTA1 \$ ICOL(NADS+9,1)=NADS+4	COEFADS	75
C	A(NADS+9,2)=-SZTA2 \$ ICOL(NADS+9,2)=NADS+8	COEFADS	76
C	A(NADS+9,3)=1. \$ ICOL(NADS+9,3)=NADS+3	COEFADS	77
C	A(NADS+9,4)=-SZTP1 \$ ICOL(NADS+9,4)=NADS+12	COEFADS	78
C	A(NADS+9,5)=-SZTP2 \$ ICOL(NADS+9,5)=NADS+16	COEFADS	79
C	A(NADS+10,1)=GEL7T \$ ICOL(NADS+10,1)=NADS+9	COEFADS	80
C	A(NADS+10,2)=1. \$ ICOL(NADS+10,2)=NADS+10	COEFADS	81
C	A(NADS+11,1)=-KB17T \$ ICOL(NADS+11,1)=NADS+10	COEFADS	82
C	A(NADS+11,2)=1. \$ ICOL(NADS+11,2)=NADS+11	COEFADS	83
C	A(NADS+11,3)=-KB1FP \$ ICOL(NADS+11,3)=NADS+14	COEFADS	84
		COEFADS	85
		COEFADS	86
		COEFADS	87
		COEFADS	88
		COEFADS	89
		COEFADS	90
		COEFADS	91

COEFADS 92
COEFADS 93
COEFADS 94
COEFADS 95
COEFADS 96
COEFADS 97
COEFADS 98
COEFADS 99
COEFADS 100
COEFADS 101
COEFADS 102
COEFADS 103
COEFADS 104
COEFADS 105
COEFADS 106
COEFADS 107
COEFADS 108
COEFADS 109
COEFADS 110
COEFADS 111
COEFADS 112
COEFADS 113

A(NADS+12,1)=-GMLB1 \$ ICOL(NADS+12,1)=NADS+11
A(NADS+12,2)=1. \$ ICOL(NADS+12,2)=NADS+12

A(NADS+13,1)=-SBPA1 \$ ICOL(NADS+13,1)=NADS+4
A(NADS+13,2)=-SBPA2 \$ ICOL(NADS+13,2)=NADS+9
A(NADS+13,3)=-SBPA1 \$ ICOL(NADS+13,3)=NADS+12
A(NADS+13,4)=1. \$ ICOL(NADS+13,4)=NADS+13
A(NADS+13,5)=-SBPA2 \$ ICOL(NADS+13,5)=NADS+16

A(NADS+14,1)=GELPF \$ ICOL(NADS+14,1)=NADS+13
A(NADS+14,2)=1. \$ ICOL(NADS+14,2)=NADS+14

A(NADS+15,1)=-KB27T \$ ICOL(NADS+15,1)=NADS+10
A(NADS+15,2)=-KB2RP \$ ICOL(NADS+15,2)=NADS+14
A(NADS+15,3)=1. \$ ICOL(NADS+15,3)=NADS+15

A(NADS+16,1)=-GMLB2 \$ ICOL(NADS+16,1)=NADS+15
A(NADS+16,2)=1. \$ ICOL(NADS+16,2)=NADS+16

RETURN
END

COMPLEX FUNCTION G(S,N,R)		
COMPLEX GI,LPF,AAACMP,AAECMP,APAP,EPAP,AFBLO,EFRLP,	FUNCTIONS	2
1 AEQVBP,EEQVBP,XINTNT,A,R,F,S	FUNCTIONS	3
COMPLEX GFZT,GCZT,GERI,GAR1,GBR1,GLB11,GLB12,GFOP,GCOP,	FUNCTIONS	4
1 GFB2,GAB2,GBR2,GLB21,GLB22,GFZT,GERI,GELBP,GBLB1,GBLB2,	FIRST	10
2GFYT,GCYT,GFAT,GAAT,GAAT,GLA11,GLA12,	FIRST	11
3 GFAP,GCAP,GAAT,GAAT,GAAT,GLA21,GLA22,	FIRST	12
4 CELYT,GELAP,GBLA1,GBLA2,GBSHO3,GBLOMPS	FIRST	13
REAL KZT,KBP,KB1,KB2,KYT,KAP,KAI,KAZ,KR2ZT,	COMPEIL2	14
1 KPIBP,KR2BP,KAIYT,KAZYT,KAIAP,KAZAP	FIRST	15
REAL P,EPPO,ETAO,EPST,ETAI	FIRST	16
DIMENSION R(80)	FUNCTIONS	5
	FUNCTIONS	6
COMMON/ALL/P(150),NR,NW,ISTART,METHOD	FUNCTIONS	7
COMMON/AAIII/ETAO,EPPO,AK,EK,CA,CE,XKA,XKE,AZMOT,ELMOT,AJ,EJ,	FUNCTIONS	8
1 AOPTG,EOPTG,XG1,XG2,LPF,AAACMP,AAECMP,APAP,EPAP,AFBLO,EFRLP,	FUNCTIONS	9
2 XINTNT,EEQVBP,AEQVBP	FUNCTIONS	10
	FUNCTIONS	11
	FUNCTIONS	12
	FUNCTIONS	13
COMMON /CADAS/ SYTAA,SAPAA,AZTAA,SBPAA,SYTBA,SAPBA,SZTBA,S3PBA,	FIRST	17
1 YT,AP,ZT,GP,KYT,KAP,KAI,KAZ,KZT,KBP,KBI,KO2,	FIRST	18
2 YTCW2,YTCW1,APCW2,APCW1,ZTCW2,ZTCW1,BPCW2,BPCW1,	FIRST	19
3 YTSKAN,APSGAN,A1MFRQ,A2MFRQ,	FIRST	20
4 7TSKAN,BPSKAN,R1MFRQ,B2MFRQ,	FIRST	21
5 A1LSF,A2LSF,R1LSF,B2LSF,	FIRST	22
6 WFTY,ZFTY,WFA1,ZFA1,WFA2,ZFA2,	FIRST	23
7 WLA11,ZLA11,WLA12,ZLA12,WLA21,ZLA22,ZLA22,	FIRST	24
8 WFTZ,ZFTZ,WFBP,ZFBP,WFB1,ZFB1,WFB2,ZFB2,	FIRST	25
9 WLB11,ZLB11,WLB12,ZLB12,WLB21,ZLB22,ZLB22,	FIRST	26
Z SYTA1,SYTA2,SYTB1,SYTB2,SAPA1,SAPA2,SAPB1,SAPB2,	FIRST	27
B S7TA1,S7TA2,S7TB1,S7TB2,S3PA1,S3PA2,S3PB1,S3PB2,	FIRST	28
C KB1ZT,KR2ZT,KB1BP,KB2BP,KAIYT,KAZYT,KAIAP,KAZAP,	FIRST	29
D SYTGA,SAPGA,SZTGA,S3PGA	FIRST	30
E		

C

C	5	PACK-IN TO A2 AMPLIFIER OUTPUT G=R(NADS+3)/GBSMOD/GLA22/GLA21/A2LSF/GAA2*2. RETURN	FIRST	59
C			FIRST	60
C	6	PACK-IN TO A1 AMPLIFIER OUTPUT G=R(NADS+4)/GBSMOD/GLA12/GLA11/A1LSF/GAA1*2. RETURN	FIRST	61
C			FIRST	62
C	7	PACK-IN TO P2 AMPLIFIER G=R(NADS+16)/GBSMOD/GLP22/GLP21/P2LSF/GAR2*2. RETURN	FIRST	63
C			FIRST	64
C	8	PACK-IN TO B1 AMPLIFIER G=R(NADS+12)/GBSMOD/GLB12/GLB11/B1LSF/GAB1*2. RETURN	FIRST	65
C			FIRST	66
C	9	TORQUE OUTPUT FROM A1 MOTOR (NODE 17) G=R(NADS+4)/GBSMOD/GLA12/GLA11/A1LSF RETURN	FIRST	67
C			FIRST	68
C	10	TORQUE OUTPUT FROM A2 MOTOR (NODE 18) G=R(NADS+3)/GBSMOD/GLA22/GLA21/A2LSF RETURN	FIRST	69
C			FIRST	70
C	11	TORQUE OUTPUT FROM B1 MOTOR (NODE 19) G=R(NADS+12)/GBSMOD/GLB12/GLB11/B1LSF RETURN	FIRST	71
C			FIRST	72
C	12	TORQUE OUTPUT FROM B2 MOTOR (NODE 20) G=R(NADS+16)/GBSMOD/GLB22/GLB21/P2LSF RETURN	FIRST	73
C			FIRST	74
			FIRST	75
			FIRST	76
			FIRST	77
			FIRST	78
			FIRST	79
			FIRST	80
			FIRST	81
			FIRST	82
			FIRST	83
			FIRST	84
			FIRST	85
			FIRST	86
			FIRST	87
			FIRST	88
			FIRST	89
			FIRST	90

C	13	Y- TRANS OPEN LOOP RESPONSE TRUE	PROVEIT	1
		G=(R(NADS+4)*SYTA1+R(NADS+8)*SYTA2)/R(NADS+1)	PROVEIT	2
		RETURN	FIRST	93
C			FIRST	94
C	14	ALPHA-P OPEN LOOP RESPONSE TRUE	PROVEIT	3
		G=(R(NADS+8)*SAPA2)+(R(NADS+4)*SYTA1)/(R(NADS+5))	PROVEIT	4
		RETURN	FIRST	97
C			FIRST	98
C	15	BETA-P OPEN LOOP RESPONSE	FIRST	99
		P=R(NADS+16)*SBPR2/R(NADS+13)	FIRST	100
		RETURN	FIRST	101
C			FIRST	102
C	16	Z-TRANS OPEN LOOP RESPONSE	FIRST	103
		G=R(NADS+12)*SZTR1/R(NADS+9)	FIRST	104
		RETURN	FIRST	105
C			FIRST	106
C	17	A1 MIRROR DEFLECTION	FIRST	107
		G=R(NADS+4)	FIRST	108
		RETURN	FIRST	109
C			FIRST	110
C	18	A2 MIRROR DEFLECTION	FIRST	111
		G=R(NADS+8)	FIRST	112
		RETURN	FIRST	113
C			FIRST	114
		END	FIRST	115

THIS PAGE IS BEST QUALITY PRACTICABLE
FROM COPY FURNISHED TO DDC

103	COEF	
104	COEF	
105	COEF	
106	COEF	
107	COEF	
108	COEF	
109	COEF	
110	COEF	
111	COEF	
112	COEF	
113	COEF	
114	COEF	
115	COEF	
116	COEF	
117	COEF	
118	COEF	
119	COEF	
120	COEF	
121	COEF	
122	COEF	
123	COEF	
124	COEF	
1	FIRST	
2	FIRST	
3	FIRST	
4	FIRST	
5	FIRST	
6	FIRST	
7	FIRST	
8	FIRST	
9	FIRST	
127	COEF	
128	COEF	
129	COEF	
130	COEF	
131	COEF	


```

C      IAPT = 0
C      JAPT = 0
C      CALL COEFAPT(A,R,ICOL,NEQN,NROW,NCOL,S,N,R,IAPT,JAPT)
C
C      NEXT PLACE AA INTO MATRIX A, AA WILL START AT A(34,34)
C
C      NAAS = 33
C      CALL COEFAAS(A,R,ICOL,NEQN,NROW,NCOL,S,N,R,NAAS)
C
C      SET COMMON TERMS BETWEEN APT AND AAS
C
C      A(NAAS+15,3)=2./S      SICOL(NAAS+15,3)=20+JAPT
C      A(NAAS+7,3)=2./S      SICOL(NAAS+7,3)=5+JAPT
C      A(NAAS+6,3)=COS(FPSO)  SICOL(NAAS+6,3)=10+JAPT
C      A(NAAS+14,3)=1.        SICOL(NAAS+14,3)=25+JAPT
C
C      NEXT PLACE ADAS INTO MATRIX A, ADAS WILL START AT A(50,50)
C
C      NADS = 49
C      ISOL=P(100)+NADS
C      B(ISOL)=(1.0,0.0)
C      KKK=ISOL-1
C      DO 175 I=1,KKK
C      C(I)=(0.0,0.0)
C      KKK=ISOL+1
C      DO 176 I=KKK,NROW
C      B(I)=(0.0,0.0)
C      CALL COEFADS(A,R,ICOL,NEQN,NROW,NCOL,S,N,R,NADS)
C      GO TO 99
C
C      175
C      176
C
C      THERE ARE NO COUPLING TERMS BETWEEN ADAS AND APT
C      OR ADAS AND AA AT PRESENT COUPLING

```


AD-A056 093

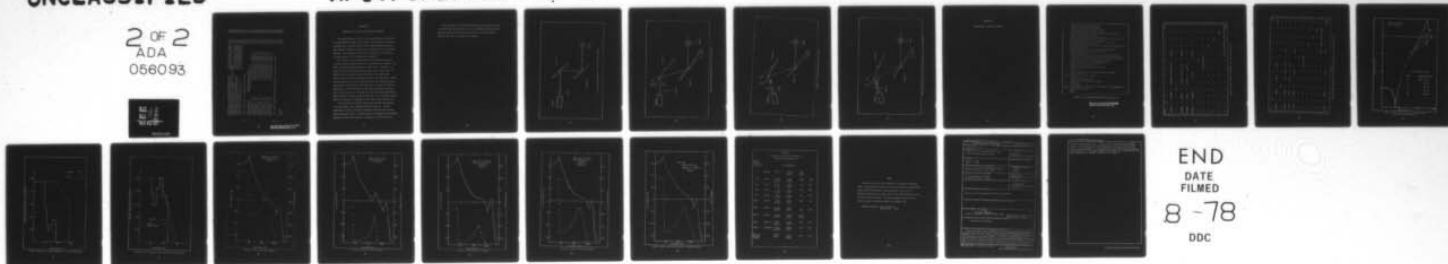
AIR FORCE INST OF TECH WRIGHT-PATTERSON AFB OHIO SCH--ETC F/G 20/6
ANALYSIS AND DESIGN MODIFICATION OF AN AIRBORNE MIRROR ALIGNMEN--ETC(U)
MAR 78 P D NUTZ

UNCLASSIFIED

AFIT/GAE/AA/78M-12

NL

2 OF 2
ADA
056093



END
DATE
FILMED
8-78
DDC

```

233      A(NOPT+1,1) = (1./MTEL)*SIN(EPSTO-ETAO)      SICOL(NOPT+1,1) = 5+NADS      COEF
234      A(NOPT+1,2) = (1./MTEL)*COS(EPSTO-ETAO)      SICOL(NOPT+1,2) = 13+NADS      COEF
235      A(NOPT+1,3) = -(1./MTEL)      SICOL(NOPT+1,3) = 1+NADS      COEF
236      A(NOPT+1,4) = -(MTEL-1.)/MTEL*GI      SICOL(NOPT+1,4) = 5+IAPT      COEF
237      A(NOPT+2,1) = -(1./MTEL)*SIN(EPSTO-ETAO)      SICOL(NOPT+2,1) = 13+NADS      COEF
238      A(NOPT+2,2) = (1./MTEL)*COS(EPSTO-ETAO)      SICOL(NOPT+2,2) = 5+NADS      COEF
239      A(NOPT+2,3) = -(1./MTEL)      SICOL(NOPT+2,3) = 9+NADS      COEF
240      A(NOPT+2,4) = -(MTEL-1.)/MTEL*GI      SICOL(NOPT+2,4) = 25+IAPT      COEF
241      COEF
242      COEF
243      COEF
244      COEF
245      COEF
246      COEF
247      COEF
248      COEF
249      COEF
250      COEF
251      COEF
252      COEF
253      COEF
254      COEF
255      COEF
256      COEF
257      COEF
258      COEF
259      COEF
260      COEF
261      COEF
262      COEF
263      COEF

```

DEFINE FIVE EXTRA EQUATIONS FOR SPARES

```

      A(NOPT+1,5) = 1.      SICOL(NOPT+1,5) = NOPT+1
      A(NOPT+2,5) = 1.      SICOL(NOPT+2,5) = NOPT+2
      A(NOPT+3,1) = 1.      SICOL(NOPT+3,1) = NOPT+3
      A(NOPT+3,2) = -1.      SICOL(NOPT+3,2) = NOPT+1
      A(NOPT+4,1) = 1.      SICOL(NOPT+4,1) = NOPT+4
      A(NOPT+4,2) = -1.      SICOL(NOPT+4,2) = NOPT+3
      A(NOPT+5,1) = 1.      SICOL(NOPT+5,1) = NOPT+5
      A(NOPT+5,2) = -1.      SICOL(NOPT+5,2) = NOPT+4
      A(NOPT+6,1) = 1.      SICOL(NOPT+6,1) = NOPT+6
      A(NOPT+6,2) = -1.      SICOL(NOPT+6,2) = NOPT+5
      A(NOPT+7,1) = 1.      SICOL(NOPT+7,1) = NOPT+7
      A(NOPT+7,2) = -1.      SICOL(NOPT+7,2) = NOPT+6
      A(NOPT+8,1) = 1.      SICOL(NOPT+8,1) = NOPT+8
      A(NOPT+8,2) = -1.      SICOL(NOPT+8,2) = NOPT+7

```

USE ABOVE EQUATIONS WITHOUT CHANGES TO CALLING ROUTINES

```

      RETURN
      END

```

C C C

C C C C

Appendix B

Diagrams of Two for One Beam Steering Movement

The understanding of the two for one mirror movement is crucial in understanding the ADAS control system. The need for the 2:1 ratio is discussed in the main section of this report and again in Ref. 1. This appendix attempts to explain the need through the use of several diagrams. These diagrams are not of the actual layout of the beam steering mirrors but the principle still applies.

Fig. 19 shows the initial position of each mirror, the sensor location, and the nominal position of the optical beam on target. The beam is completely aligned along its nominal path. In Fig. 20, the beam has a pure translational misalignment X at the sensor face. In order to move the beam to strike the center of the target both mirrors must be moved counterclockwise exactly the same amount. Mirror #1 must always move to such an angle that the beam strikes the hinge (pivot) point of Mirror #2. This hinge point is called the "critical hinge point." Fig. 21 depicts the beam with pure angular misalignment at the sensor face. To correct for this pure angular disturbance Mirror #1 must move twice as far as Mirror #2. In a continuous system, Mirror #1 would also be required to move twice as fast as Mirror #2.

It is possible to have both angular and translational misalignment of the beam. This condition is shown in Fig. 22. For the combination of errors, the mirror movement ratio (1:2) will be somewhere between 2:1 and 1:1. The actual ratio will depend on the relative magnitude of each error involved. In Fig. 22, the ratio is 1.8:1.

This principle of beam steering movement may be directly applied to the ADAS beam steering mirrors. The only difference between these figures and the physical beam steering mirrors is that the errors may also occur due to movement of the target.

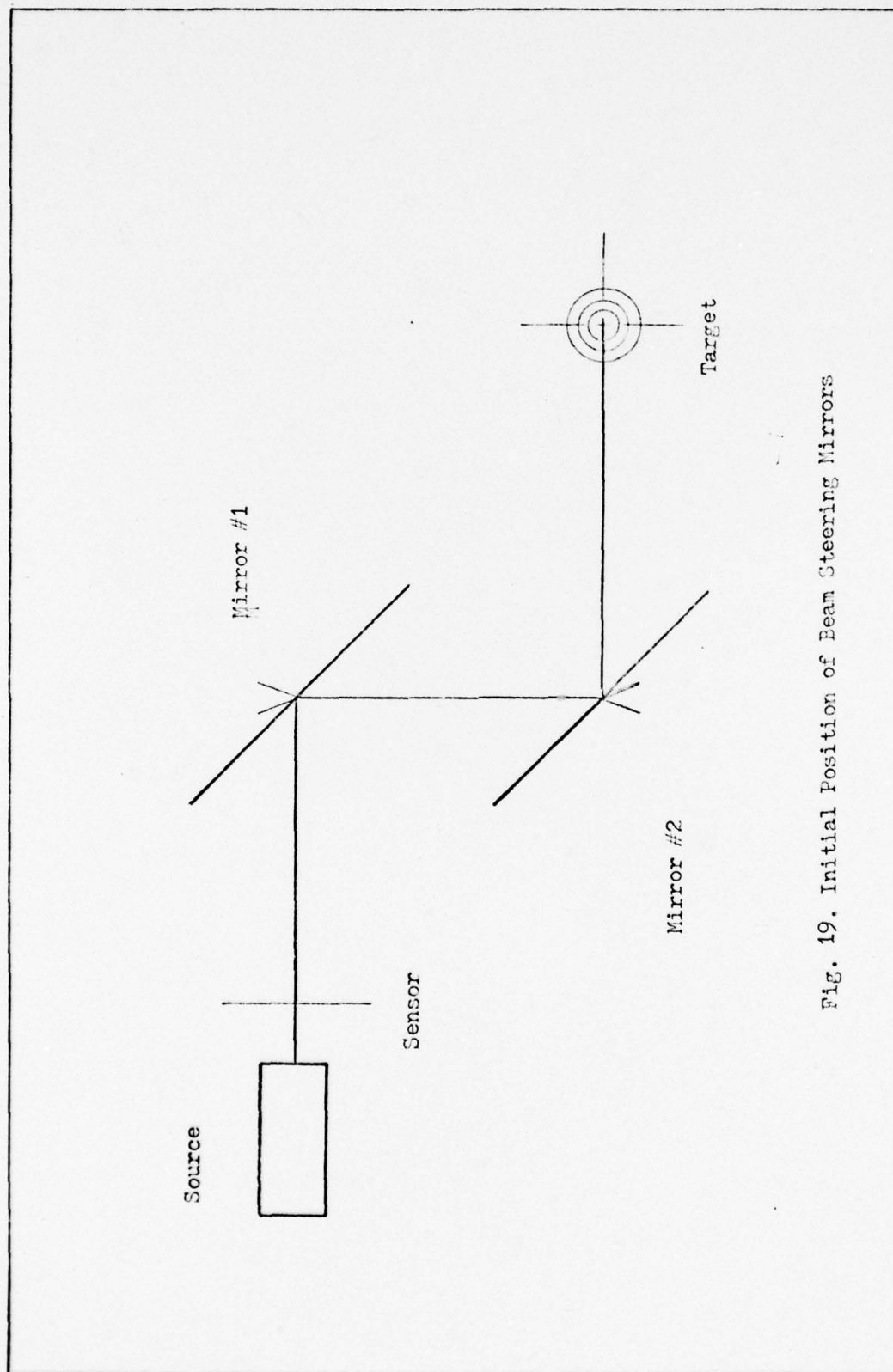


Fig. 19. Initial Position of Beam Steering Mirrors

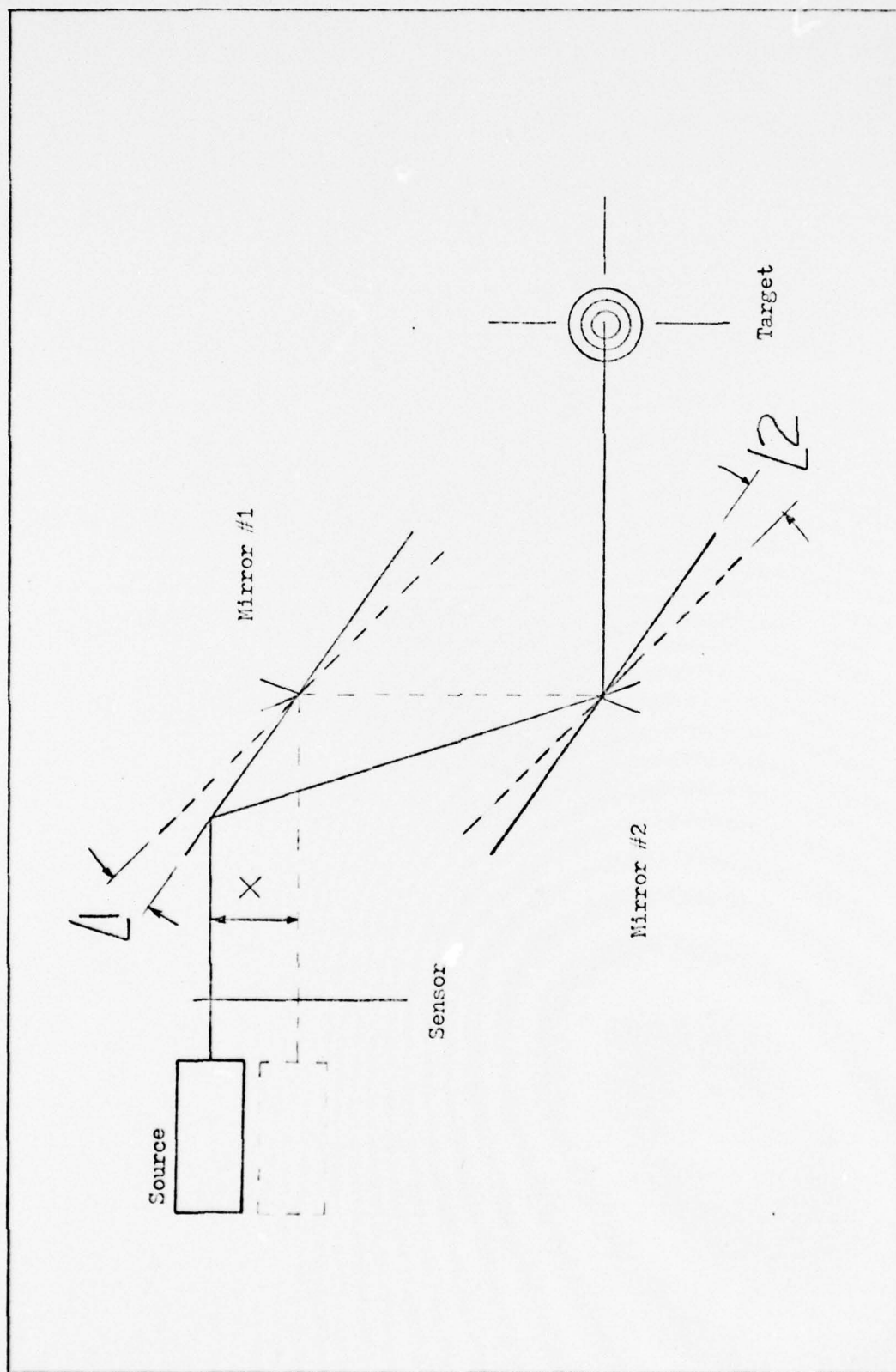


Fig.20. Pure Translational Error in Beam Alignment

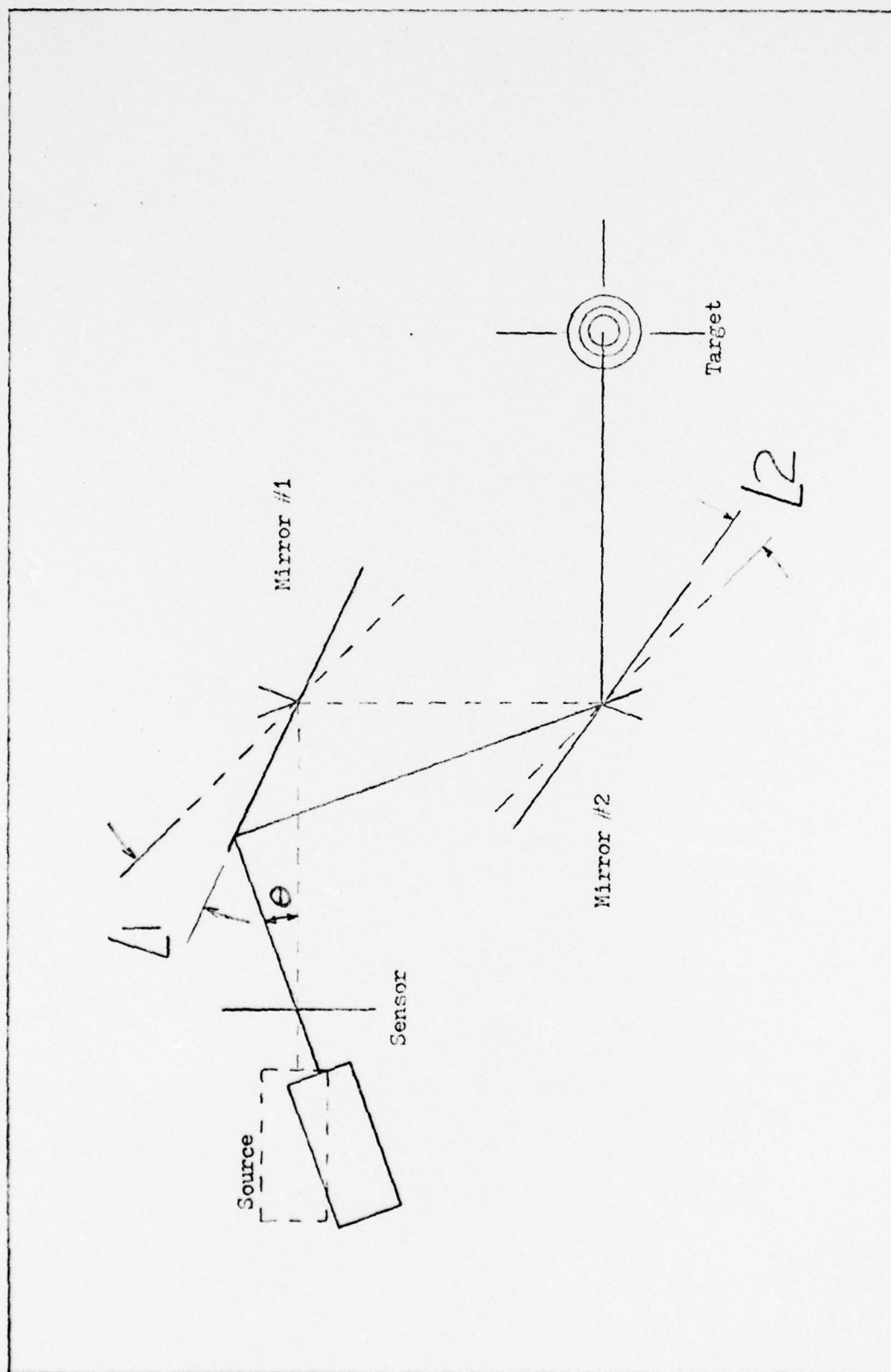


Fig.21. Pure Angular Error in Beam Alignment

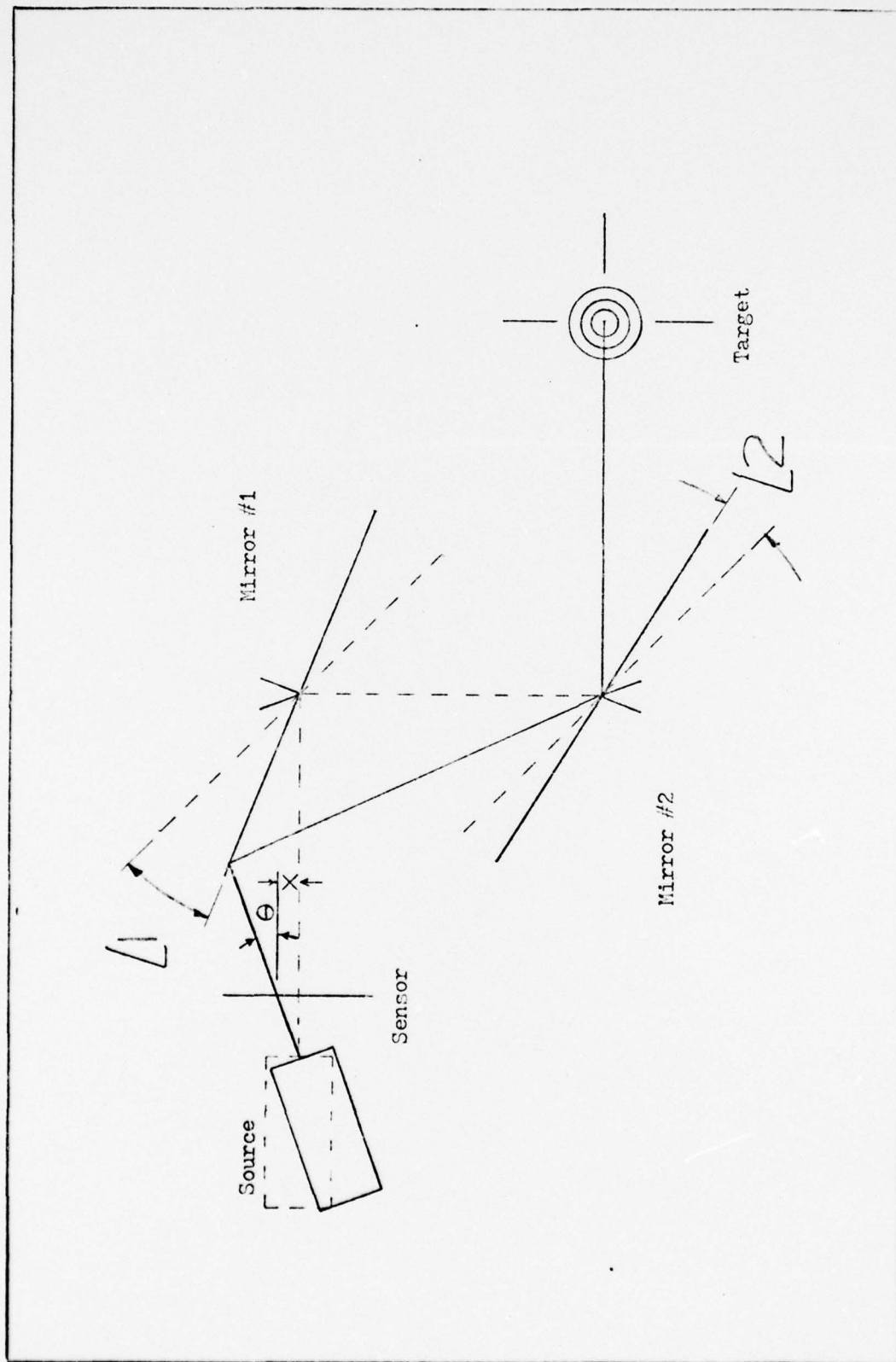


Fig. 22. Combination of Angular and Translational Beam Misalignment

Appendix C

Supplimentary Figures and Tables


```

PROGRAM EIGEN(INPUT,OUTPUT)
DIMENSION A(13,13),WORK(26)
COMPLEX EIGVAL(13),EIGVEC(13,13)
DATA(A(1,I),I=1,13)/0,1.0,11*0/
DATA(A(2,I),I=1,13)/4.03E+6,0,-8.5E+6,0,33.5,
10,1.58E+6,0,0,0,0,12.0/
DATA(A(3,I),I=1,13)/0,0,0,1.0,9*0/
DATA(A(4,I),I=1,13)/-2.25E+7,0,1.89E+7,0,3.23E+1,
19.16E+1,1.59E+6,0,6.77E+6,4*0/
DATA(A(5,I),I=1,13)/-3.41E+8,0,7.17E+8,0,
1-3.14E+3,0,-1.42E+8,6*0/
DATA(A(6,I),I=1,13)/2.50E+9,0,-2.55E+9,0,0,-9.3E+3,
10,0,-6.4E+8,4*0/
DATA(A(7,I),I=1,13)/0,0,0,0,0,0,0,1.0,5*0/
DATA(A(8,I),I=1,13)/0,0,0,0,0,0,0,
1-1.42E+5,-7.54E+2,5*0/
DATA(A(9,I),I=1,13)/0,0,0,0,0,0,0,0,1.0,3*0/
DATA(A(10,I),I=1,13)/0,0,0,0,0,0,0,0,0,1.0,0,0/
DATA(A(11,I),I=1,13)/0,0,0,0,0,0,0,0,0,0,1.0,0/
DATA(A(12,I),I=1,13)/0,0,0,0,0,0,0,0,0,
1-3.97E+9,-6.34E+7,-3.79E+5,-1.0E+3,0/
PRINT*, "ENTER ROW 13 OF MATRIX A"
READ*, (A(13,I),I=1,13)
PRINT 50, ((A(I,J),J=1,13),I=1,13)
50  FORMAT(4E15.6)
IND=1
CALL PGEIG(13,13,A,IND,EIGVAL,EIGVEC,WORK)
PRINT 100,IND
100  FORMAT("  ERROR = "I5/)
DO 10 I=1,13
PRINT 200, EIGVAL(I)
PRINT 300, (EIGVEC(J,I),J=1,13)
10  CONTINUE
CALL EXIT
200  FORMAT(///"  EIGENVALUE = "2F13.3/"  EIGENVECTOR =")
300  FORMAT(14X,2F13.3)
STOP
END

```

Fig.23 . ADAS State Space Model Computer Program

THIS PAGE IS BEST QUALITY PRACTICABLE
FROM COPY FURNISHED TO DDC

[illegible]

* = 0

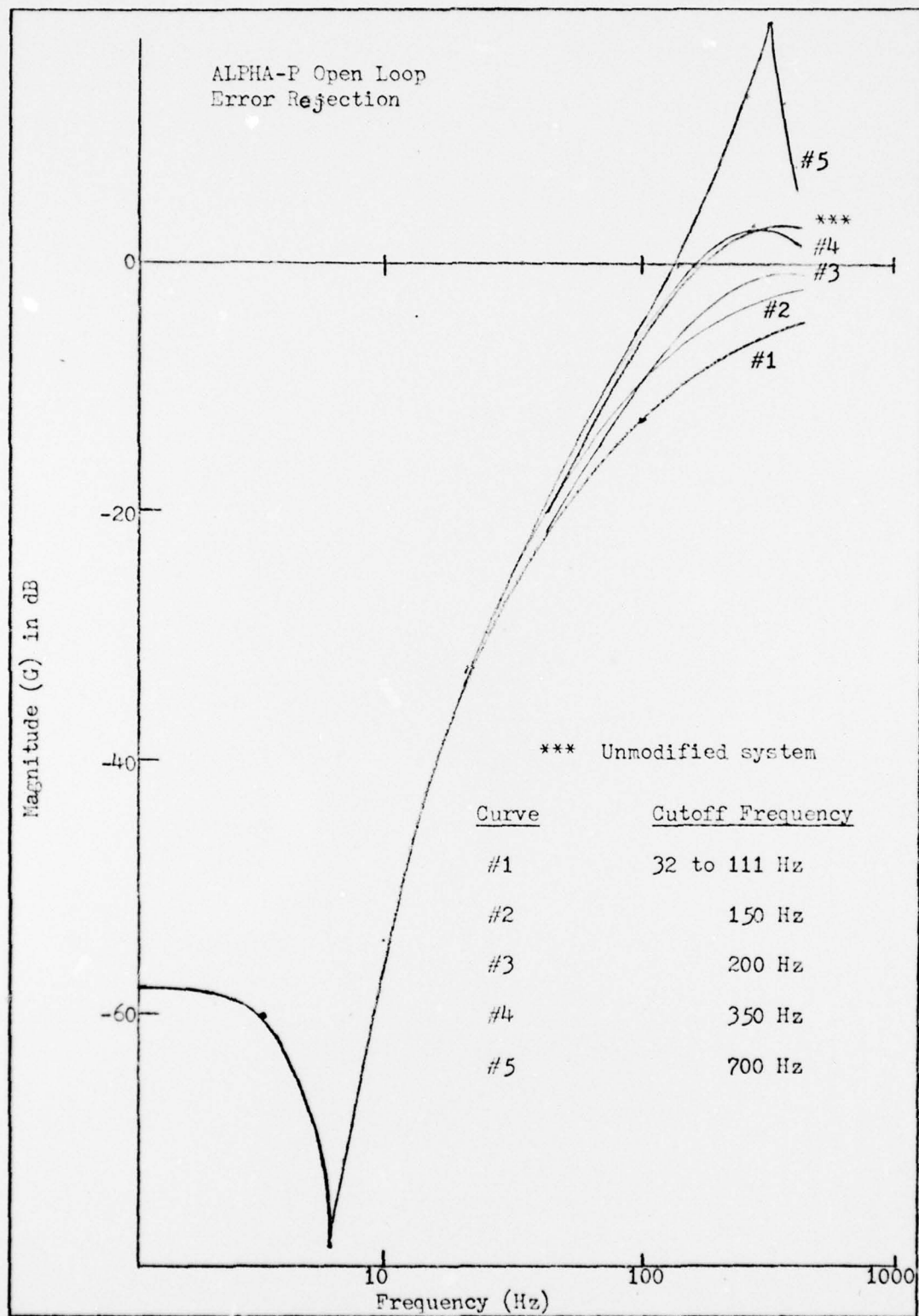


Fig.26. ALPHA-P Open Loop Error Rejection with
Various Cutoff Frequencies

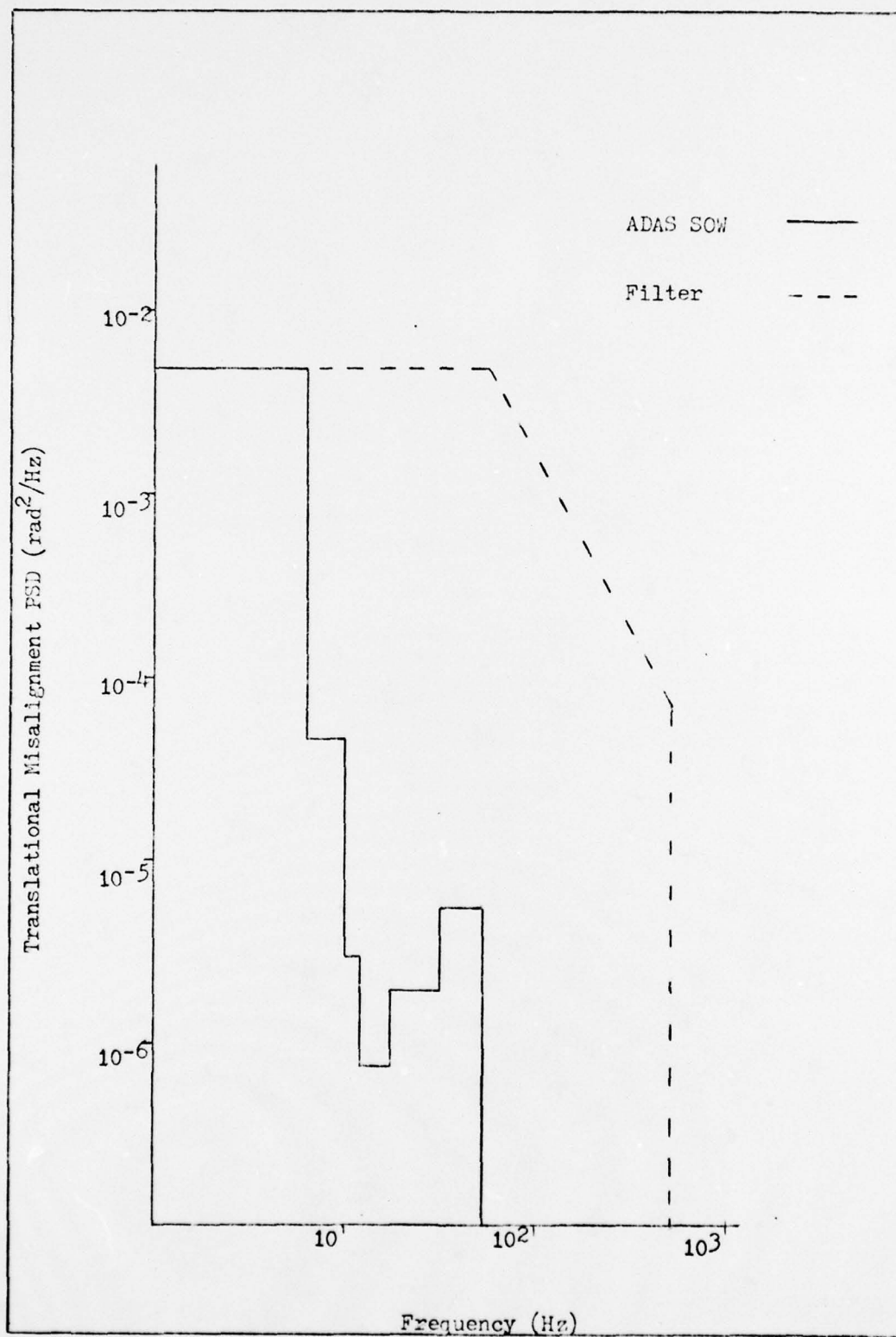


Fig.27. Comparison of Translational ADAS SOW and Filter PSDs

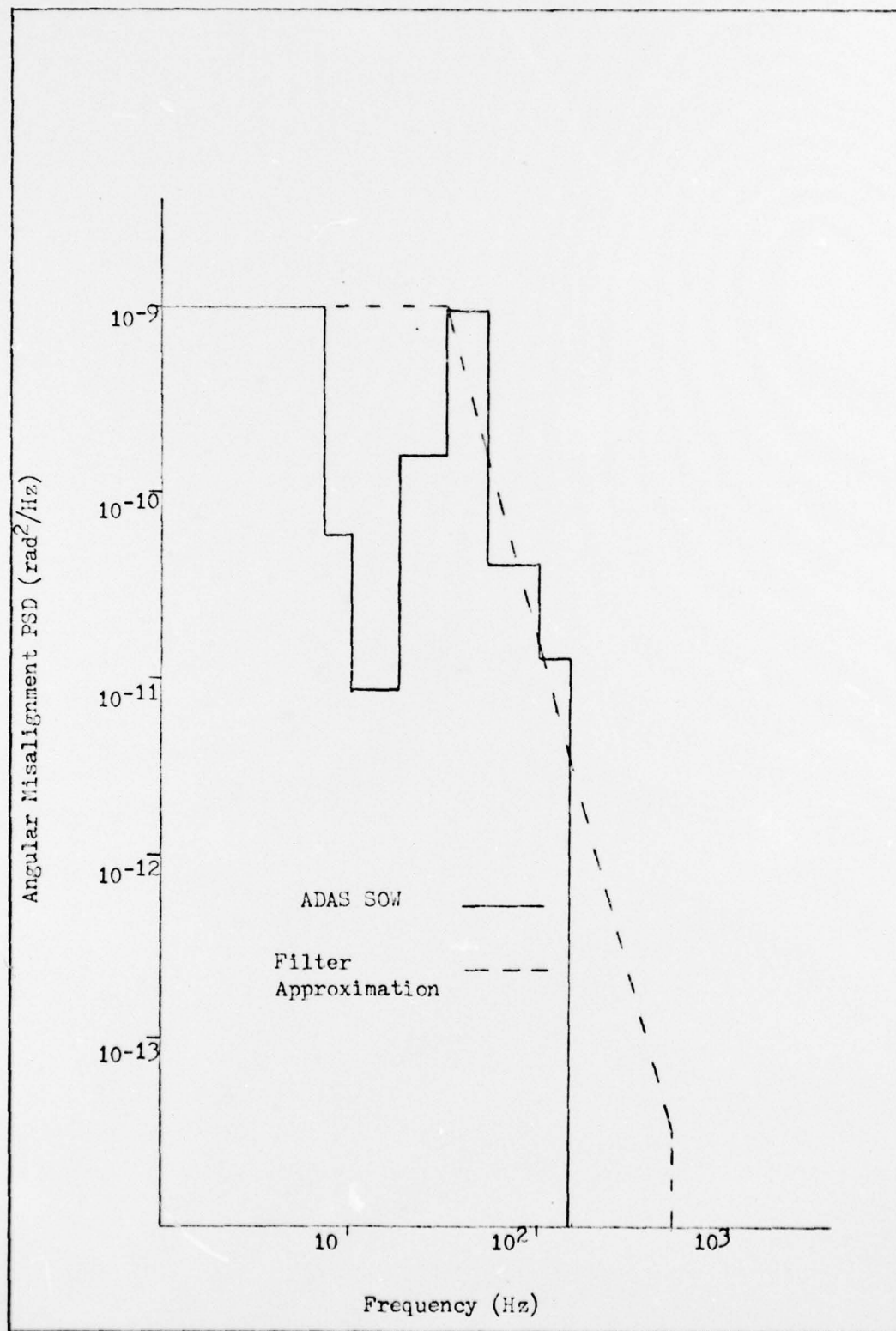


Fig.28. ADAS SOW PSD and State Space Filter Approximation

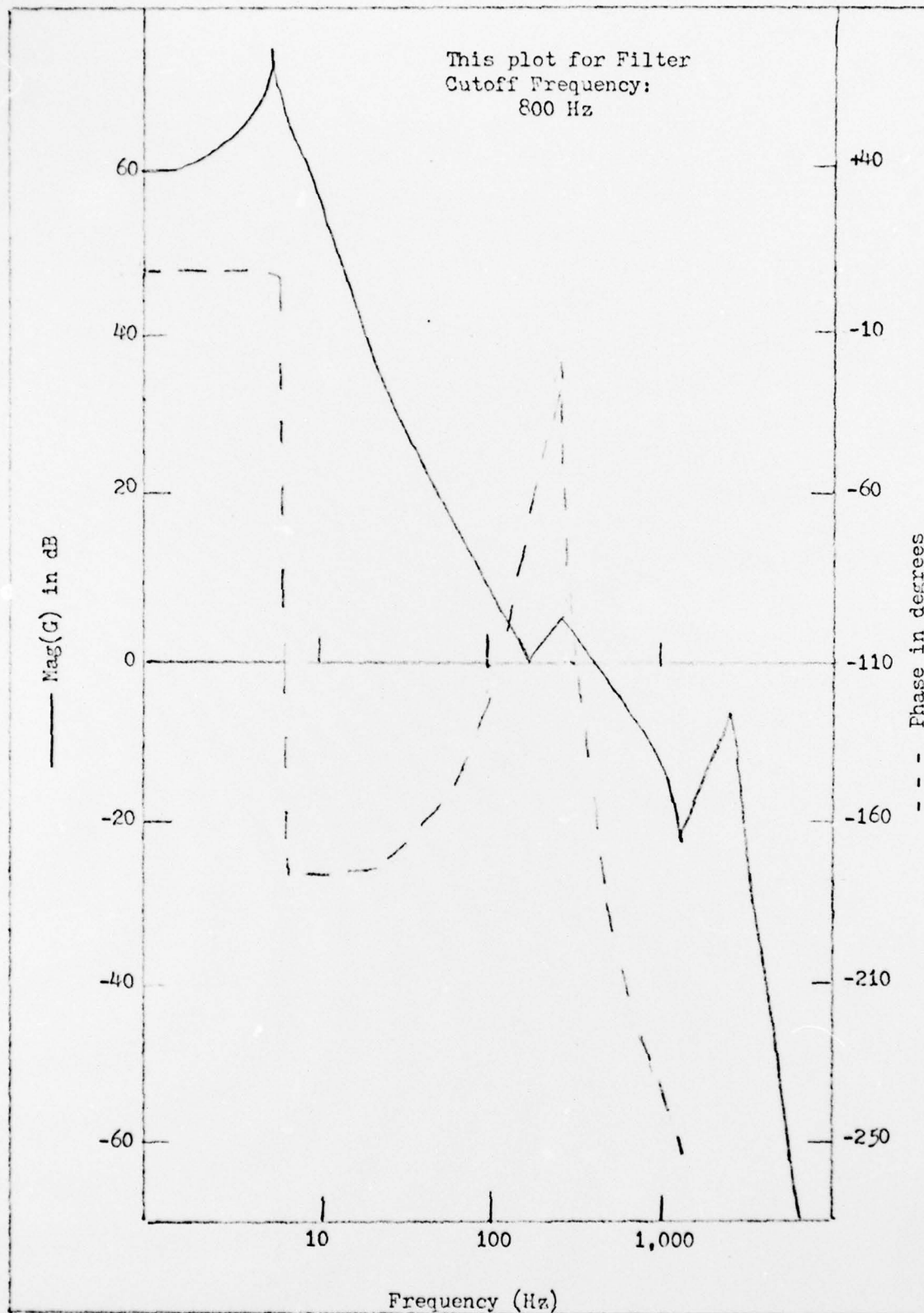


Fig. 29. ALPHA-P Open Loop Response

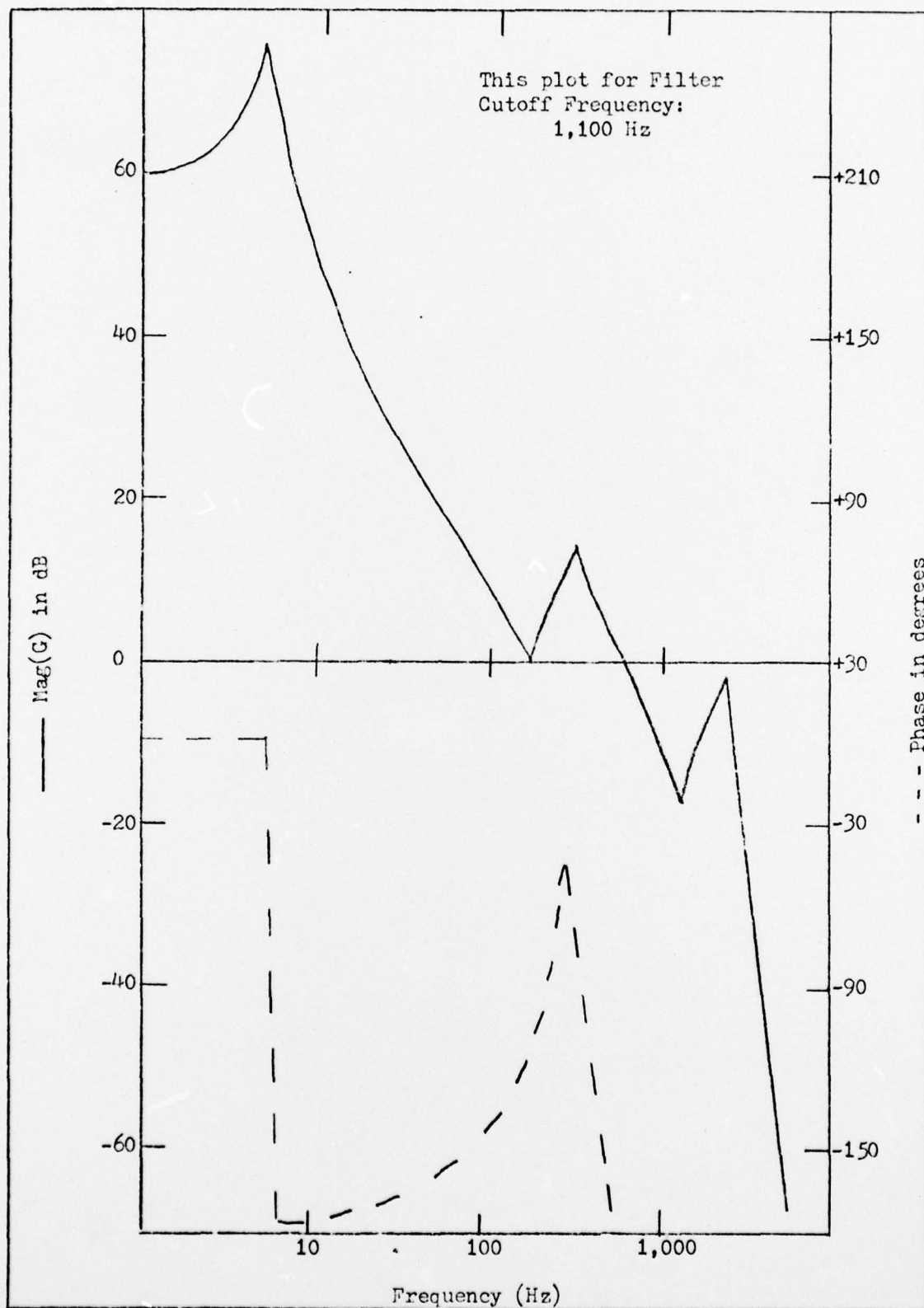


Fig. 30 . ALPHA-P Open Loop Response

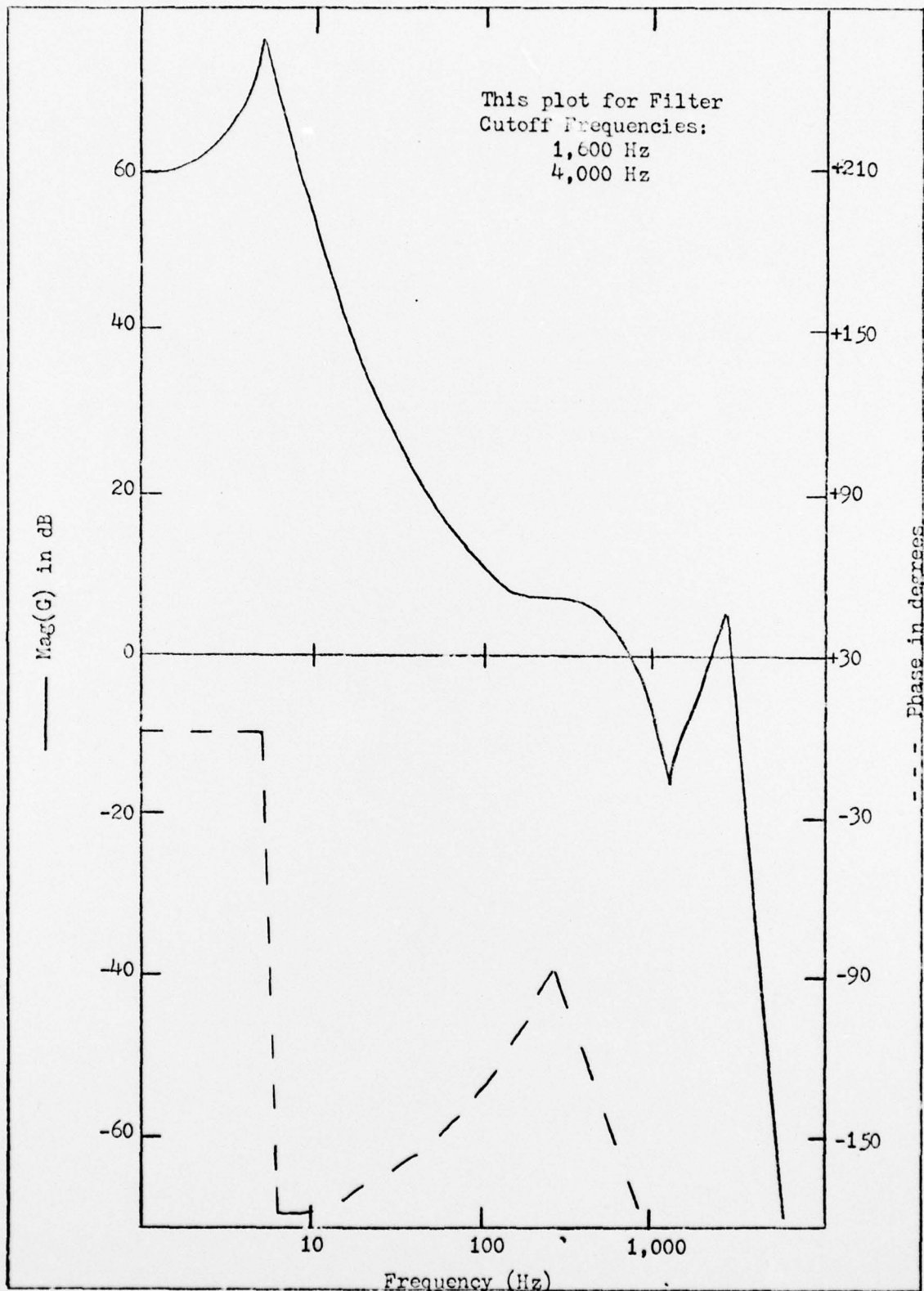


Fig.31 . ALPHA-P Open Loop Response

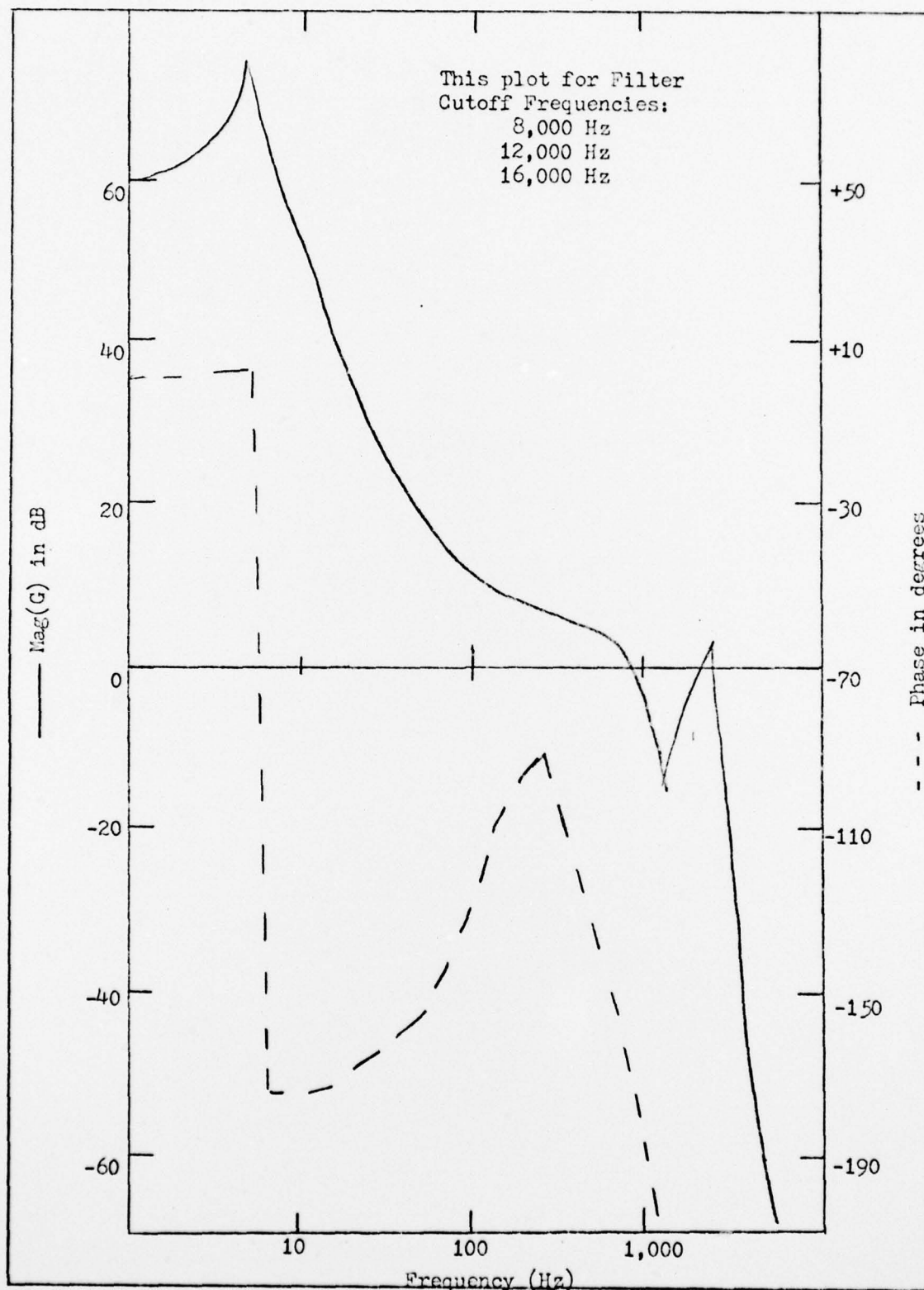


Fig. 32 . ALPHA-P Open Loop Response

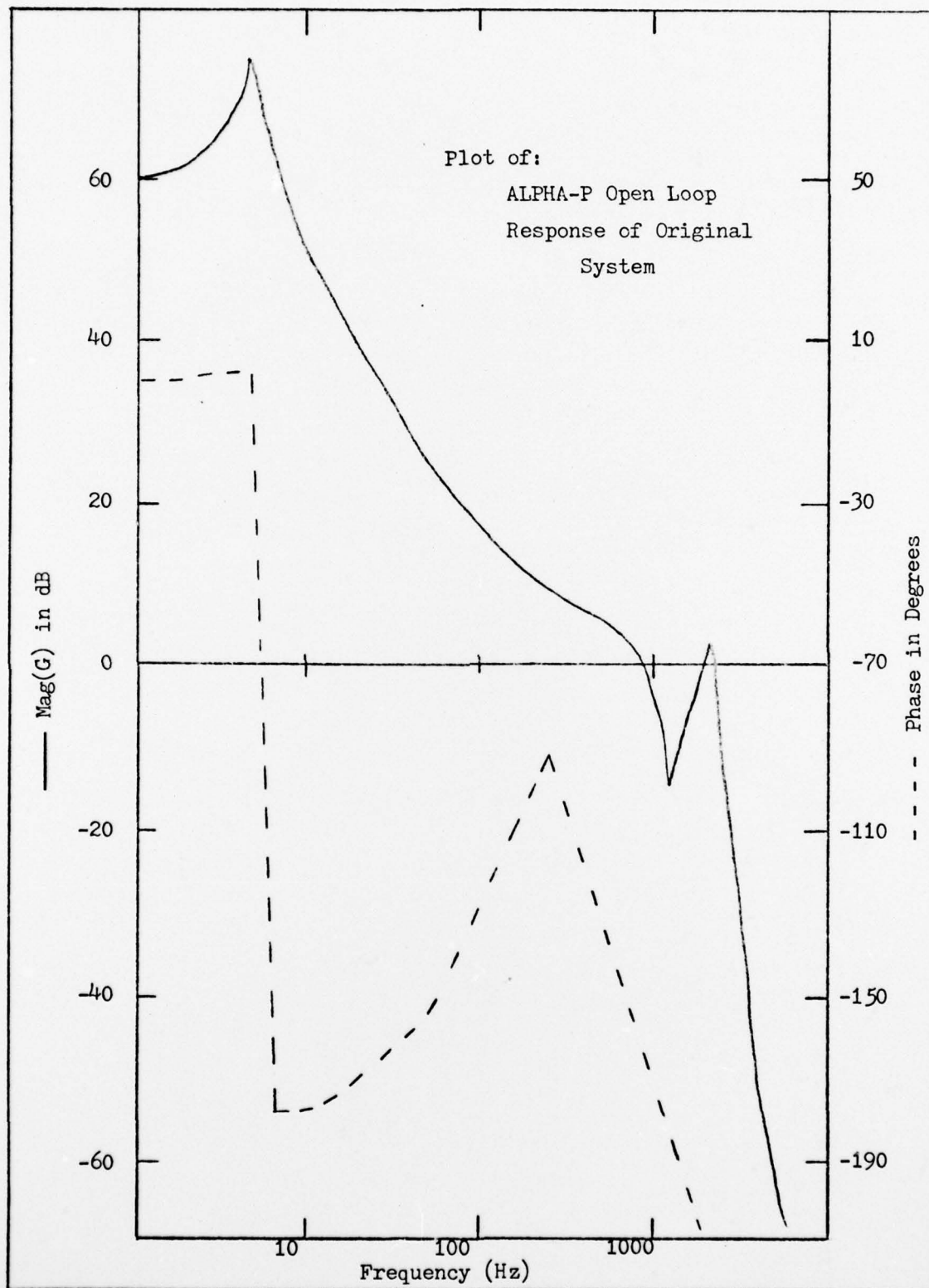


Fig.33. ALPHA-P Open Loop Response of Original System

Table XI

Eigenvalue Comparison with Various
Filter Cutoff Frequencies

Cutoff Frequency (Hz)	<u>Eigenvalues</u>				
0	-11,517	+2,780	-1433 <u>+1137i</u>	-418 <u>+148i</u>	
32	-11,684	+3,089 <u>+2,168i</u>	-2235 <u>+2966i</u>	-1576	-1087
160	-11,843	+1,157 <u>+ 994i</u>	-1432 <u>+1131i</u>	-805	-240
700	-13,166	+90 <u>+2,615i</u>	-1388 <u>+1138i</u>	-675	-402
800	-13,445	-170 <u>+2,797i</u>	-1431 <u>+1106i</u>	-590	-203
1,100	-14,410	-511 <u>+3,164i</u>	-1483 <u>+1071i</u>	-944	-94
1,600	-16,094	-1,250 <u>+3,338i</u>	-1437 <u>+1092i</u>	-768	-208
8,000	-51,231	-3,790 <u>+2,540i</u>	-1350 <u>+1050i</u>	-467 <u>+266i</u>	
16,000	-100,570	-3990 <u>+1860i</u>	-1390 <u>+1060i</u>	-340	-760
160,000	-1,000,000	-4,200 <u>+1,090i</u>	-1480 <u>+1080i</u>	-827	-204
Infinite (Original System)		-4,184 <u>+844i</u>	-1497 <u>+1086i</u>	-897	-179

Vita

Patrick D. Nutz was born in Midland, Pennsylvania in February, 1954. He attended the University of Pittsburgh School of Engineering under a AFROTC scholarship. After graduating with a B.S. in Mechanical Engineering in April, 1976, he was commissioned a 2d Lt in the U.S. Air Force Reserve. His first assignment was to the Air Force Institute of Technology WPAFB in September, 1976.

Permanent address: 1111 Avondale Dr.
Industry, Pa. 15052

REPORT DOCUMENTATION PAGE		READ INSTRUCTIONS BEFORE COMPLETING FORM
1. REPORT NUMBER AFIT/GAE/AA/78M-12	2. GOVT ACCESSION NO.	3. RECIPIENT'S CATALOG NUMBER
4. TITLE (and Subtitle) ANALYSIS AND DESIGN MODIFICATION OF AN AIRBORNE MIRROR ALIGNMENT SYSTEM		5. TYPE OF REPORT & PERIOD COVERED MS Thesis
		6. PERFORMING ORG. REPORT NUMBER
7. AUTHOR(s) Patrick D. Nutz 2d Lt USAF		8. CONTRACT OR GRANT NUMBER(s)
9. PERFORMING ORGANIZATION NAME AND ADDRESS Air Force Institute of Technology (AFIT-EN) Wright-Patterson AFB, Ohio 45433		10. PROGRAM ELEMENT, PROJECT, TASK AREA & WORK UNIT NUMBERS 19870164
11. CONTROLLING OFFICE NAME AND ADDRESS Air Force Weapons Laboratory LRO/Kirtland AFB, NM 87115		12. REPORT DATE March 1978
		13. NUMBER OF PAGES 116
14. MONITORING AGENCY NAME & ADDRESS (if different from Controlling Office)		15. SECURITY CLASS. (of this report) Unclassified
		15a. DECLASSIFICATION/DOWNGRADING SCHEDULE
16. DISTRIBUTION STATEMENT (of this Report) Approved for public release; distribution unlimited		
17. DISTRIBUTION STATEMENT (of the abstract entered in Block 20, if different from Report)		
18. SUPPLEMENTARY NOTES Approved for public release; IAW AFR 190-17 Jerry F. Guess, Captain, USAF Director of Information		
19. KEY WORDS (Continue on reverse side if necessary and identify by block number) Airborne Mirror Alignment		
20. ABSTRACT (Continue on reverse side if necessary and identify by block number) This study deals with an electronic control system modification to solve a torque limitation problem in the Airborne Dynamic Alignment System aboard the Airborne Laser Lab. This control system is reduced in complexity and modeled in the frequency and state space domains. Closed loop system response over a desired frequency range is obtained from the frequency domain model. Stability data is calculated through eigenvalue analysis of the state space model. A low pass filter is introduced to decrease the demand on the torque saturated motor. The main result of this modification is that the filter does not appreciably		

UNCLASSIFIED

SECURITY CLASSIFICATION OF THIS PAGE (When Data Entered)

alter the closed loop response. This is due to the fact that the cutoff frequency of the filter must be extremely high to keep the modified system stable. It is concluded that the complimentary filter does not solve the torque saturation problem. A recommendation is made that further analysis be concentrated in the time domain through modern state space techniques and the design approach to an optimal controller is presented.

SECURITY CLASSIFICATION OF THIS PAGE (When Data Entered)